U.S.NRC
United States Nuclear Regulatory Commission
Protecting People and the Environment

NUREG/CR-7171
ORNL/TM-2013/263

A Review of the Effects of Radiation on Microstructure and Properties of Concretes Used in Nuclear Power Plants

Office of Nuclear Regulatory Research

AVAILABILITY OF REFERENCE MATERIALS IN NRC PUBLICATIONS

NRC Reference Material

As of November 1999, you may electronically access NUREG-series publications and other NRC records at NRC's Public Electronic Reading Room at http://www.nrc.gov/reading-rm.html. Publicly released records include, to name a few, NUREG-series publications; *Federal Register* notices; applicant, licensee, and vendor documents and correspondence; NRC correspondence and internal memoranda; bulletins and information notices; inspection and investigative reports; licensee event reports; and Commission papers and their attachments.

NRC publications in the NUREG series, NRC regulations, and Title 10, "Energy," in the *Code of Federal Regulations* may also be purchased from one of these two sources.

1. The Superintendent of Documents
   U.S. Government Printing Office Mail Stop SSOP
   Washington, DC 20402–0001
   Internet: bookstore.gpo.gov
   Telephone: 202-512-1800
   Fax: 202-512-2250
2. The National Technical Information Service
   Springfield, VA 22161–0002
   www.ntis.gov
   1–800–553–6847 or, locally, 703–605–6000

A single copy of each NRC draft report for comment is available free, to the extent of supply, upon written request as follows:

Address: U.S. Nuclear Regulatory Commission
Office of Administration
Publications Branch
Washington, DC 20555-0001
E-mail: DISTRIBUTION.RESOURCE@NRC.GOV
Facsimile: 301–415–2289

Some publications in the NUREG series that are posted at NRC's Web site address http://www.nrc.gov/reading-rm/doc-collections/nuregs are updated periodically and may differ from the last printed version. Although references to material found on a Web site bear the date the material was accessed, the material available on the date cited may subsequently be removed from the site.

Non-NRC Reference Material

Documents available from public and special technical libraries include all open literature items, such as books, journal articles, transactions, *Federal Register* notices, Federal and State legislation, and congressional reports. Such documents as theses, dissertations, foreign reports and translations, and non-NRC conference proceedings may be purchased from their sponsoring organization.

Copies of industry codes and standards used in a substantive manner in the NRC regulatory process are maintained at—

The NRC Technical Library
Two White Flint North
11545 Rockville Pike
Rockville, MD 20852–2738

These standards are available in the library for reference use by the public. Codes and standards are usually copyrighted and may be purchased from the originating organization or, if they are American National Standards, from—

American National Standards Institute
11 West 42nd Street
New York, NY 10036–8002
www.ansi.org
212–642–4900

Legally binding regulatory requirements are stated only in laws; NRC regulations; licenses, including technical specifications; or orders, not in NUREG-series publications. The views expressed in contractor-prepared publications in this series are not necessarily those of the NRC.

The NUREG series comprises (1) technical and administrative reports and books prepared by the staff (NUREG–XXXX) or agency contractors (NUREG/CR–XXXX), (2) proceedings of conferences (NUREG/CP–XXXX), (3) reports resulting from international agreements (NUREG/IA–XXXX), (4) brochures (NUREG/BR–XXXX), and (5) compilations of legal decisions and orders of the Commission and Atomic and Safety Licensing Boards and of Directors' decisions under Section 2.206 of NRC's regulations (NUREG–0750).

U.S.NRC
United States Nuclear Regulatory Commission
Protecting People and the Environment

NUREG/CR-7171
ORNL/TM-2013/263

A Review of the Effects of Radiation on Microstructure and Properties of Concretes Used in Nuclear Power Plants

Manuscript Completed: August 2013
Date Published: November 2013

Prepared by:
Kaspar William
University of Houston
Department of Civil and Environmental Engineering
Houston, TX 77204-4003

Yunping Xi
University of Colorado
Department of Civil, Environmental and Architectural Engineering
Boulder, CO 80309-0428

Dan Naus
Oak Ridge National Laboratory
Materials Science and Technology Division
Oak Ridge, TN 37831-6069

Herman L. Graves, III, NRC Technical Monitor

NRC Job Code N6978

Prepared for:
Division of Engineering
Office of Nuclear Regulatory Research
U.S. Nuclear Regulatory Commission
Washington, DC 20555-0001

ABSTRACT

The current understanding of the effects of radiation on concrete materials is summarized. Much of the research related to this topic was conducted from the 1960s into the 1970s in support of development of prestressed concrete reactor vessels for high-temperature reactors and radioactive waste storage facilities. From the 1970s until 2012, the efforts addressed development of computational models of radiation damage to concrete and assessment of the effects of radiation on concrete durability. Concrete structures used as biological shields and as support for the reactor pressure vessel in current light-water reactor plants are subjected to two types of radiation, gamma and neutron. Gamma and neutron radiation are described, and their interactions with concrete constituents are noted. A summary of the effects of neutron and gamma radiation on the mechanical and physical properties of concrete is provided. Information is presented on thermal effects due to gamma heating of the concrete. Coupling effects of mechanical loading, thermal effect, moisture content, and radiation are described, and an example provided using a computational model to indicate radiation damage in a shield for a next-generation nuclear facility. Nondestructive testing methods are identified for assessment of the condition of reinforced concrete structures. Radiation limits for neutron and gamma exposure are listed. Finally, recommendations are provided to (1) expand the very limited database on the effect of neutron and gamma radiation on concrete's microstructure and mechanical and physical properties, (2) conduct calculations to establish the neutron and gamma fields that develop in concrete shields and support structures after various operating periods, and (3) quantify the interaction of temperature and irradiation effects.

FOREWORD

Commercial nuclear power plants (NPPs) in the United States contain concrete structures whose performance and function are necessary for the protection and safety of plant operating personnel, the general public, and the environment. Typical safety-related concrete structures contained in light-water reactor (LWR) plants are generally grouped into four categories: primary containments, containment internal structures, secondary containments/reactor buildings, and other structures. These safety-related concrete and other structures must be capable of maintaining structural integrity for the operating life of the plant.

Since 2008 the Office of Nuclear Regulatory Research (RES) staff has had discussions with other NRC staff, U.S. industry and academic representatives, and Japanese researchers on the topic of the effects of radiation fluences on concrete. Based on these discussions, RES planned and managed a research program to provide information on the effect of radiation on concrete structures, particularly in operating environments for existing LWRs and for some new reactor designs.

The objective of this research is threefold: (1) to determine whether current methods used to evaluate the effects of gamma and neutron radiation fluences on concrete structures are sufficient in determining the concrete properties for new reactor designs, (2) to determine the changes in the dimensional or physical properties of concrete that will be brought about by the elevated temperatures and the radiation fluences anticipated in new, high-temperature reactor designs, and (3) how these changes may also affect long-term NPP operation.

This NUREG/CR provides a review of concrete as a nuclear shielding material and the effects of nuclear radiation on the mechanical properties of concrete. Also discussed are computational models for radiation damage of concrete, assessment techniques to evaluate radiation damage, and radiation exposure limits for concrete NPP structures. The information in this report, coupled with the applicable code provisions discussed, could form the basis for new regulatory guidance on the review of radiation effects on concrete used in NPP structures.

CONTENTS

LIST OF FIGURES

LIST OF TABLES

EXECUTIVE SUMMARY

This document summarizes the current understanding of the effects of irradiation on concrete materials. Much of the research related to this topic was conducted from the 1960s into 1970s in support of development of prestressed concrete reactor vessels for high-temperature gas-cooled reactors and radioactive waste storage facilities. Concrete structures used as biological shields and as support for the reactor pressure vessel in current LWR plants are subjected to two types of radiation, gamma and neutron.

Gamma radiation refers to electromagnetic radiation of high frequency; high energy per photon. Gamma rays typically have energies above 100 keV and wavelengths less than 10 picometers. Gamma rays have an insignificant effect on solid materials composed of ionic and metallic bonds, but they can result in the destruction of anisotropic chemical bonds such as covalent bonds. Water in the concrete can be decomposed by gamma rays by a process called radiolysis and can be converted to hydrogen, oxygen, and hydrogen peroxide. Water can also be removed from the concrete by evaporation due to heat generated by gamma radiation. Because most of the water in concrete is contained in the cement paste, gamma radiation has a greater effect on the cement paste than it has on the aggregate materials.

In the instance of neutron irradiation, the neutrons do not interact with the electrons but with the nuclei of atoms. Because neutrons interact with the nuclei of atoms, the lattice spacing within the material may change after the collisions. Therefore, the neutrons have a more significant effect on dense and well-crystallized materials (e.g., aggregates) than on randomly structured materials with high porosity (e.g., cement paste). Interactions between nuclear radiation and the internal structure of concrete produce geometric changes of the structure resulting from displacements of atoms from their lattice sites and phase transformations of the concrete constituents resulting in a reduction in porosity and/or formation of microcracks. These interactions result in changes in the various concrete properties.

A summary of the effects of neutron and gamma radiation on the mechanical and physical properties of concrete is provided. Information is presented on thermal effects due to gamma heating of the concrete. Coupling effects of mechanical loading, thermal effect, moisture content, and radiation are described, and an example provided using a computational model to indicate radiation damage in a shield for a next-generation nuclear facility. Nondestructive testing methods are identified for assessment of the condition of reinforced concrete structures. Radiation limits for neutron and gamma exposure are listed. Finally, potential gaps are identified to (1) expand the very limited database on the effect of neutron and gamma radiation on concrete's microstructure and mechanical and physical properties, (2) conduct calculations to establish the neutron and gamma fields that develop in concrete shields and support structures after various operating periods, and (3) quantify the interaction of temperature and irradiation effects.

ACKNOWLEDGMENTS

The authors would like to acknowledge the continuing support and guidance throughout the program provided by U.S. Nuclear Regulatory Commission Technical Monitor, Mr. Herman L. Graves, III.

The authors also would like to acknowledge Mr. Walter Koncinski of Oak Ridge National Laboratory for his detailed review and many contributions to the report.

The authors wish to take this opportunity to recognize the fundamental contributions of our former colleague and friend Professor Hubert Hilsdorf towards understanding radiation effects on properties of concrete.

ABBREVIATED TERMS

AASHTO	American Association of State Highway and Transportation Officials
AC	alternating current
ACI	American Concrete Institute
ASME	American Society of Mechanical Engineers
ANSI	American National Standards Institute
ASR	alkali-silica reaction
ASTM	American Society for Testing and Materials
BS	British Standard
BWR	boiling-water reactor
CDP	combined damage plasticity
CH	calcium hydroxide
C-S-H	calcium silicate hydrate
DP	Drucker-Prager
EPRI	Electric Power Research Institute
ESEM	environmental scanning electron microscopy
HCP	hardened cement paste
HVT	half-value thickness
INFN	Italian Institute for Nuclear Physics
LET	linear energy transfer
LWR	light-water reactor
NDT	nondestructive test
NPP	nuclear power plant
OPC	ordinary Portland cement
PP	polypropylene
PWR	pressurized-water reactor
SEM	scanning electron microscopy
SHRP	Strategic Highway Research Program
SPES	Selective Production of Exotic Species
w/c	water-to-cement ratio

1. INTRODUCTION

Compared with other construction materials, concrete has a high shielding capacity against nuclear radiation, good long-term durability, and good high-temperature resistance, all at relatively low construction costs. Therefore, concrete is widely used for primary and secondary containment structures of nuclear power plants (NPPs) exposed to radiation and elevated temperatures. Besides being a basic infrastructure material, concrete is used to build shielding structures and interim storage facilities for spent nuclear fuel. Radiation and temperature effects on the properties of concrete depend on a range of variables, such as the intensity of the radiation field, the temperature level, and the period of exposure. In addition to the separate effects of radiation and temperature, there is also a one-way coupling effect between the two (i.e., a radiation-induced thermal effect).

There are two types of radiation in NPPs, neutron radiation and gamma rays. Neutron radiation is the emission of neutrons; gamma rays are a special form of photon radiation. The two types of radiation interact with concrete in different ways. A variety of concrete materials, with different types of cement, aggregates, and additives, have been used in NPPs. Some concretes are more susceptible to gamma radiation, and others are more susceptible to neutron radiation, depending on the constituent materials used in the mix.

Elevated temperatures have two different effects on concrete. One involves phase transformations of the concrete constituents under high temperatures; the other refers to mechanical damage in the form of spalling. Both effects may result in significant deterioration of the stiffness, strength, and ductility of concrete and concomitant loss of load-bearing capacity. Phase transformations depend primarily on the temperature level, but not on the rate of temperature changes. Spalling damage occurs under high heating or cooling rates. A moderate elevation in temperature can occur in concrete exposed to gamma radiation.

This report summarizes the results of research on the effects of radiation and temperature on the material properties of concrete [i.e., mechanical properties, such as strength, stiffness, and ductility (energy absorption capacity), and durability properties, such as time- and rate-dependent creep and shrinkage and environmental aging]. Basic information on neutron and gamma radiation is introduced first. That is followed by a description of the internal structure of concrete and by detailed discussions on heating due to radiation and its effects on the properties of concrete. The effect of radiation on the properties of concrete and the concomitant coupling effect of radiation and temperature are further examined, in addition to testing methods of the effects of radiation and high temperatures on concrete structures. Radiation limits for neutron and gamma exposure of NPP structures are identified. Areas for additional research are noted.

2. GAMMA RAY AND NEUTRON ATTENUATION

Nuclear reactions are driven by the transformation of atoms; typically, atoms of one element are converted into atoms of another element. This process is different from chemical reactions. Chemical reactions usually involve electrons being shared, or transferred, to form compounds. Instead of the electrons taking part in the reaction, nuclear reactions are characterized by the atom's nuclei undergoing changes. Nuclear reactions yield large changes in energy and measurable changes in mass (Silberberg 2007). In addition, when an atom transforms, it emits radiation. The magnitude of the released energy is equivalent to the energy difference between the atom's initial state and the atom's final state.

Radioactivity of nuclei is associated with unstable nuclides, which transform to a more stable form by emitting radiation. The stability of a nucleus is related to the ratio of N/Z, where N is the neutron number and Z is the proton number. The sum of N and Z equals the mass number A (A = N + Z). The N/Z ratio of stable light nuclei (A < 20) is close to 1.0; the ratio for heavy nuclei such as uranium-235 can reach 1.554 (N = 143, Z = 92, and A = 235). The N/Z ratio of a stable nuclide can be changed into an unstable nuclide artificially by bombarding stable nuclides with neutrons or high-energy particles produced by nuclear reactors.

Irradiation by charged particles such as electrons and protons can lead directly to a gain or a loss of charge of an atom, which is called direct ionizing radiation (ionization is the process of an atom gaining or losing electrons). Irradiation by noncharged particles such as neutrons and photons does not lead directly to a change in charge of an atom, and thus is called indirect ionizing radiation. Although uncharged particles do not cause direct ionization of atoms, they do release charged particles (electrons or protons) as a consequence of their interaction with matter and will subsequently cause direct ionization of atoms. Therefore, both direct and indirect ionizing radiation can cause ionization.

The literature distinguishes between radiation that is electrically charged and radiation that is electrically neutral. The electrically charged radiation includes alpha and beta particles. Alpha rays are high-speed, high-energy particles expelled from unstable nuclei; each alpha particle is the nucleus of a helium atom, which is made up of two protons and two neutrons. Alpha radiation is a weak form of direct ionizing radiation that is readily stopped by a sheet of paper. Beta particles, which are much lighter, are given off by the nucleus of an unstable isotope to restore an energy balance. The beta particles are high-energy, high-speed electrons or positrons (a positron has an electric charge of +1e, spin of ½, and has the same mass as an electron; an electron has an electric charge of -1e and a spin of ½). Beta radiation is also a direct ionizing radiation and is stronger than alpha radiation. It can be halted by a thin lead plate.

Gamma rays and neutrons are electrically neutral. Gamma rays are energetic photons or light waves in the same electromagnetic family as light and x rays. Photons are considered gamma radiation when they possess an energy level that is higher than 0.1 MeV. Gamma radiation, which is much stronger than alpha or beta radiation, is an indirect ionizing radiation and is biologically hazardous. X rays are also electromagnetic radiation, but their energy level is lower than that of gamma rays. X rays are also distinguished from gamma rays in that x rays are emitted by electrons whereas gamma rays are emitted by the atomic nucleus. Neutrons are also electrically neutral particles, and thus, when emitted by an atomic nucleus, are also classified as an indirect form of ionizing radiation.

In direct ionizing irradiation, the charged particles interact strongly with the materials in a radiation shield and are attenuated by the shield. In the case of alpha ray irradiation, a positively

charged helium atom travels through a shielding material, gains two negatively charged electrons, and becomes a neutral helium atom. In indirect ionizing irradiation, noncharged particles such as neutrons and gamma photons interact less strongly with shielding materials. In general, the indirect ionizing radiation is more hazardous than the direct ionizing radiation. In the following two sections, the interactions of photons and neutrons with shielding materials will be discussed.

2.1 GAMMA RADIATION

Gamma radiation refers to electromagnetic radiation of high frequency; high energy per photon. Gamma rays typically have energies above 100 keV and wave lengths less than 10 picometers. The absorbed dose in a small volume element is equal to the energy imparted by ionizing radiation to the material in a volume element divided by the mass of the material in the volume element. The unit of absorbed dose is a gray having units of joule kg^{-1}: 1 Gy = 100 rad. Photons interact with shielding materials in three different ways: photoelectric effect, Compton scattering, and pair production. Each involves the ejection of electrons from atoms, as shown in Figure 2.1. For the photoelectric effect, a gamma ray is absorbed, resulting in the ejection of an orbital electron. For Compton scattering, the gamma ray is not absorbed but deflected (scattered), and an electron is also ejected. For pair production, the gamma ray is absorbed, and a pair (consisting of a positron and an electron) is ejected.

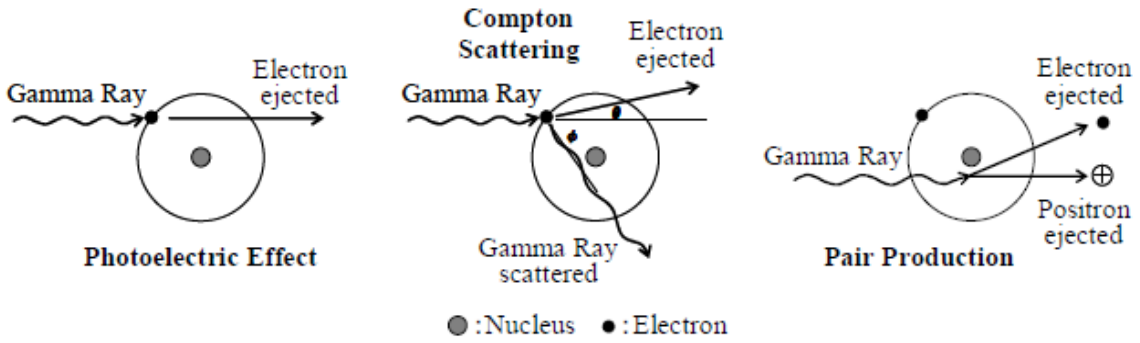

Figure 2.1. The photoelectric effect, Compton scattering, and pair production of gamma radiation. (Kontani et al. 2010)

From a radiation-shielding point of view, the relative importance of the three interactions between photons and the shielding material depends on both photon energy and the atomic number of the shielding material. According to Kaplan's review (1989), when the atomic number is 20, the photoelectric effect is dominant if the photon energy is from 0.01 to 0.1 MeV, and Compton scattering is dominant if the photon energy is from 0.1 to 100 MeV. When the atomic number is 60, the photoelectric effect is dominant if the photon energy is from 0.01 to 0.5 MeV, Compton scattering is dominant if the photon energy is from 0.5 to 5 MeV, and pair production is dominant if the photon energy varies from 5 to 100 MeV. According to Kontani et al. (2010), the energy range of gamma rays produced by nuclear reactors varies from 100 KeV to 10 MeV. Compton scattering is the dominant interaction mechanism in that energy range. The dominant ranges of the three types of interactions are illustrated in Figure 2.2. In general, with shielding materials that have a high atomic number, the dominant interaction mechanism for photon radiation depends on the photon energy level. High photon energy results in pair production, low energy causes photoelectric effect, and Compton scattering is dominant in between.

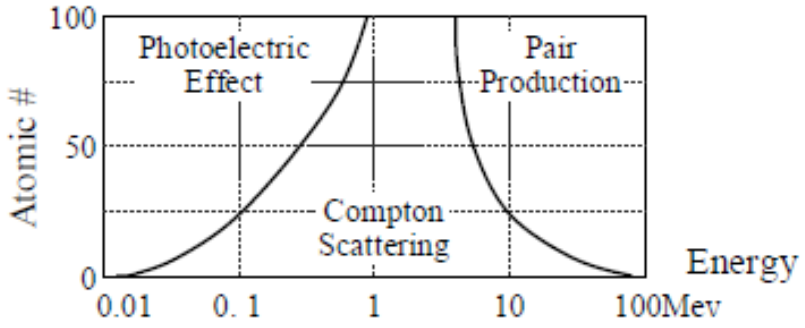

Figure 2.2. Relationship among gamma ray energy, atomic number, and interaction mechanisms. (Kontani et al. 2010)

Compton scattering reduces the energy of a gamma ray by transferring a portion of its energy to the ejection of an electron and deflects the gamma photon from its original path. Because they are deflected and not totally absorbed during the Compton scattering process, the gamma rays can be scattered numerous times before completely passing through the material, and thus a buildup of gamma radiation may occur within the shielding material. This effect can actually increase the total amount of radiation passing through the shielding and needs to be considered when designing a radiation shield.

Because gamma rays are attenuated by interactions with electrons, concrete to be used as a gamma-shielding material should be designed to maximize the density of electrons within it. This can be done by (1) using a type of cement with higher number of electrons per atom content, (2) increasing the density of concrete by better compaction, and (3) using heavier aggregate (Callan 1953). The first two methods are difficult to apply in practice because there are only a few types of Portland cement available. Also, a concrete mixture can be compacted to a point where the coarse aggregate in the mix may become segregated. A more practical approach would be to use heavier aggregates, such as iron, iron ore aggregates, and various other high-density aggregates in the concrete mixture (Callan 1953; Kaplan1989).

Gamma rays have an insignificant effect on the solid materials composed of ionic and metallic bonds, but they can break anisotropic chemical bonds such as a covalent bond. Siliceous materials may be degraded by gamma rays because the Si-O bond is a covalent bond (Kontani et al. 2010). See the discussion of the alkali-silica reaction (ASR) in Section 6.1.

Gamma rays can reduce the water content in a shielding material such as concrete by two mechanisms. The gamma rays can decompose water through a process called radiolysis which converts the water to hydrogen, oxygen, and hydrogen peroxide (Bouniol and Aspart, 1998). Water can also be driven from concrete by evaporation caused by the heat generated by gamma-ray irradiation. In concrete, most of the water is contained in the cement paste, not in the aggregate, and thus the effect of gamma-ray irradiation on cement paste is more significant than its effect on aggregate.

2.2 NEUTRON RADIATION

Neutron radiation interacts with the nuclei of atoms; however, the interaction depends mainly on the kinetic energy of the neutrons. The neutrons are classified by their energy into three types: thermal neutrons, epithermal neutrons, and fast neutrons. The energy level of thermal neutrons

is less than 1 eV, epithermal neutron energy levels are between 1 eV and 0.1 MeV, and the energy level of fast neutrons is greater than 0.1 MeV (Hilsdorf et al. 1978). The epithermal neutrons are also referred to as intermediate or resonance neutrons. The amount of neutron radiation absorbed is typically expressed by the fluence (Shultis and Faw 2000). Neutron fluence is the measure of the number of neutrons *n* that penetrate a unit area, typically expressed in terms of neutrons per square centimeter. The rate of neutron radiation is measured in units of flux, typically expressed in terms of neutrons per square centimeter per second.

When a high-energy (i.e., fast) neutron collides with a nucleus, the neutron loses some energy, and the nucleus generates scattered gamma rays and ejects a neutron. The ejected neutron (compared with the incoming neutron) and the nucleus both change their directions. The process is called inelastic scattering. This process may repeat many times until the fast neutron becomes an intermediate neutron. When an intermediate neutron collides with a nucleus, the nucleus ejects a neutron, and the ejected neutron (compared with the incoming neutron) and the nucleus both change their directions. The intermediate neutron does not have enough energy to cause the nucleus to release gamma rays. This process is called elastic scattering; however, the intermediate neutron will lose some energy during the process. The elastic scattering process may repeat until an intermediate neutron becomes a thermal neutron. When a thermal neutron collides with a nucleus, no further neutron ejection occurs, no gamma rays are released, and all the energy is absorbed in the collision. The inelastic and elastic scattering processes of neutron radiation are illustrated in Figure 2.3.

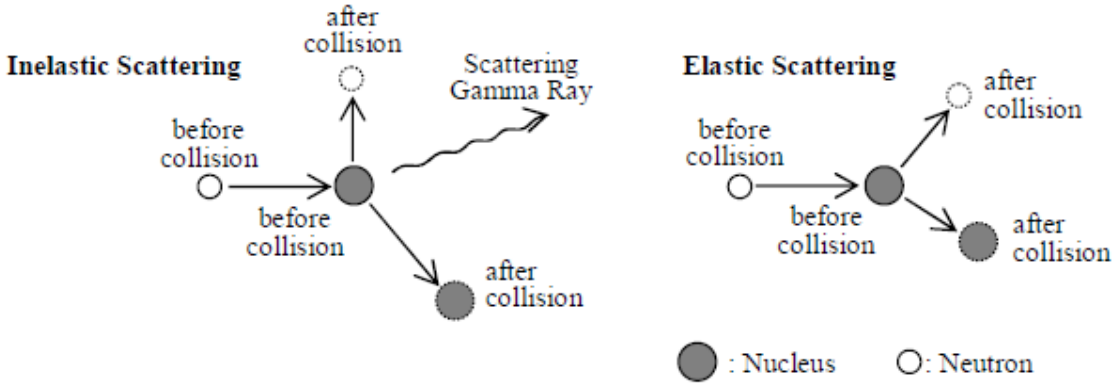

Figure 2.3. Inelastic and elastic scattering processes of neutron radiation. (Kontani et al. 2010)

Increasing the density of a material is desirable for neutron attenuation because this will increase the number of atoms per unit volume as well as the probability of the collision between neutrons and nuclei.

Because neutrons interact with nuclei of atoms, the lattice spacing within the material may change after the collision of neutrons with nuclei. Therefore, neutrons have a more significant effect on dense and well-crystallized materials than on randomly structured materials with high porosity. In concrete, aggregates (coarse and fine aggregates) are in a crystallized phase, and cement paste is an amorphous phase, and thus, neutron radiation causes more distortion and damage to the internal structure of aggregates than to the structure of cement paste. The neutrons collide with nuclei in cement paste, but the nuclei do not accumulate enough damage to alter the properties of

the cement paste because of the high porosity and randomly layered internal structure of cement paste, which will be described in detail in Chapter 3.

2.3 RADIATION SHIELDING EFFECTS

For radiation shielding, a higher transfer of energy corresponds to a more effective radiation shield, but the radiation also has an effect on the shielding material. Therefore, if a concrete biological shield attenuates gamma rays and neutrons effectively, it will be affected to a greater extent by the irradiation than a less effective radiation shielding material. This greater absorption should be observed as a change in the mechanical and physical properties of the shield material.

The attenuation mechanisms of concrete are different with photons and neutrons. The radiation shielding for photons can be calculated relatively accurately based on three processes for photons: photoelectric effect, Compton scattering, and pair production. The radiation shielding for neutrons can be calculated less accurately than that for photons. Kaplan (1989) has an extensive review on radiation attenuation of photons and neutrons by concrete.

The intensity of photons that pass through a shield can be experimentally measured in different ways, depending on the experimental setup (see Figure 2.4): narrow-beam attenuation (e.g., with photons passing through a collimator) and broad-beam attenuation (i.e., without a collimator). The radiation intensities of photons after travelling through a shielding material are given by

$$I = I_0 e^{-\mu x} \tag{2.1}$$

$$I = I_0 B e^{-\mu x} \tag{2.2}$$

where I_0 is the photon intensity at the source, B is the broad-beam buildup factor, μ is the linear attenuation coefficient in cm^{-1}, and x is the depth in centimeters in the shielding structure from the surface of the shielding material. The difference of Eq. (2.1) and Eq. (2.2) is the factor B. Equation (2.2) is for broad-beam attenuation whereas Eq. (2.1) is for narrow-beam attenuation. In both equations, the attenuation coefficient μ determines the rate of attenuation. It depends on the energy of the photons and the radiation resistance of the shielding material.

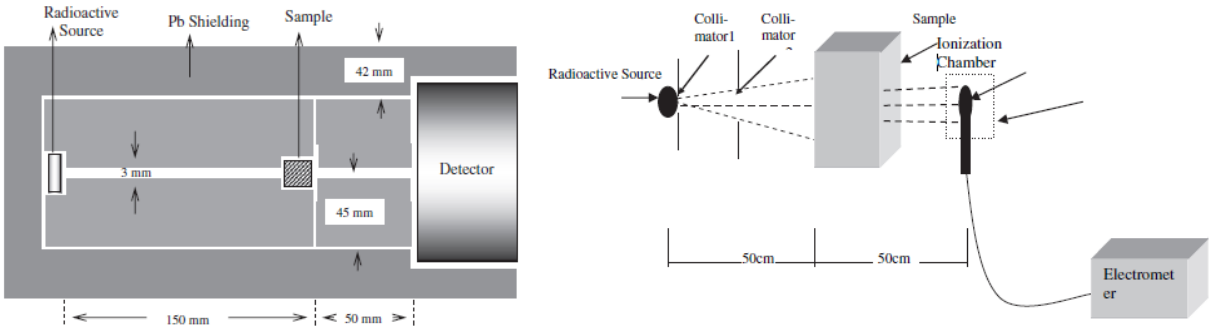

Figure 2.4. Experimental setups for measuring mass attenuation coefficients. (Yilmaz et al. 2011 on the left and Kharita et al. 2011 on the right.)

For neutron irradiation, determination of the reduction in the radiation intensity is more complicated than for photon irradiation. This is because there are primary and secondary

neutrons that are produced in the interaction process, and photons are produced from inelastic scattering. Therefore, attenuation of both neutrons and photons needs to be considered. In general, neutron attenuation can be calculated by the transport theory used for calculation of photon attenuation, but the solutions are more complicated and less accurate. The attenuation of fast neutrons can be calculated approximately by Eq. (2.3):

$$I = I_0 e^{-\Sigma_R x} \tag{2.3}$$

where $\sum_R$ is the macroscopic removal cross section in cm^{-1}. The absorption for thermal neutrons is given by Eq. (2.4):

$$I = I_0 e^{-x/L_N} \tag{2.4}$$

where L_N is the diffusion length (in centimeters), which depends on neutron radiation resistance of the material.

3. CONCRETE AS A NUCLEAR SHIELDING MATERIAL

The internal structure of concrete can be considered as a multiple-scale structure such as shown in Figure 3.1. At the mesoscale, concrete can be considered as a two-phase composite material with aggregate as inclusions and cement paste as a matrix. At the microscale, the internal structure of hydrated cement paste can be divided into several hydration products at different scale levels.

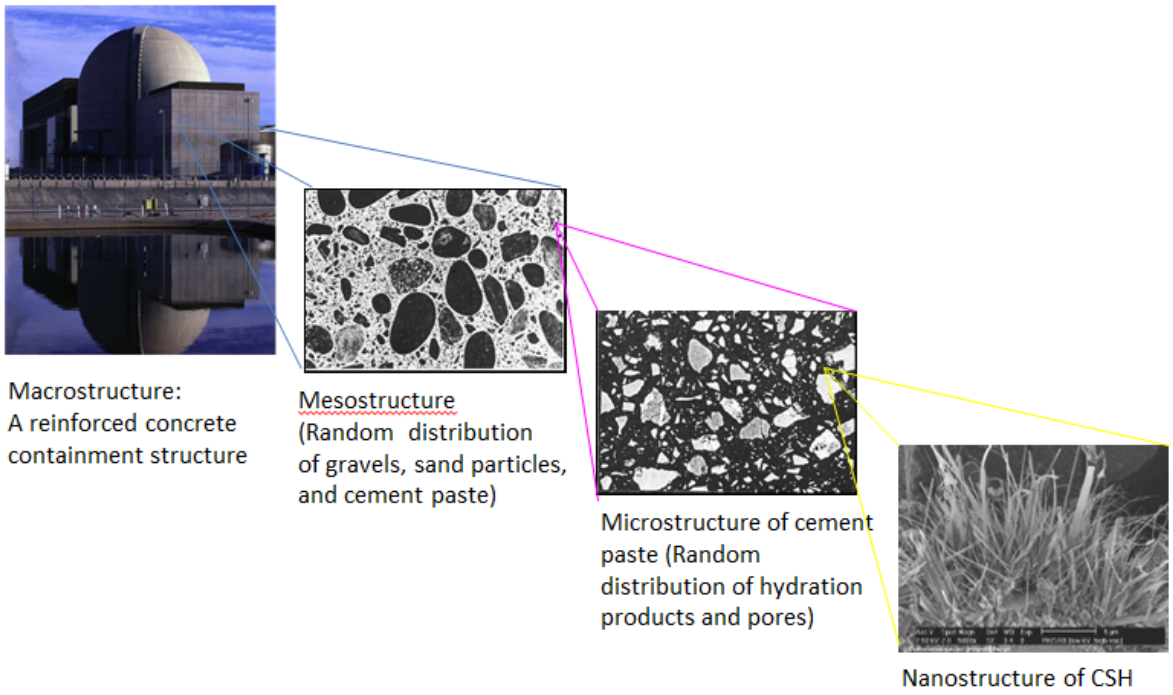

Figure 3.1. Multiple-scale internal structure of concrete (schematic).

The internal structure of aggregates is more or less of a crystalline nature, but the internal structure of hydrated cement paste is not. This is important because the response of a crystalline material to gamma rays and neutron irradiation can be different from that of a noncrystalline material.

3.1 AGGREGATES USED IN CONCRETE FOR SHIELDING STRUCTURES

Aggregates can be classified in different ways. Aggregates can be divided into coarse and fine aggregate, in which the sizes of coarse aggregate particles are larger than 4.75 mm, and the sizes of fine aggregate particles are smaller than 4.74 mm. In accordance with mineralogical compositions, aggregates can be divided into rock types, such as siliceous aggregates and calcareous aggregates, or by density (e.g., normal weight, lightweight, and heavyweight). Table 3.1 presents examples of aggregates and concrete unit weights for each of the density classifications.

Table 3.1. Examples of aggregates based on density (Kaplan 1989)

Type aggregate	Density (kg/m^3)	Examples	Concrete density (kg/m^3)
Normal weight	1520–1680	Limestone, granite, sandstone	2400
Light weight	< 1120	Volcanic pumice, blast furnace slag, cinder	< 1850
Heavy weight	> 2080	Magnetite, barytes, ferrophosphorus	> 4000

Typically, normal-weight aggregates have been used in the biological shields of pressurized water reactors, and heavyweight aggregates have been used in the shields and support structures of a few boiling water reactors (BWRs).

Several different types of aggregates have been studied for use in shielding structures, including the following (Kaplan 1989).

- **Hydrous aggregates.** Hydrous aggregates are good materials for radiation shielding because of their high hydrogen content, which is beneficial in the attenuation of neutrons. The hydrogen in the aggregate comes mainly from chemically bound water. Commonly used hydrous aggregates are serpentine, limonite, goethite, and bauxite.

- **Heavy aggregates.** The density of the shielding material is important for the attenuation of photons. Therefore, high-density (heavy) aggregates are used to increase the density of concrete in radiation shields and thus reduce the section-thickness requirements to achieve a given level of shielding. Typical heavy aggregates can be naturally occurring ores such as magnetite, witherite, barytes, ferrophosphorus or synthetics such as iron and steel. In one case, where a 3.05 m thickness of ordinary concrete would be required, a thickness of only 2.4 m of magnetite concrete gave equivalent shielding efficiency (Callan 1953).

- **Boron-containing aggregates.** Boron-containing aggregates can be used for radiation shields because of their large neutron cross section. Neutron attenuation often leads to production of secondary “hard” gamma radiation. Elements with a large neutron cross section will produce “soft” gamma radiation instead, which is less penetrating into the shielding structure. Boron aggregates include colemanite, borocalcite, and ferroboron.

Table 3.2 summarizes radiation attenuation characteristics for several of the aggregates considered for use in shielding structures. Guidance is available for assessing aggregates for specific use in radiation-shielding concretes (Lee et al. 2013).

Table 3.2. Properties of aggregates for radiation attenuation (Kaplan, 1989)*

	ρ (g/cm^3)	μ (1/cm)	Σ_R (1/cm)	L_N (cm)
Barytes	3.50	0.0945	0.0926	4.72
Magnetite	3.55	0.0959	0.1060	2.67
Limonite-steel	4.54	0.1226	0.1210	1.96
Ferrophosphorus	4.68	0.1264	0.1250	1.93

* ρ is density of aggregate, μ is linear attenuation coefficient, Σ_R is effective removal cross section, and L_N is diffusion length.

3.2 IMPACT OF IRRADIATION ON THE CRYSTALLINE STRUCTURE OF AGGREGATES

Under nuclear irradiation, the atomic structure of some aggregates can be converted from crystalline structure to distorted amorphous structure with a decrease in specific gravity and an increase in volume (Kontani et al. 2010). Two negative impacts are associated with the conversion. One is that the distorted internal structure leads to higher reactivity of the converted aggregates, which may make the aggregates more reactive to certain aggressive chemicals. A typical example is the ASR of concrete, which is discussed in detail in Section 6. The other negative impact is that the increase in volume can cause microcracking of concrete.

The effect of nuclear irradiation on quartz was studied by several researchers (Ichikawa et al., 2002). Crystalline quartz, or α-quartz, with specific gravity of about 2.65 is converted to distorted amorphous quartz with specific gravity of 2.27 under a fluence of 1×10^{20} n/cm^2 for fast neutrons with an energy level > 0.1 MeV, and under a dose of 1×10^{12} Gy for beta and gamma rays. Figure 3.2 shows the density of quartz as a function of fast neutron fluence. Regular amorphous quartz can be converted into distorted amorphous quartz by a fluence of 0.2×10^{20} n/cm^2 for fast neutrons and a dose of 0.1×10^{12} Gy for beta and gamma rays, which are both lower than the values for crystalline quartz. The volume expansion (i.e., density reduction) associated with the conversion is quite large (a 14% difference between the two specific gravities). The conversion of aggregate usually starts at its surface layer.

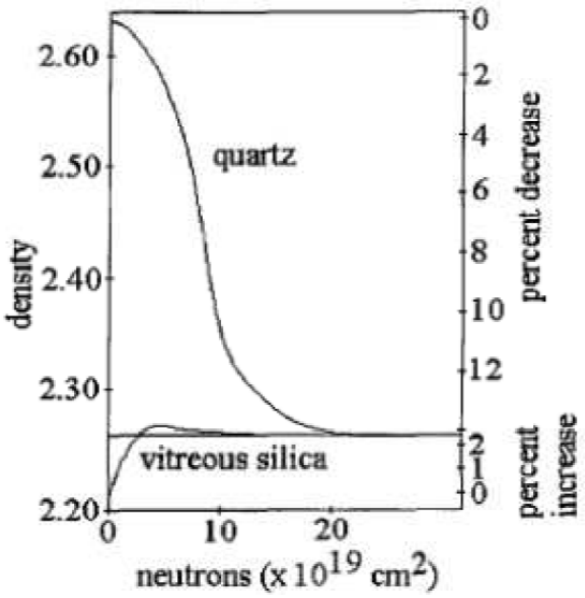

Figure 3.2. Density of quartz as a function of fast neutron fluence.(Bouniol 2011.)

3.3 CEMENTS AND INTERNAL STRUCTURE OF CEMENT PASTE

The chemical composition of cement paste depends on the type of cement used in construction. Portland cement is the most commonly used cement for concrete shielding structures. Other cements with different chemical compositions are available (Mehta and Monteiro 1993) but have not been used in construction of NPP concrete structures.

Mixing water and Portland cement makes cement paste. It is composed of several hydration products of Portland cement. For example, the volume of calcium hydroxide (CH) particles is about 25% of the total volume of cement paste. CH particles are needle- or plate-shaped crystals and have a significant effect on long-term properties of concrete. Calcium silicate hydrate ($C_3H_2S_3$, or simplified as C-S-H) has a nonstoichiometric amorphous structure. The crystalline structure of C-S-H in cement paste has not been fully resolved. The volume of C-S-H is about 50% of the total volume of cement paste. Ettringite ($C_6AS_3H_{32}$) particles are needle-shaped crystals. Their formation is associated with large volume expansion. The volume of ettringite is about 15% of the total volume of cement paste. The remainder of the cement paste volume consists of capillary water and empty capillary pores.

Calcium hydroxide and ettringite are crystalline materials, but C-S-H is not. The atomic structure of C-S-H is important because C-S-H is the material that binds all components together and produces the strength of concrete. The atomic structure of C-S-H has been studied extensively and theoretically (Jennings and Xi 1992). However, until recently, the experimental techniques could not provide direct visualization of the detailed structure of C-S-H at the nanometer level. Light microscopy, scanning electron microscopy (SEM), and environmental SEM provide resolution at the micrometer level. Transmission electron microscopy, x-ray diffraction (XRD), and atomic force microscopy methods provide more-detailed resolution. Using indirect test methods such as adsorption of nitrogen or water, and mercury intrusion porosimetry, average structural information of C-S-H has been obtained. Because these properties give no

information as to how the pores are arranged in space, the conclusions about the pore structure of C-S-H were drawn by inference. For example, the internal surface areas measured for C-S-H are around 200 m^2/g based on adsorption isotherms, which is very high. Because of the very high internal surface areas measured, some basic nanostructure models were proposed for C-S-H. They are layered structures with plate-like solid layers or randomly shaped flexible layers. One of them is shown in Figure 3.3, which was proposed by Powers and Brownyard (1948); another model, shown in Figure 3.4, was proposed by Feldman and Sereda (1968).

The Powers Model (Powers and Brownyard 1948) is supported by water adsorption test data. The model considers that the colloidal particles of C-S-H are made up of two or three layers of thin sheets that are bonded together. Bond forces are mainly surface forces. The water within the particles or between the layers is interlayer water, and the water on the surface of the particles is adsorbed water (see Figure 3.3). The maximum and minimum average distances between the layers are 30Å and 4Å, respectively, which can be obtained by analysis of surface area based on water adsorption test data. If the water between the layers is removed, it will not reenter. This irreversible interlayer water loss corresponds to irreversible shrinkage of cement paste. Feldman and Sereda (Feldman and Sereda 1968) suggested that C-S-H is a completely irregular array of single layers (see Figure 3.4). Bonding between layers is considered to be through solid-solid contacts. The interlayer water can move reversibly in and out of the interlayer space.

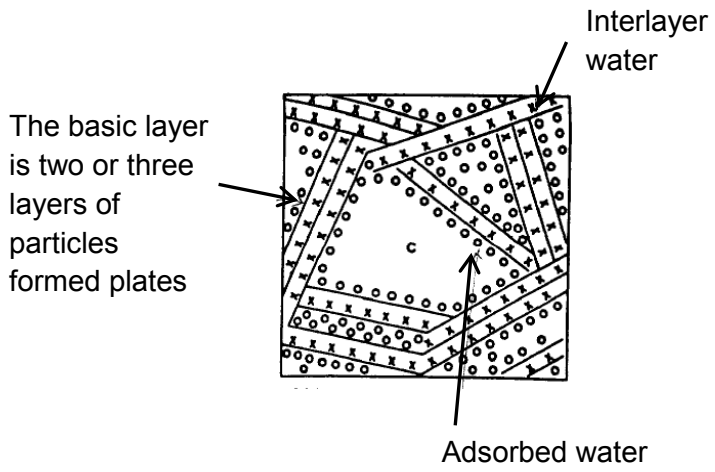

Figure 3.3. Powers' model for the internal layered structure of C-S-H. (Powers and Brownyard 1948)

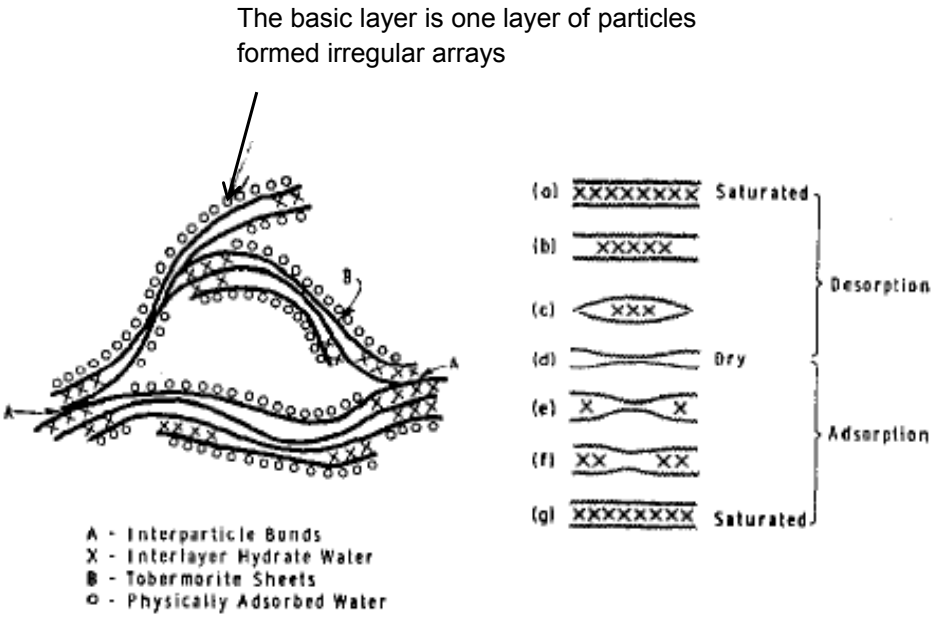

Figure 3.4. Feldman and Sereda's model for the internal layered structure of C-S-H. (Feldman and Sereda 1968)

Taylor (Taylor 1986, Taylor 1997) reported a model for C-S-H at the molecular level. It rationalizes results from thermal gravimetric analysis, density, selected-area electron diffraction, and analysis of composition by analytical electron microscopy. The proposed structure is an intimate mixture of imperfect Jennite and 1.4 nm tobermorite formed into an imperfect array of layers [see Figure 3.5(a)], and the prefix refers to the layer thickness. This structure explains many of the chemical characteristics of C-S-H.

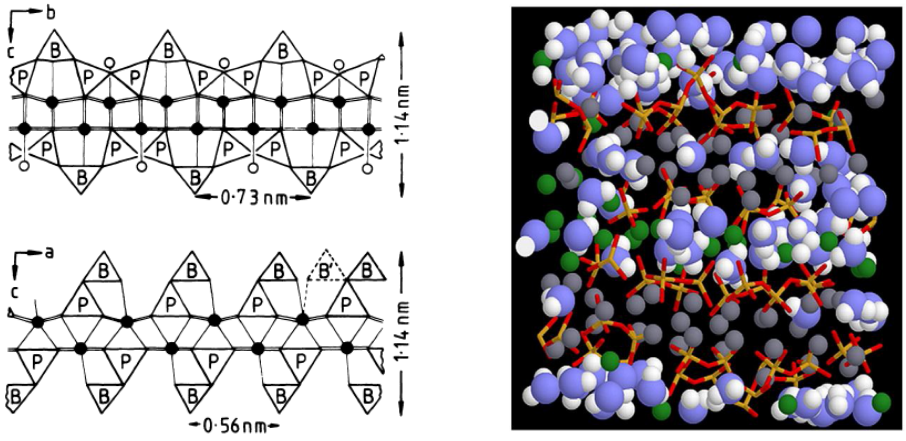

Figure 3.5. (a) Internal structure of 1.4 nm tobermorite for C-S-H (Taylor 1986, 1997); (b) Detailed molecular structure of C-S-H (Pellenq et al. 2009). Yellow and red lines are for Si-O bond, green and gray spheres are calcium, and blue and white spheres are oxygen and hydrogen atoms of water molecules.

One important feature related to the present topic is that when being heated at 55ºC, the 1.4 nm tobermorite loses interlayer water and undergoes unidimensional lattice shrinkage, giving 1.1 nm tobermorite ($C_5S_6H_5$ approximately). Under radiation heating, 55ºC is a temperature frequently reached. Thus the loss of interlayer water may lead to significant shrinkage of cement paste.

Jennings (1986) proposed that the basic element of C-S-H, called "basic building block," be considered to be an 11 nm diam sphere with a specific surface area of 210 m^2/g. The internal structure of the element is layered of the type proposed by the Taylor model. The elements are assembled into one of the three types of structures, each with its own structure of specific porosity. Various material properties can be predicted by varying the proportion of each of the three structures formed in the cement paste, which depend on material parameters such as the ratio of water to cement. The movement of water is reversible, but associated changes in structure are irreversible.

Figure 3.5(b) shows molecular dynamic simulation of C-S-H, including the position and binding of water molecules in the interstitial pores (Pellenq et al. 2009). The model can predict the changes in structure at different calcium contents, the location and binding energy of impurities, and the amount and location of water under various ambient conditions (Jennings and Bullard 2011).

These structural models were proposed to explain experimental results of adsorption isotherms (pore size distribution and surface area), creep, shrinkage, and some transport properties of concrete, such as chemical diffusivity, mainly because those properties are related to the nanostructure of concrete. On the other hand, strength and stiffness of concrete are mainly controlled by microcracks, packing density of solid particles, and the interface bond between cement paste and aggregate, not by the nanostructural features.

Lowinska-Kluge and Piszora (2008) conducted a study on the microstructure of cement paste under various doses of gamma radiation. The microscopic images of the cement paste tested shown in Figure 3.6 indicate that pseudomorphoses had taken place after a dose of 130 MGy and that the microstructure of cement paste was changed significantly by the gamma radiation.

Figure 3.7 shows SEM images of irradiated cement paste with silica fume as an additive. Pseudomorphs were observed at a dose of 290 MGy. With increasing dose, microcracks appeared in the sample. At a dose of 1188 MGy, a completely amorphous cement matrix and microcracking was produced, as shown in Figure 3.7(4). Figure 3.8 shows SEM images of irradiated cement paste with fly ash as an additive. Pseudomorphs appeared at a dose of 290 MGy, which is similar to the results for the cement paste made with a silica fume additive. Bubbles observed in Figure 3.8(3) are the effect of separation of chemically bonded water. With increasing dose of radiation, microcracks appeared, and the paste was completely destroyed at a dose of 1188 MGy, as shown in Figure 3.8(4).

These studies indicate that radiation affects the microstructure of cement paste. The changes in microstructure can impact the effectiveness of the concrete as a shielding material. Additional research is recommended to increase the understanding of the effect of neutron and gamma irradiation on the nanostructure of concrete.

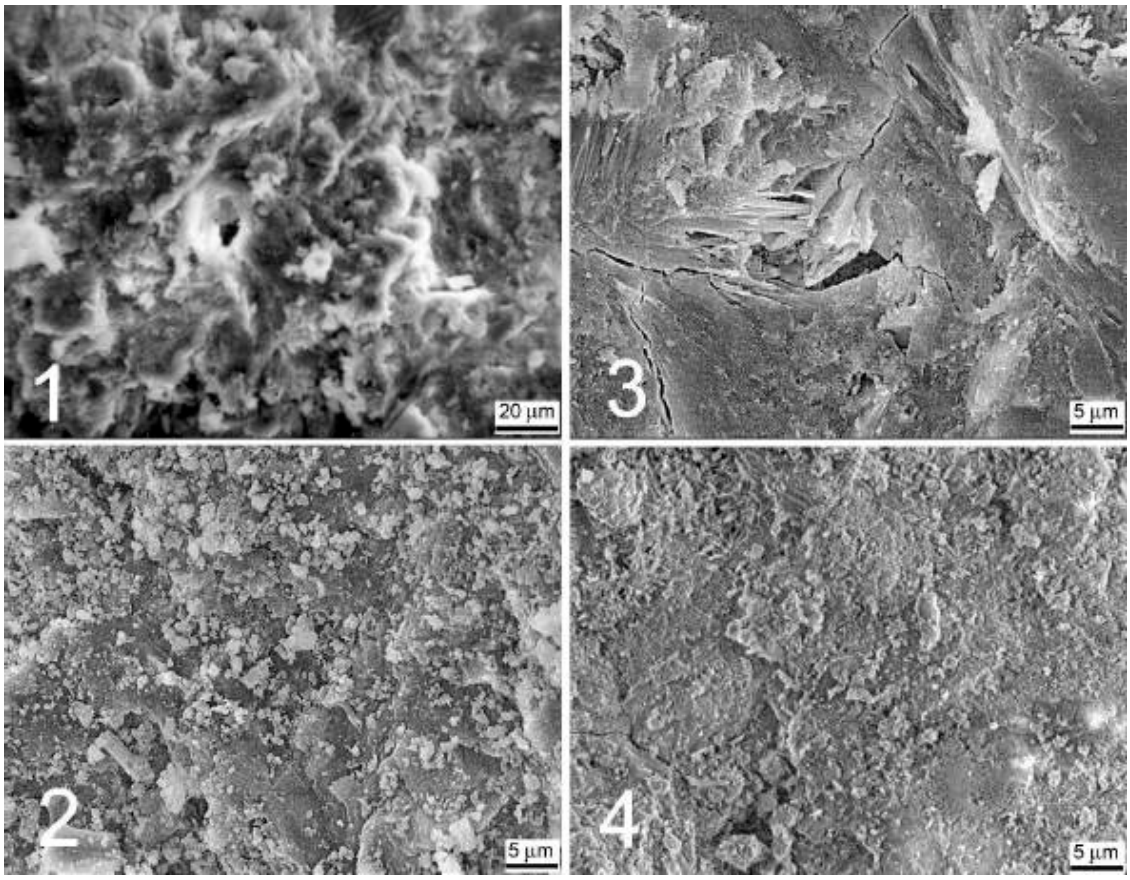

Figure 3.6. SEM images of cement paste irradiated with gamma radiation. (1) 0 MGy, (2) 130 MGy, (3) 290 MGy, and (4) 836 MGy. (Lowinska-Kluge and Piszora 2008). Note the change in scale between (1) and (2), (3), and (4).

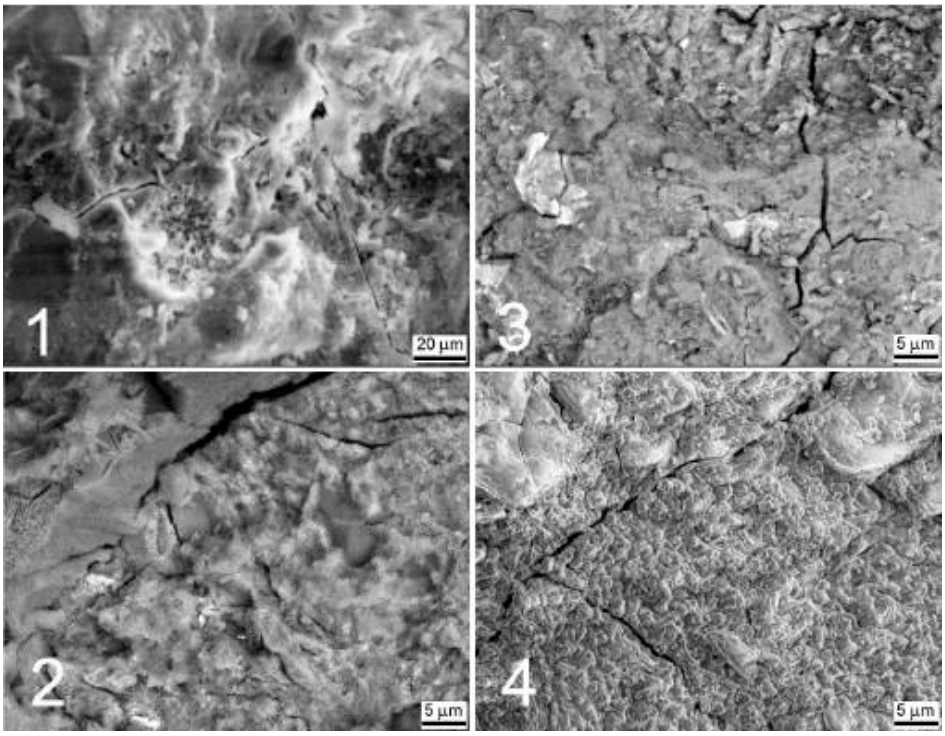

Figure 3.7. SEM images of cement paste that was made with a silica fume additive and irradiated with gamma radiation. (1) 0 MGy, (2) 290 MGy, (3) 466 MGy, and (4) 1188 MGy. (Lowinska-Kluge and Piszora 2008). Note the change in scale between (1) and (2), (3), and (4).

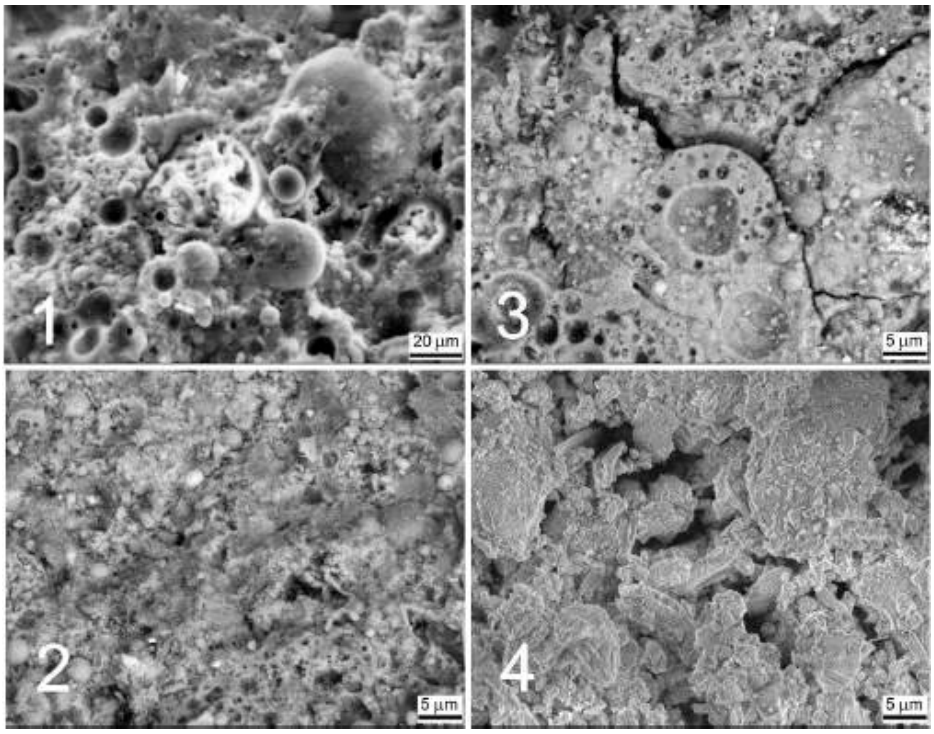

Figure 3.8. SEM images of cement paste that was made with a fly ash additive and irradiated with gamma radiation.
(1) 0 MGy, (2) 290 MGy, (3) 466 MGy, and (4) 1188 MGy. (Lowinska-Kluge and Piszora 2008). Note the change in scale between (1) and (2), (3), and (4).

3.4 RADIATION SHIELDING PROPERTIES OF CONCRETE

Concrete is a composite material with aggregates and a cement paste binder as components. Shielding properties of concrete depend on the shielding properties of its constituents. The linear attenuation coefficient for gamma rays in Eq. (2.1) can be written independently of mass density:

$$I = I_0 e^{-(\mu/\rho)\rho x} = I_0 e^{-(\mu/\rho)d} \tag{3.1}$$

where ρ is the density of the shielding material (g/cm^3) and d is density times distance traveled (g/cm^2). The mass attenuation coefficient, μ/ρ, of a composite material can be written in terms of its components:

$$\mu/\rho = \sum_{i=1}^{N} w_i (\mu/\rho)_i \tag{3.2}$$

where
i is the ith constituent,
N is the total number of constituents,
w_i is the weight fraction of the ith constituent,
$(\mu/\rho)_i$ is the mass attenuation coefficient of the ith constituent.

Another parameter that is related to the linear attenuation coefficient μ, called the half-value thickness, *HVT*, is the depth of shielding where the intensity of the primary photon beam is reduced by 50%. [HVT is different from half-life, which is defined as a time interval during which activity of the radionuclide decreases to one half of the initial value (Hala and Navratil 2003)]:

$$HVT = X_{1/2} = \frac{\ln 2}{\mu} \tag{3.3}$$

Research on the radiation-shielding properties of concrete has been extensive. Table 3.3 lists some of the test data on linear attenuation coefficients (Abdo et al. 2002, Kharita et al. 2008, Yilmaz et al. 2011, Sahin et al. 2011). Theoretical values for the mass attenuation coefficients (μ/ρ) of concretes can also be calculated by analytical models (Schmidt 1969, Bashter 1997) and numerical programs, such as WinXCom (Gerward et al. 2004) and the NXcom (El-Khayatt 2011). One can see from Table 3.3 that the linear attenuation coefficients decrease through an increase in energy and that the concrete mix affects the HVT.

Similarly, the macroscopic removal cross section $\sum_R$ for neutron radiation can also be related to the properties of the constituents:

$$\Sigma_R / \rho = \sum_{i=1}^{N} w_i \left(\Sigma_R / \rho\right)_i \tag{3.4}$$

Because of the interactions between concrete and neutrons during the operation of a nuclear reactor, many elements in shielding concrete become radioactive. The activity of the affected shielding concrete should be measured after decommissioning of the reactor (Alhajali et al. 2009).

Table 3.3. Measured linear attenuation coefficients μ (1/cm) and half-value thicknesses (X1/2 in cm) of 12 concrete mixtures at different energies (Yilmaz et al. 2011)

Concrete	Linear attenuation coefficients μ (cm^{-1}) and HTV (cm)					
	59.5 keV			661 keV		
	$\mu_{Exp.}$	$(\chi_{1/2})_{Exp.}$		$\mu_{Exp.}$	$(\chi_{1/2})_{Exp.}$	
		1st method	2nd method		1st method	2nd method
M0	0.593	1.168±0.110	1.053±0.022	0.175	3.97±0.372	3.174±0.076
MS2.5	0.450	1.540±0.147	1.045±0.024	0.198	3.50±3.343	3.647±0.080
MS5	0.389	1.781±0.178	1.237±0.027	0.202	3.430±0.346	3.678±0.088
MS10	0.383	1.809±0.179	1.301±0.031	0.179	3.871±0.375	3.673±0.095
MF5	0.380	1.823±0.178	1.322±0.033	0.182	3.807±0.350	3.795±0.087
MF10	0.328	2.112±0.215	1.430±0.031	0.171	4.052±0.409	3.749±0.101
MF20	0.296	0.341±0.243	1.573±0.040	0.169	4.100±0.422	4.285±0.102
MF30	0.272	2.547±2.241	1.64±0.045	0.161	4.304±0.421	4.125±0.094
MB5	0.302	2.294±0.222	1.643±0.044	0.157	4.414±0.428	4.293±0.107
MB10	0.298	2.325±0.239	1.613±0.041	0.172	4.029±0.382	4.208±0.088
MB20	0.319	2.172±0.204	1.488±0.034	0.173	4.005±0.408	3.250±0.084
MB30	0.275	2.520±0.252	1.593±0.039	0.171	4.052±0.393	3.611±0.090

Several studies were conducted to calculate the shielding capacity of concrete slabs made of different aggregates. Tables were prepared for nuclear engineering applications. The tables give the dose equivalent per unit incident fluence as a function of the mass thickness of the concrete slabs (Wyckoff and Chilton 1973, Shultis and Faw 2000).

3.5 THE STATES OF WATER IN CONCRETE AND THE FUNCTION OF WATER FOR RADIATION SHIELDING

The water content in cement paste is important to the effect of radiation on the properties of concrete. States of water in cement paste can be divided into free water, adsorbed water, and chemically combined water. Free water is water available to react with the cement and is found in air voids and capillary pores. Free water can evaporate with its rate dependent on the relative humidity, temperature, and airflow over the concrete surface. When represented by adsorption isotherms, free water is also called capillary water, as shown in Figure 3.9. Adsorbed water consists of water molecules that are physically adsorbed onto the surface of solids in the hydrated cement paste (e.g., gel pores and interlayer space). The gel water is lost at relatively low relative humidity levels (e.g., 30%) and causes shrinkage of cement paste whereas water associated with the interlayers (see Figure 3.3 and Figure 3.4) is evaporable only under high vacuum. They are shown as gel water in Figure 3.9.

Chemically combined water is the water reacted with Portland cement to form CH, C-S-H, and ettringite. This type of water, shown as “nonevaporable water” in Figure 3.9, is not evaporable in dry air and or under high vacuum (i.e., it is unaffected by relative humidity). It can be released at high temperature, which is called dehydration.

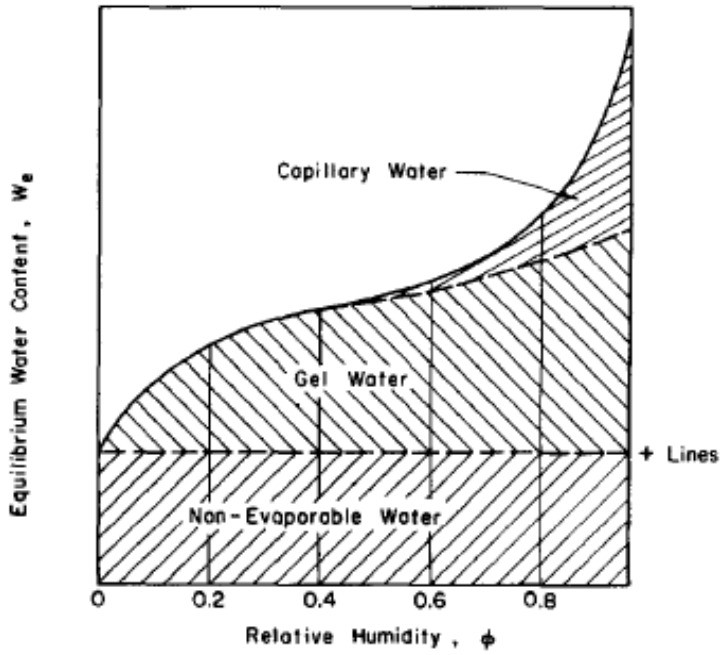

Figure 3.9. Relationship between equilibrium water content of hardened cement paste and relative vapor pressure. (Hilsdorf 1967)

The change of water content in concrete is important for radiation shielding because the loss of adsorbed water and interlayer water, by change of temperature and/or relative humidity, is one of the causes for drying shrinkage, which can result in shrinkage cracking. The loss of adsorbed water by a change of loading is one of the causes for creep; the loss of chemically combined water through dehydration reduces both the strength and stiffness of concrete.

The energy transfer during the collision of a neutron and a nucleus is proportional to the mass of the neutron and the mass of the nucleus. If the mass of the nucleus is similar to the mass of the neutron, larger energy transfer will occur. Therefore, elements with nuclei that have a mass closer to the neutron mass will attenuate the neutron radiation more effectively. Hydrogen and oxygen have nucleus masses that are similar to neutron mass and are therefore desirable in terms of neutron radiation shielding. Hydrogen and oxygen are the elements found in water, so a greater proportion of water in the concrete mixture will improve its ability to shield neutron radiation. Specifically, the mass of a neutron is 1.008 u whereas the mass of a hydrogen nucleus consisting of one proton is 1.007 u (where u is the atomic mass unit, u = 1.66×10^{-27} kg) (Kaplan 1989). The mass of one Oxygen-16 atom is 15.995 u.

Most of the hydrogen in concrete comes from water. To be conservative, it was assumed that only the chemically bound water is considered to remain in the concrete. The total amount of chemically bound water can be estimated by

$$W_b = 0.24\, m\, C \tag{3.5}$$

where W_b is the weight of bound water, C is the total weight of cement, and m is a maturity factor. The maturity factor is determined by the conditions (temperature and relative humidity) under which the concrete was cured. If the conditions are reasonable, the maturity factor is 0.8 (ANSI/ANS 2006a). If the conditions are less than optimal, a lower maturity factor is used. Hilsdorf (1967) developed a model to calculate the water content in hardened concrete made from Portland cement cured at different levels of relative humidity.

The description above implies that more water in cured concrete can provide better radiation shielding. In order to find out whether this is true, Kharita et al. (2010) conducted a systematic experimental study on 75 concrete samples with various water/cement ratios (w/c), by weight, and found that w/c has no significant effect on shielding properties of concrete under room-temperature conditions. The test data are shown in Figure 3.10. However, using w/c as an experimental parameter resulted in other major changes in the concretes. The concrete strength was reduced by increasing w/c, as shown in Figure 3.11. Therefore, the effect of water in concrete on radiation shielding properties is actually quite complicated. On one hand, increase in w/c reduces the strength of concrete because the porosity of concrete increases. As a result, the shielding properties of concrete with high w/c should have decreased. On the other hand, the increased amount of water helped to improve the shielding properties. The combined effect of the two opposing trends may result in the insignificant variation of shielding properties of concrete over a large range of w/c. Thus the actual water content of the concrete, not the w/c, will be a better experimental parameter for future studies of the effect of water on radiation shielding properties of concrete.

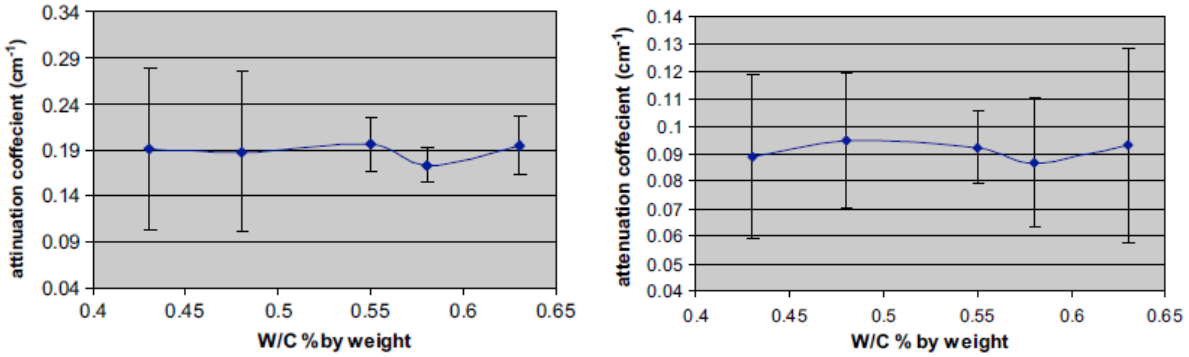

Figure 3.10. Changes in the linear attenuation coefficients of concrete versus the changes in w/c (a) for a broad beam of gamma radiation from a Cs-137 source and (b) for a broad beam of neutron radiation from an Am–Be source. (Kharita et al. 2010)

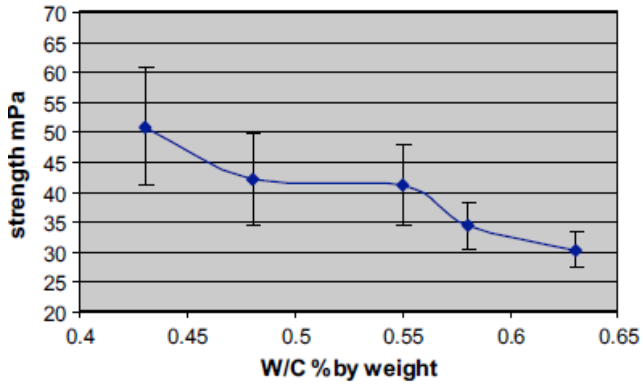

Figure 3.11. Changes in strength of concrete versus the changes in w/c.
(Kharita et al. 2010)

3.6 THE EFFECT OF POLYMER FIBERS

It is well known that fibers can improve mechanical properties of concrete, including compressive and tensile strength and post-peak ductility, but very few studies have investigated the effect of nuclear radiation on fiber-reinforced concrete. A recent experimental study by Martinez-Barrera et al. (2011) showed indirectly the effect of gamma radiation on the mechanical properties of concrete reinforced with polypropylene (PP) fiber. The concrete specimens were exposed to different gamma radiation doses (5, 10, 50, 100, and 150 kGy) in air at room temperature with a dose rate of 3.5 kGy/h. Then, strength and stiffness tests were performed on the irradiated concrete samples.

As shown in Figure 3.12(a) and (b), gamma irradiation can impact the compressive strength and the compressive modulus of PP-fiber-reinforced concrete. Depending on the gamma dose,

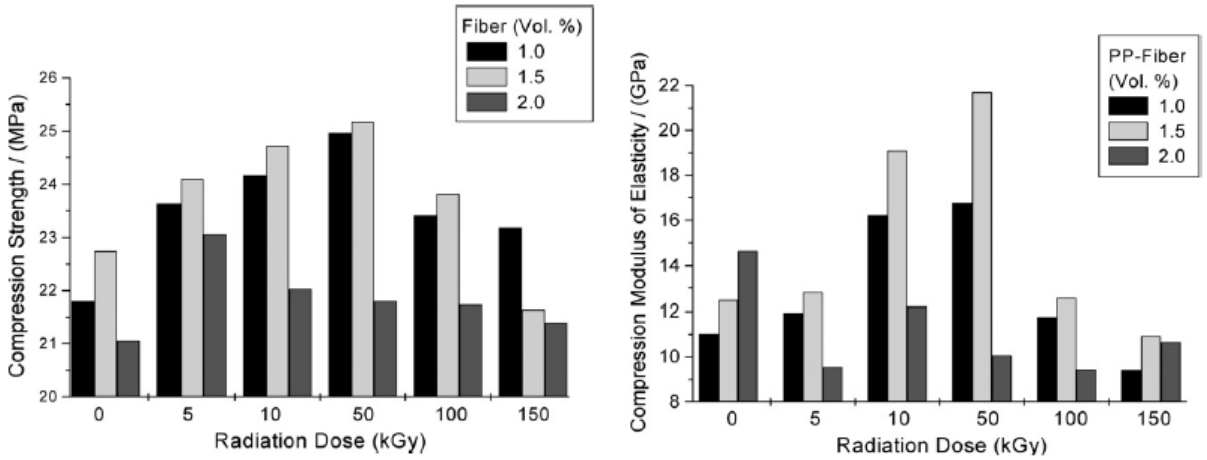

(a) **(b)**

Figure 3.12. (a) Compressive strength data with various radiation doses and (b) modulus of elasticity test data with various radiation doses. (Martinez-Barrera et al. 2011.)

gamma radiation can increase or decrease mechanical properties of concrete that has been reinforced with polymer fibers. Based on the above test data, the mechanical properties of PP-fiber-reinforced concrete with fiber contents of $\leq$ 1.5%, by volume, improve with increasing fiber content and increasing dose up to 50 kGy. The improvement is considered to be due to the ionizing energy generating more surface contacts between the fibers and the hydrated cement phase. However, at higher doses (100 and 150 kGy), the mechanical properties are decreased.

3.7 DESIGN OF CONCRETE RADIATION SHIELDING

Design of concrete radiation shielding for NPP structures (e.g., nuclear reactors, hot cells, radiochemical plants, nuclear fuel fabrication facilities) is an involved process. Basic design procedures have been noted to involve several basic steps (Kaplan 1989):

1. Determine the type and intensity of the radiation source to be shielded. This type of information is normally provided by the designers or users of the nuclear installation for which the shielding is required.

2. Decide the maximum level of radiation that can be permitted at the external surface of the shield. This is generally based on recommendations of the regulatory authority (e.g., the International Commission on Radiological Protection).

3. Determine the required attenuation or reduction factor resulting from (1) and (2).

4. Consider the potential choices and proportioning of materials that could be used in the concrete mix to achieve the desired results.

5. Determine the nuclear shielding properties of various concretes under consideration (e.g., estimate the thickness required to achieve the required photon and neutron attenuation).

6. Determine the temperature distribution in the concrete shield so that thermal stresses may be calculated to establish whether they are within acceptable limits.

7. Decide, based on the above, the type of concrete that would be most suitable for the shield and develop a detailed design.

A more-detailed discussion related to each of these basic steps is provided in the source reference (Kaplan 1989). Additional information on concrete radiation shields for NPPs related to specifications, analysis, design, and testing is available (e.g., ANSI/ANS 1987, 1999, 2006a, 2006b; Jaeger 1968, 1975; Shultis and Faw 2000; USNRC 2009).

4. HEAT OF RADIATION AND THE THERMAL STRESS DUE TO RADIATION

Irradiation of concrete by neutron and gamma radiation can lead to an increase in temperature of up 250°C (Fillmore 2004). Such a large increase in temperature can have significant impacts on the mechanical and radiation-shielding properties of concrete. Granata and Montagnint (1972) and Acevedo and Serrato (2010) reported that concrete samples were heavily damaged when heated to 280°C (a temperature commonly reached in heavy-water reactors) and at a fluence of 10^{20} n/cm^2.

In general, high temperature causes two forms of damage in concrete. One is the deterioration in mechanical properties of concrete, such as physico-chemical changes of the cement paste and aggregate (so-called phase transformations), and thermal incompatibility between the aggregate and the cement paste. The other one is spalling of concrete. Spalling can result in severe reduction of cross-sectional area, leading to the exposure of the interior concrete to excessive temperatures, which in turn causes further spalling damage, called progressive spalling damage. There are several theories explaining the spalling mechanisms of concrete under high temperature, which will not be discussed here (See Willam et al., 2009). Experimental results have shown that spalling damage occurs under a high heating rate in the temperature range of 200°C to 350°C. In some of the tunnel fires in Europe, the heating rate reached 100°C/min to 200°C/min, and the maximum temperature could have reached above 1000°C in a few minutes (CEMENBUREAU, 2004). Spalling of concrete typically occurs near the concrete surface, but may occur at depths up to 50% its cross section thickness. Concrete spalling is not expected to occur as a result of heat generated by radiation.

The heat of radiation affects properties of concrete at two levels: the structural level and the microstructural level. At the structural level, the thermal gradient due to the heat of radiation results in thermal stress, which may be high enough to create damage in concrete. At the microstructural level, the mismatch of thermal strains in cement paste and in aggregate responding to the heat of radiation may cause a large stress at the interface between the aggregate and cement paste, which may cause microcracking in the cement paste.

4.1 HEAT GENERATED BY GAMMA AND NEUTRON IRRADIATION

Radiation energy is converted to heat when absorbed by a shield. The heat generated by irradiation can reach quite high temperatures, depending on the shielding material used and the configuration of the shielding structure. Hilsdorf et al. (1978) noted a temperature as high as 250°C was developed in some of the investigations he summarized, which is high enough to generate considerable damage in shielding materials. Therefore, the heat generated by gamma and neutron radiation is very important in that it can impact the functional and performance requirements of the shield.

In the case of photon radiation, kinetic energy is transferred from the photons to electrons in the shielding material. This energy is then transformed to heat. Equation (4.1) can be used to calculate the heat generated by photons:

$$H(r) = c\int E_P \,\mu_P(E_P, r)\Phi(E_P, r)dE_P \tag{4.1}$$

where

H(r) is the rate of heat generation at spatial position *r* in W cm^{-3},

E_P is photon energy in MeV, r is the position coordinate in cm,
$\mu_p(E_P, r)$ is the energy deposition coefficient for energy deposition in cm^{-1},
$\Phi(E_P, r)$ is the photon flux spectrum at energy E_P in photons cm^{-2} s^{-1} MeV^{-1},
c is the conversion factor, $c = 1.6 \times 10^{-13}$ W s MeV^{-1}.

At a given point in space, Eq. (4.1) is an integration over the entire photon energy spectrum. For gamma irradiation, Eq. (4.2) can be used to calculate the approximate volumetric heating rate due to gamma photons at any point x:

$$H_\gamma(x) \cong 1.6 \times 10^{-13} E_\gamma \, \mu_\gamma \, \Phi_\gamma(E_\gamma) \tag{4.2}$$

where
$H_\gamma(x)$ is the heating rate at point x in W cm^{-3},
x is the coordinate or depth in a shielding material in cm,
E_γ is the gamma ray energy in MeV,
μ_γ is the linear energy-absorption coefficient for gamma rays of energy E_γ in cm^{-1},
Φ_γ is the gamma ray flux density at energy E_γ in photons cm^{-2} s^{-1},
E_γ is the gamma ray energy in MeV.

Unlike Eq. (4.1), no integration is involved in Eq. (4.2). Equation (4.2) can be further simplified

$$H_\gamma \cong 1.6 \times 10^{-13} E_{ave} \, \Phi_{\gamma in} \tag{4.3}$$

where
H_γ is the heating rate per unit area (W cm^{-2}),
E_{ave} is the average energy of the photons in MeV,
$\Phi_{\gamma in}$ is the incident photon flux density in photons cm^{-3} s^{-1}.

In the case of neutron irradiation, the heat generated by the process can be divided into direct and indirect heat. For elastic scattering, no gamma ray is generated, and the heat generated by the interaction of neutrons and nuclei is deposited at the site of interaction. For inelastic scattering, the heat generated by the interaction is deposited on site (direct heat), but the gamma rays produced by the interaction deposit their energies at various distances from the site of reaction (indirect heat). The approximate volumetric heating rate at a point x due to neutrons may be conservatively estimated by

$$H_N(x) \cong 1.6 \times 10^{-13} \Sigma_c(E_N) \Phi_N(x) E_B \tag{4.4}$$

where
H_N is the approximate volumetric heating rate at point x in W cm^{-3},
$\Sigma_c(E_N)$ is the macroscopic capture cross section for neutrons of energy E_N in cm^{-1},
$\Phi_N(x)$ is the neutron flux density at a point x in neutrons cm^{-2} s^{-1},
E_B is the binding energy for capture reaction in MeV.

Equation (4.4) can be simplified to provide an estimate of the approximate heating per unit area for neutrons:

$$H_N \cong 1.6 \times 10^{-13} E_{KB} \, \Phi_{Nin} \tag{4.5}$$

where
H_N is the approximate heating per unit area for neutrons in W cm^{-2},

E_{KB} is the sum of average kinetic energy associated with a neutron and the average binding energy associated with neutron capture in MeV,
Φ_{Nin} is the incident neutron flux density in neutrons $cm^{-2}\ s^{-1}$.

Abdo and Amin (2001) conducted an experimental study to compare the estimations by above equations to measured data. Figure 4.1(a) is a comparison of the measured and calculated heat generated in concrete due to total thermal neutrons, in which the calculation was based on an equation similar to Eq. (4.4) (Yevick 1966; Jaeger 1968; ANSI/ANS 2006a). The basic trend is that both total thermal neutron flux and heat generation are linear functions of the shielding depth. The heat generation due to capture of total thermal neutrons, which can reach about 6.6 × 10^{-3} mW cm^{-3} at a thickness of 50 cm, generates a temperature rise of 1.7°C.

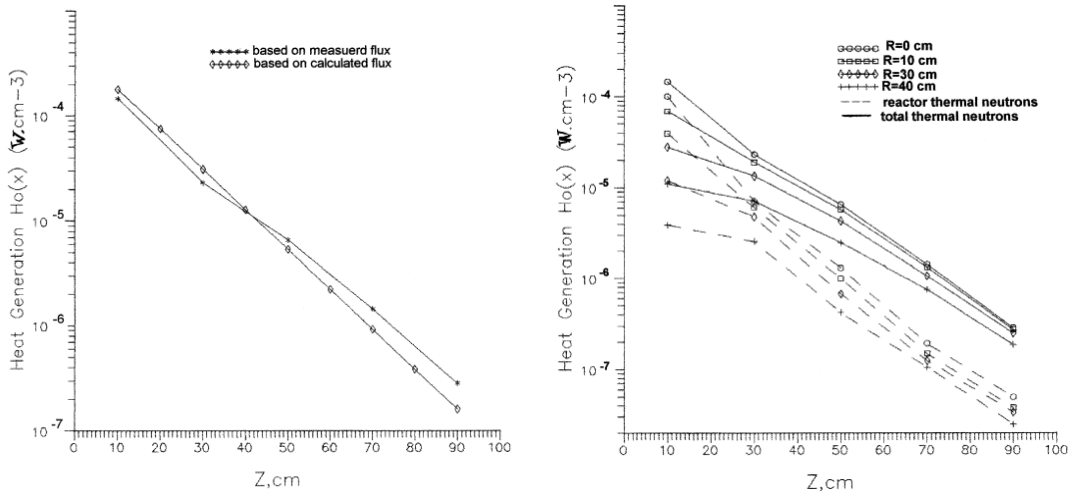

(a) **(b)**

Figure 4.1. Measured and calculated (a) heat generation due to the total thermal neutrons and (b) the calculated heat generation due to total thermal and reactor thermal neutrons in ordinary concrete (Abdo and Amin 2001).

Figure 4.1(b) shows the heat generation due to both the total thermal neutrons and the reactor thermal neutrons along the beam direction (Z-direction) and normal to it (R-direction). The figure shows a marked depression in the heat generation due to the reactor thermal neutrons in both Z- and R-directions as compared with that due to the total thermal neutrons. This depression in the heat generation reaches about 30% at a shield thickness of 10 cm in both Z- and R-directions. The depression in the heat generation reaches about 60% at 40 and 10 cm in the R- and Z-directions, respectively. The results show that the heat generation due to total thermal neutrons provides the main contribution to the heat generation, especially in the first layers of the shield compared with reactor thermal neutrons. However, at deep penetrations the contribution of the total thermal neutrons to the heat generation is comparatively small (Abdo and Amin 2001).

4.2 TEMPERATURE VARIATION DUE TO THE HEAT OF RADIATION

After the heat generated by the irradiation is determined, the temperature field in a shielding structure can be evaluated by considering the heat of radiation as a heat source in a thermal

analysis for the shielding structure. Because the irradiation effect is a long-term effect and shielding structures are usually very large (such as a thick wall of a biological shield), a one-dimensional steady-state thermal conduction equation with a heat source can be used for evaluating temperature distribution due to irradiation by gamma rays. For example,

$$k\frac{\partial^2 T}{\partial x^2} = -E_P I_0\, e^{-x/\lambda} \tag{4.6}$$

where

T is temperature distribution in °C,
k is the thermal conductivity of concrete in W cm^{-1} $°C^{-1}$,
x is the depth into the shielding structure in cm,
I_0 and E_P have the same meaning as in Eq. (2.1) and Eq. (4.1),
λ is the relaxation length in cm, and is equal to

$$\lambda = \frac{1}{\mu} \text{ for gamma radiation or } \lambda = \frac{1}{\Sigma_R} \text{ for neutron radiation} \tag{4.7}$$

where

μ is defined in Eq. (2.1)
Σ_R is defined in Eq. (2.2).

The right-hand side of Eq. (4.6) is the heat source due to the heat produced by photon radiation. A solution of temperature distribution can be obtained by integrating Eq. (4.6) twice:

$$T(x) = -\frac{\lambda^2 E_P I_0}{k} e^{-x/\lambda} + Cx + D \tag{4.8}$$

where *C* and *D* are two integration constants which can be determined based on boundary conditions of the shield structure such as the inner and outer surface temperatures of a concrete wall of a biological shield. For radiation attenuation purposes, the thickness of a shield structure is usually much larger than the relaxation length λ. When the radiation is applied only on one side of the structure (at $x = 0$), the temperature cannot vary linearly with the depth because the temperature rise due to the radiation in the deep part of the shield must be zero, and thus *C* must be 0 in Eq. (4.8), and Eq. (4.8) becomes

$$T(x) = -\frac{\lambda^2 E_P I_0}{k} e^{-x/\lambda} + D \tag{4.9}$$

Using the boundary condition at the surface $x = 0$, $T(0) = 0$ (no temperature rise on the surface of the shielding structure due to the radiation), we have $D = \lambda^2 E_P I_0/k$, and then

$$T(x) = \frac{\lambda^2 E_P I_0}{k}\left(1 - e^{-x/\lambda}\right) \tag{4.10}$$

Because of the boundary condition used in Eq. (4.9), $T(0) = 0$, $T(x)$ in Eq. (4.10) should be the temperature rise due to radiation, $\Delta T(x)$:

$$\Delta T(x) = \frac{\lambda^2 E_P I_0}{k}\left(1 - e^{-x/\lambda}\right) \tag{4.11}$$

The thermal stress in the shielding structure depends on the temperature gradient and, in absence of kinematic restraints, it does not depend on uniform temperature rise in the material. The temperature gradient can be obtained by taking a derivative of Eq. (4.10) with respect to *x:*

$$\frac{dT}{dx} = \frac{\lambda E_P I_0}{k} e^{-x/\lambda} \tag{4.12}$$

It is obvious that at the surface x = 0, the temperature gradient reaches the maximum, which means that the thermal stress due to the radiation reaches the maximum on the surface of the shielding structure.

Abdo and Amin (2001) conducted an experimental study to compare the temperature estimates with the measured temperature data. Figure 4.2 shows a comparison of the measured and calculated temperature rise generated by gamma rays, in which the temperature calculation was based on Eq. (4.11) (Yevick 1966, Jaeger 1975, Kaplan 1989). Figure 4.2 shows the temperature rise in ordinary concrete because of gamma rays due to capture of the total thermal neutrons (measured and calculated) and that due to reactor thermal neutrons. The figure shows that the temperature rise has its maximum values in the first layer of the shield thickness and that it decreases rapidly at deep depths in the shield. The figure shows also that the maximum evaluated temperature rise is about 1.7 ºC, which has no effect on dehydration of the concrete.

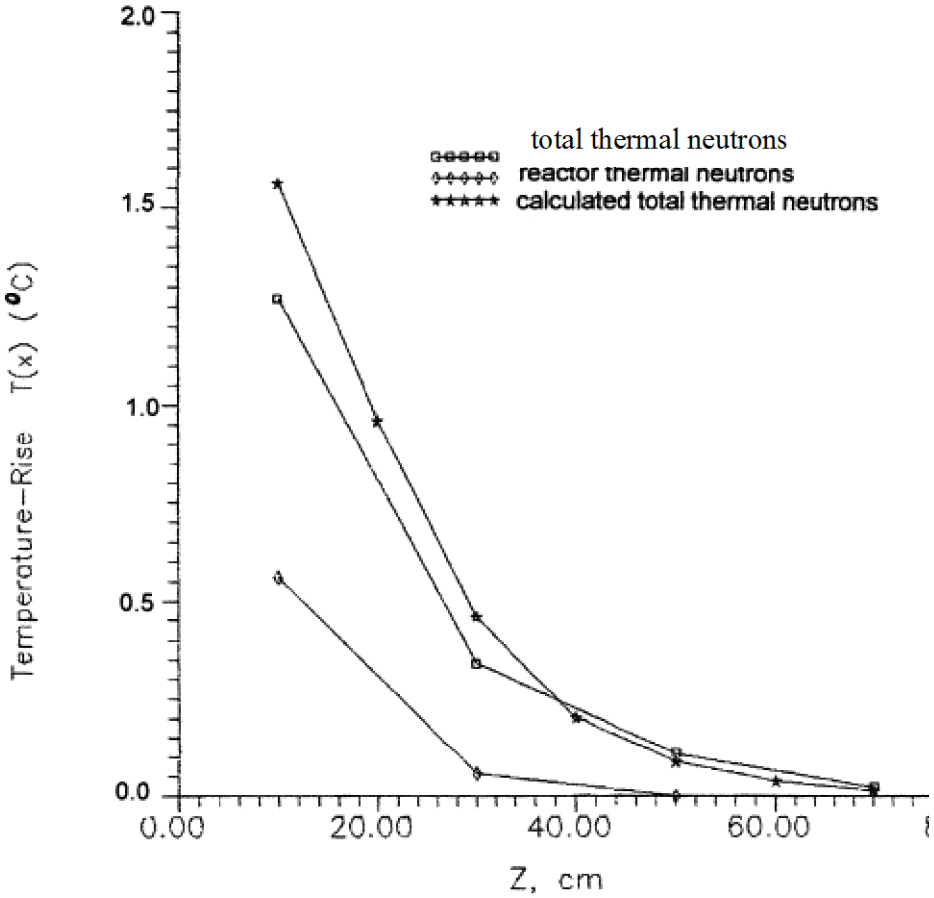

Figure 4.2. Temperature rise in ordinary concrete because of gamma rays due to capture of thermal neutrons (Abdo and Amin 2001).

4.3 MACROSCOPIC THERMAL STRESS IN SHIELDING STRUCTURES DUE TO RADIATION

Thermal stresses occur in a shielding material due to the heat of radiation at two different scale levels. One, which is due to the temperature gradient as noted in Eq. (4.12),may be called macroscopic thermal stress.. The other one, which is due to the differential thermal expansions of the constituent phases in the shielding material that occur even under a uniform heating of radiation, may be called microscopic thermal stress. The macroscopic thermal stress due to the gamma and neutron irradiation is discussed in this section. Microscopic thermal stress is discussed in the Section 4.4.

With the thermal gradient of Eq. (4.11) and given properties of a shielding wall such as coefficient of thermal expansion, modulus of elasticity, and Poisson's ratio, thermal stress in a shielding structure can be evaluated. For example, the thermal stress in a large shielding wall subjected to irradiation on one side of the wall can be calculated as follows (Kaplan 1989):

$$\sigma(x) = \sigma_{ave} + \frac{\alpha E \Delta T}{1-\nu} \tag{4.13}$$

where

σ_{ave} is the average stress due to radiation heating,
α is the linear coefficient of thermal expansion of the shielding material,
E is the modulus of elasticity of the shielding material,
ν is Poisson's ratio of the shielding material,
ΔT is the temperature rise at point x given by Eq. (4.11).

The average stress is given by

$$\sigma_{ave} = \sigma_0 - \frac{\alpha E E_P I_0 \lambda^2}{k(1-\nu)}\left[1 - 2\frac{\lambda}{L} - \left(1 - 2\frac{\lambda}{L}\right)e^{-L/\lambda}\right] \tag{4.14}$$

where σ_0 is the stress before radiation heating, L is the thickness of shielding wall in cm, and other parameters having the same meaning as noted previously. Compressive and tensile stresses are indicated by positive and negative values, respectively.

The thermal stress calculated this way is the thermal stress induced by the heat of radiation. The effect of irradiation on transport and mechanical properties of shielding materials must also be considered. For example, gamma and neutron radiation can have an impact on the thermal conductivity, coefficient of thermal expansion, modulus of elasticity, and Poisson's ratio. These effects will be discussed in the following chapters.

4.4 MICROSCOPIC THERMAL STRESS IN CONCRETE DUE TO RADIATION

When exposed to neutron irradiation, concrete increases in volume, with the increase mainly due to a change in volume of the aggregate in the concrete (Kontani et al. 2010). When subjected to fast neutron irradiation, the lattice structure of the minerals in aggregates is disturbed, leading to an increase in volume. The crystalline lattice structure present in the aggregates is much more affected by neutrons than the more-amorphous lattice structure of the cement paste. On the other hand, the volume of cement paste decreases, exhibiting shrinkage that is due to the evaporation of pore water under the heat of radiation and due to the phase change of water under irradiation. The mismatch of expansion in aggregate and shrinkage of

cement paste may cause damage in the interface between the two phases. A method to deal with this type of damage development is described in this section; the studies on the expansion and shrinkage mechanisms resulting from irradiation will be described in Chapter 5.

Microscopic thermal stress analysis is more complicated than macroscopic thermal stress analysis. The damage development depends on both the size and shape of the aggregates. An assumption of spherical aggregate shape is made to simplify the problem. For the effect of aggregate size, two different situations may be considered. The first is to consider a special situation in which all aggregates are of the same size. Based on the result of this special situation, the second situation is to consider a general case in which there is a continuous distribution of particle sizes. Only the model for the first situation is briefly described in this report. This model was originally developed to simulate the expansion of ice formed in spherical pores and the damage development near the pores (Eskandari-Ghadi et al. 2013). The model can be used for the damage development in the interface of aggregate and cement paste under the heat of radiation.

To evaluate the onset of the damage and the effect of damage due to aggregate expansion on the properties of concrete under irradiation, concrete is considered as a two phase material with cement paste as matrix and many spherical particles of size r_s (the radius of spheres) as inclusions. Figure 4.3 is a sketch for a concrete with many different sizes of aggregates. This sketch can also be used for concrete with the same size of aggregate, in which all inclusions are spheres of the same radius.

Taking any one element out of the concrete will yield Figure 4.4, in which Phase 1 is the aggregate, Phase 2 is the damaged cement paste near the aggregate, Phase 3 is the original cement paste, and Phase 4 is the effective porous medium (i.e., concrete). Because of the volumetric increase of the aggregate due to the heat of radiation and the expansion of lattice structure, there is a pressure *p* generated by the aggregate on the surrounding cement paste, as shown in Figure 4.5. The pressure results in a tensile stress in the surrounding cement paste, which may cause damage in the cement paste in the vicinity of the aggregate.

In the case of a spherical aggregate, the distribution of stresses in the cement paste matrix is determined as follows (Timoshenko and Goodier 1970):

$$\sigma_R = -p\frac{r_s^3}{R^3},\ \sigma_\theta = \sigma_\phi = p\frac{r_s^3}{2R^3} \quad \text{(other stresses are zeros)} \tag{4.15}$$

where σ_R is the radial stress, and σ_θ and σ_φ are the two tangential stresses at any point in the concrete due to the pressure *p* on the surface of the spheres. *R* in Eq. 4.15 and Figure 4.5 is the radial coordinate in spherical coordinate system when the center of the aggregate is the origin of the coordinate system, σ_R is a compressive stress, and σ_θ and σ_φ are tensile stresses. The tensile stresses are equal to *p/2* at $R = r_s$, and they decrease with the cube of the distance from the center of the sphere.

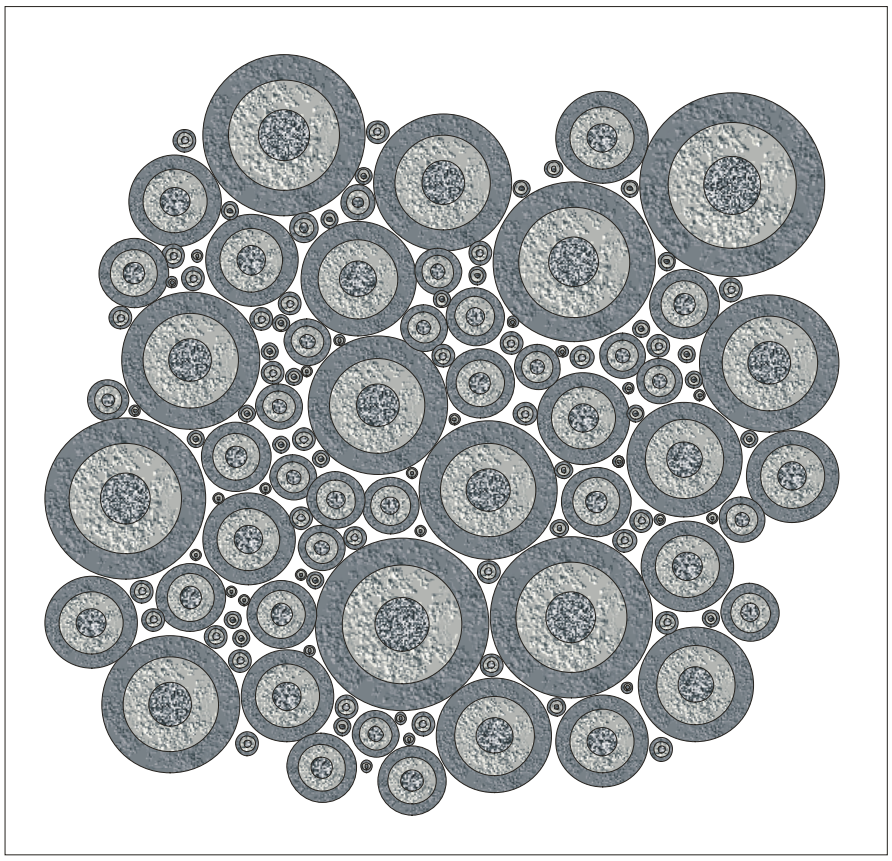

Figure 4.3. A model for concrete with aggregates of different sizes for analyzing the microscopic stress at the aggregate–cement paste interface due to the heat of radiation (the internal structure of each aggregate element is explained in Figure 4.4).

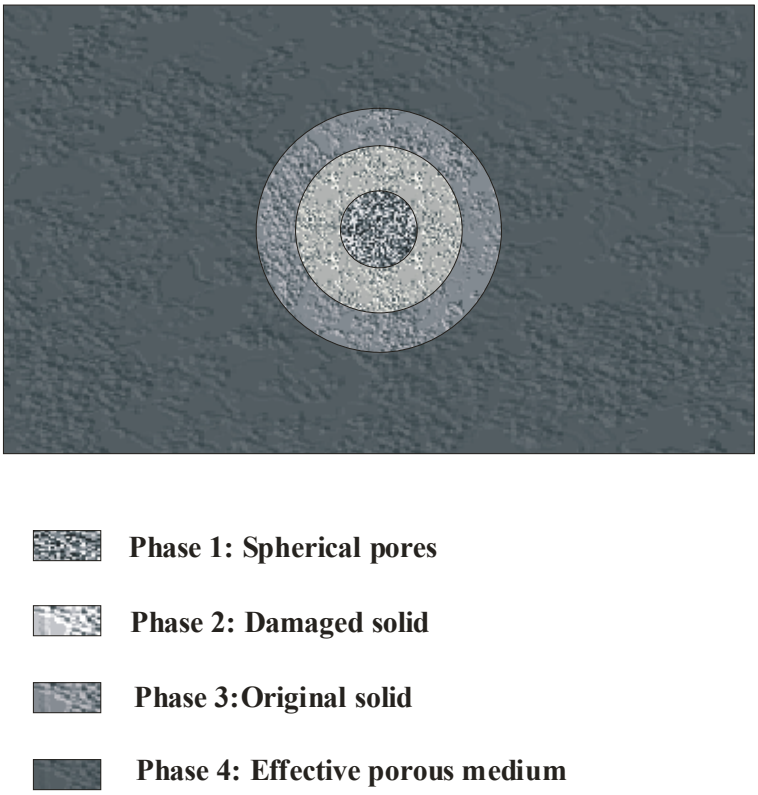

Figure 4.4. The four phases in each element in Figure 4.3.

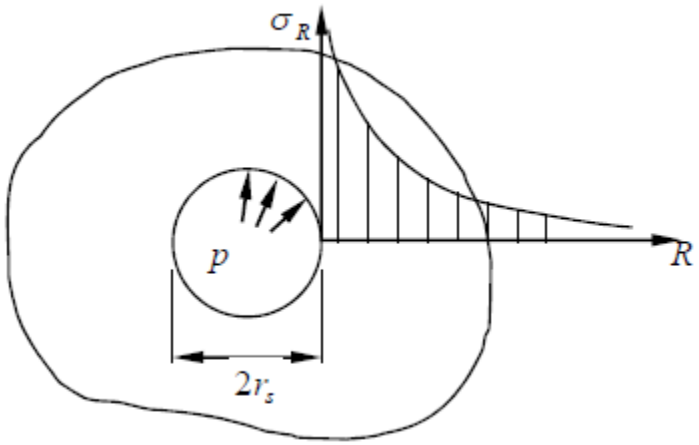

Figure 4.5. The interface pressure *p* induced by the expansion of aggregate under radiation.

Drucker-Prager (DP) plasticity may be applied to the cement paste in concrete when the damage generated by the interface pressure due to the heat of radiation is being considered. DP plasticity is used here to facilitate the discussion, although any other constitutive theory suitable for the material under consideration could be applied. With DP plasticity, the following equation can be obtained to evaluate plastic behavior of the concrete:

$$\alpha I_1 + \sqrt{J_2} = k,\ \alpha = \sqrt{\frac{2}{3}}\frac{f_c - f_t}{f_c + f_t},\ \text{and}\ k = \sqrt{\frac{2}{3}}\frac{2 f_c f_t}{f_c + f_t} \tag{4.16}$$

where

I_1 is the first invariant of stress tensor,
J_2 is the second invariant of the deviatoric stress tensor,
f_c is the compressive strength of the material,
f_t is the tensile strength of the material.

For the stress components given by Eq. (4.16), I_1 is zero and $\sqrt{J_2} = p r_s^3 \sqrt{3} / (R^3 \sqrt{2})$. The maximum value of $\sqrt{J_2}$ is $p\sqrt{3/2}$ at $R = r_s$. Thus if p equals $4 f_c f_t / [3(f_c + f_t)]$, then there will be damage due to plastic behavior at $R = r_s$. If p is larger than $4 f_c f_t / [3(f_c + f_t)]$, then the damaged part will start to grow in the radial direction. Assuming a slow variation of pressure with respect to time, which is true for most of the radiation processes, the damage growth is usually a small value with respect to the radius of aggregate and it can be evaluated in terms of the change of pressure (Eskandari-Ghadi et al. 2013).

The pressure increase is related to the volume expansion of aggregates, which depends on the radiation intensity and the duration of concrete irradiation. The pressure increase is also related to the shrinkage of cement paste due to a loss of water. Both the expansion of aggregate and the shrinkage of cement paste will be discussed in Section 4.5.

4.5 THERMAL EXPANSION AND THERMAL CONDUCTIVITY

Hilsdorf et al. (1978) summarized several experimental studies and concluded that for a neutron fluence up to 5×10^{19} n/cm^2 there is no significant difference between the coefficient of thermal expansion of temperature-exposed samples and that of neutron-irradiated samples. These test data imply that the neutron radiation does not generate extra expansion above the thermal expansion. Dubrovskii et al. (1966) conducted a test on the expansion of heat-resistant concrete with chromite filler as aggregate under a high level of neutron irradiation. The neutron fluence was 2.0 to 2.4×10^{21} n/cm^2, and temperatures were up to 550ºC. Their results are shown in Figure 4.6.

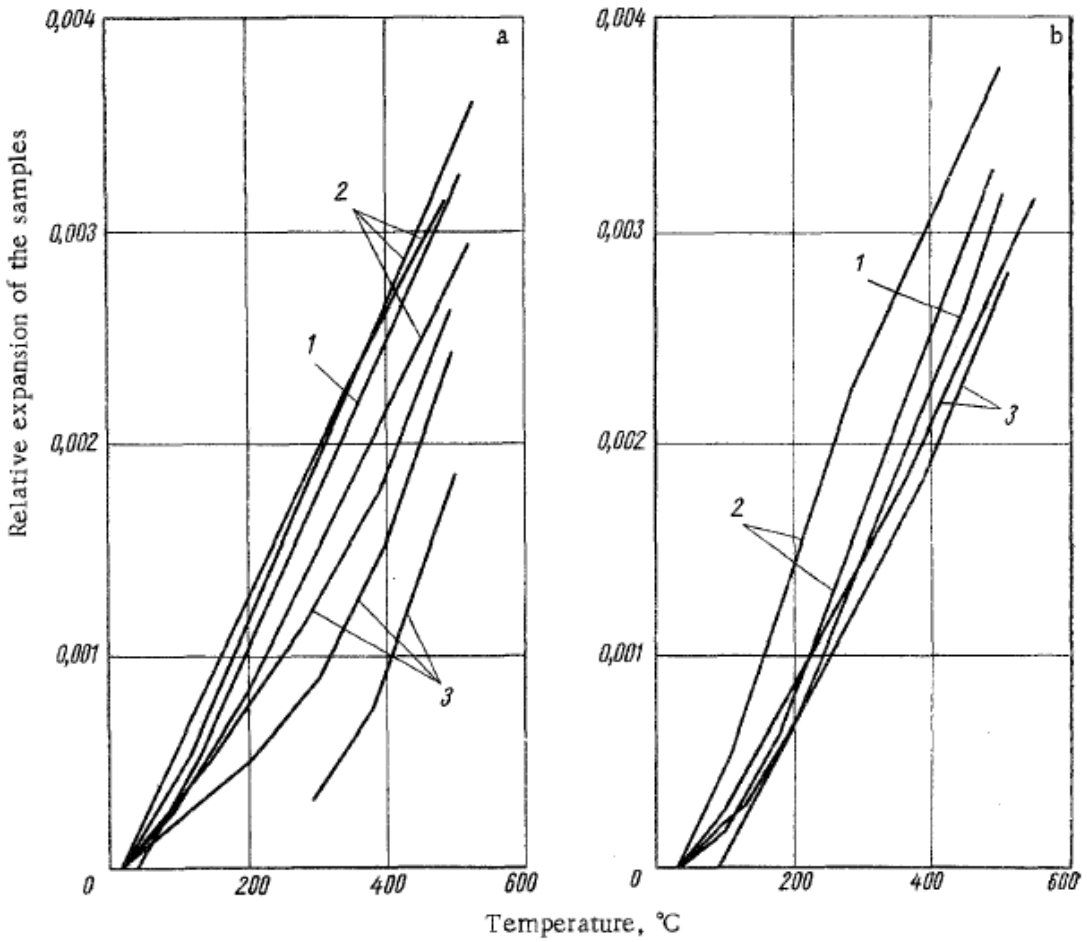

Figure 4.6. Relative expansion of concrete with chromite filler as aggregate under different temperatures: (a) first heating; (b) second heating; (1) irradiated; (2) heated; and (3) unheated. (Dubrovskii et al. 1966)

The slopes of the curves in Figure 4.6 represent the coefficient of thermal expansion of concrete. The difference between Figure 4.6(a) and Figure 4.6(b) is due to drying shrinkage during the first heating. One can see that there are no great differences between the expansions of the irradiated and heated concrete samples. The concrete samples used in the tests were made of Portland cement and chromite fillers, which is a heat-resistant concrete (or refractory concrete). In a follow-up study by Dubrovskii et al. (1967) on concrete samples made with Portland cement and sandstone and river sand, they found that the nature of thermal expansion for irradiated concrete was changed. As shown in Figure 4.7, the expansion of irradiated samples was increased significantly. Some of the samples expanded so much that they were damaged in the steel container, and the tests had to be stopped, as shown by the short curves in Figure 4.7. Again, the differences between (a) the first heating and (b) the second heating were due to drying shrinkage of cement paste.

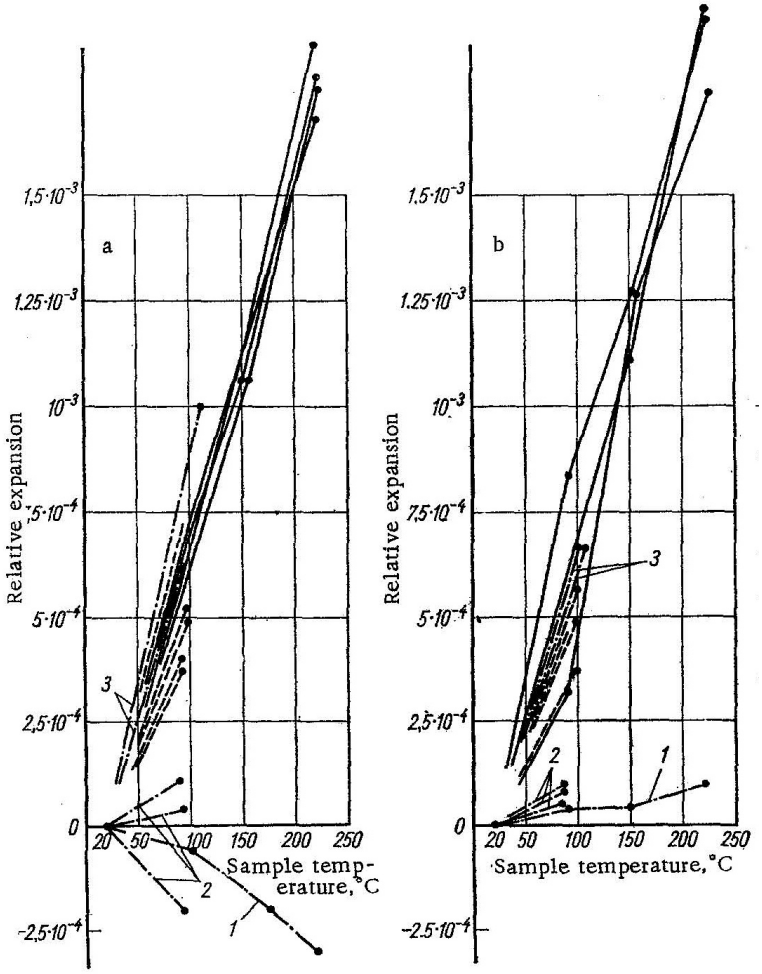

Figure 4.7. Relative expansion of concrete with sandstone and river sand aggregate under different temperatures: (a) first heating; (b) second heating; 1, 2, and 3 indicate samples irradiated to fluences of 3 × 10^{20}, 1.2 to 1.45 × 10^{20}, and 4 to 6 × 10^{19} n/c respectively;---- Control samples kept at 20°C;____ control samples kept at 20°C 220°C. (Dubrovskii et al. 1967)

The large expansion of concrete was due to the expansion of the aggregate used in the concrete. The aggregate was in the form of crystalline quartz. It is known that crystalline quartz becomes amorphous during irradiation (as shown in Figure 3.2), a process that is accompanied by anisotropic expansion and a density reduction of 15% (Bouniol 2011).

Available test data showed that nuclear radiation has a significant effect on thermal conductivity. The conductivity of irradiated concrete can be a fraction of the value of unirradiated concrete (Gray 1972, Dubrovskii et al. 1967; also see Hilsdorf et al. 1978) with the reduction in the range of 30%, as shown in Figure 4.8. However, it is not clear that the variation in thermal conductivity is due to thermal effect, radiation effect, or the combined effect of the two. Furthermore, one can see from Figure 4.8 that the reduction of thermal conductivity for normal weight concrete starts from the level of neutron radiation < 1 × 10^{19} n/cm^2 and the level of reduction remains the same up to 4 × 10^{19} n/cm^2. This indicates that the reduction mechanism is not heavily dependent on the level of radiation.

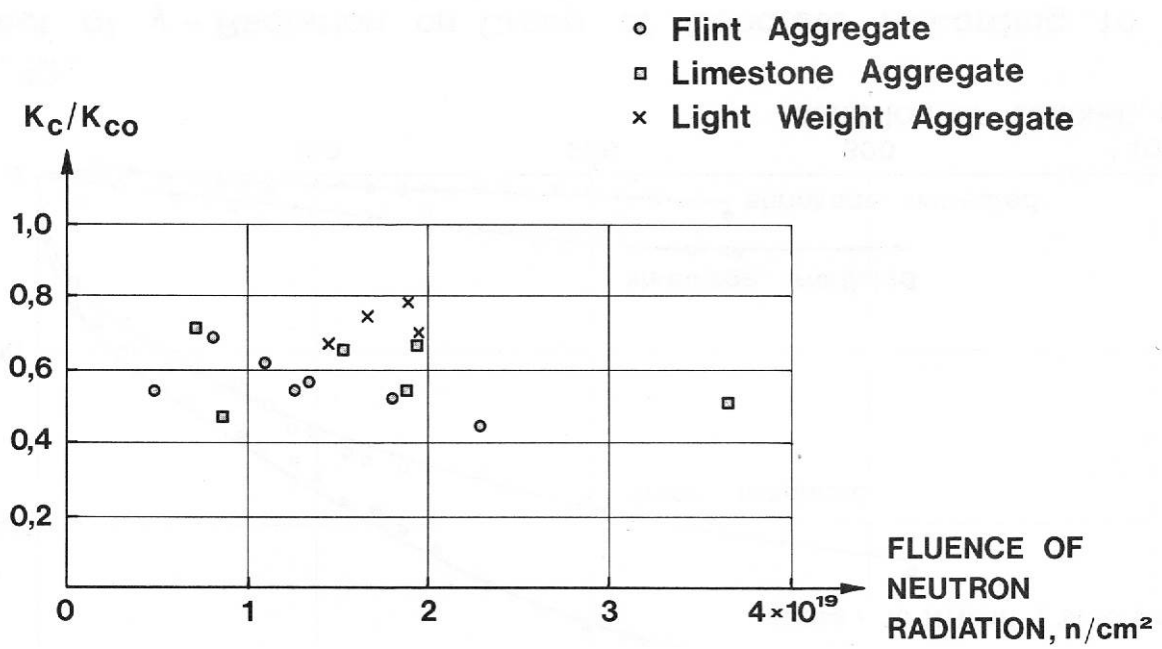

Figure 4.8. Thermal conductivity of concrete after neutron irradiation (K_c) relative to thermal conductivity of untreated concrete (K_{co}). (Gray 1972)

5. THE EFFECTS OF NUCLEAR RADIATION ON PROPERTIES OF CONCRETE

5.1 INTERACTION BETWEEN NUCLEAR RADIATION AND THE INTERNAL STRUCTURE OF CONCRETE

There are two types of interactions between nuclear radiation and the internal structure of concrete. One is related to geometric changes of the structure resulting from displacements of atoms from their lattice sites. The other is related to phase transformations of the constituents in concrete, resulting in reduction in porosity and/or formation of microcracks. As a result, the geometric changes and phase transformations can produce changes in properties of concrete. The geometric changes to the internal structure of concrete will be discussed first, followed by the phase transformations.

A crystalline structure can be visualized as a three-dimensional lattice or grid formed by an orderly arrangement of atoms. During gamma and neutron irradiation of concrete, the atoms in the lattice structure of some constituents in the concrete are displaced from their lattice sites. This displacement results in a new formation that is less stable than the previous one. This type of defect is known as a dislocation, or a lattice defect, and has an effect on the mechanical properties of materials, including strength and ductility. Dislocations can also contribute to macroscopic swelling, or geometric expansion, leading to an increase in internal stresses and strains.

Minerals with covalent bonds are more likely to be affected by radiation than those with ionic bonds (Kontani et al. 2010). Some minerals display significant changes in volume whereas others seem to be unaffected by radiation. It is difficult to distinguish the volumetric change due to radiation from the volumetric change due to the heat of radiation because radiation is typically accompanied by a temperature increase.

Bouniol and Aspart (1998) investigated the disappearance of oxygen in concrete under irradiation and the role of peroxide in radiolysis eventually resulting in carbonation. They noted that the species theoretically obtained is peroxide octahydrate that can be easily produced in aqueous solution in presence of calcium and H_2O:

$$Ca(OH)_{2\,aq} + H_2O_{2\,aq} + 6H_2O \rightarrow CaO_2.8H_2O \downarrow$$

The resulting hydrate is slightly soluble, but is capable of losing its water of crystallization in air and then decomposing with simultaneous carbonation:

$$CaO_2.8H_2O \rightarrow CaO_2 + 8H_2O$$

$$CaO_2 + H_2O \rightarrow Ca(OH)_2 + 1/2O_2$$

$$Ca(OH)_2 + CO_2 \rightarrow CaCO_3 + H_2O$$

The calcite crystals fill in pores and the porosity of concrete is reduced. The authors conducted experimental studies to verify the above (i.e., hydrated Portland cement paste was directly attacked by an aqueous solution containing 30% (by weight) H_2O_2).

Vodák et al. (2005) conducted an experimental study on the effect of gamma radiation on porosity and calcite content of concrete. Figure 5.1 shows that the specific pore surface area is reduced with increasing dose of gamma radiation, Figure 5.2 shows that the porosity of

concrete is reduced with increasing dose of gamma radiation, and Figure 5.3 shows that the relative intensity (i.e., content) of calcite is increased with an increasing dose of gamma radiation. Figure 5.3 presents results of diffraction analysis of calcite content in concrete for different values of dose. Results have been normalized to intensity of Si diffraction line that exhibits same value for all samples under consideration. These experimental results are in support of Bouniol and Aspart's proposed phase transformations under nuclear irradiation. If an excessive amount of calcite is formed during the phase transformation process, then microcracks may occur near the pores, which may contribute to the strength reduction of concrete.

The phase transformation noted above is similar to the natural carbonation reaction in concrete, a reaction of portlandite with CO_2 to form calcite and water. The difference is that the natural carbonation reaction takes place at the surface layer of concrete, where CO_2 comes from the environment and penetrates into the concrete through diffusion, whereas the radiation-induced carbonation occurs in the concrete that has been irradiated and thus is not limited to the surface of a concrete structure. Another major difference between the two types of carbonation reaction is that the natural carbonation reaction can produce an increase in concrete strength whereas the radiation-induced carbonation produces a decrease in both the size of the pore space and the strength of the concrete as the result of a succession of chemical reactions, starting with radiolysis of water and terminating in the formation of calcite crystals.

Vodák et al. (2011) conducted another experimental study to provide a more-detailed investigation on the porosity variation in cement paste under gamma irradiation as well as under natural carbonation. Figure 5.4 shows a comparison of pore size distributions in the surface layer of concrete with irradiation and without. Figure 5.5 shows a comparison of pore size distributions in the center of concrete with irradiation and without. Both figures share a similarity in that the peak in the pore size distributions around 10 to 20 nm disappeared.

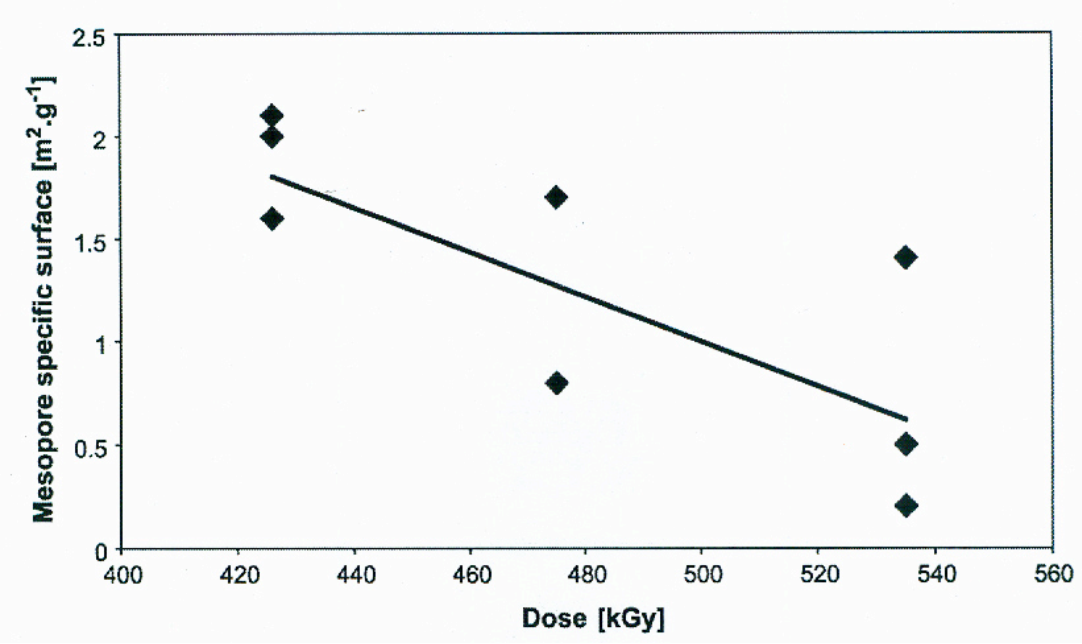

Figure 5.1. The specific pore surface area vs dose of gamma radiation. (Vodák et al. 2005)

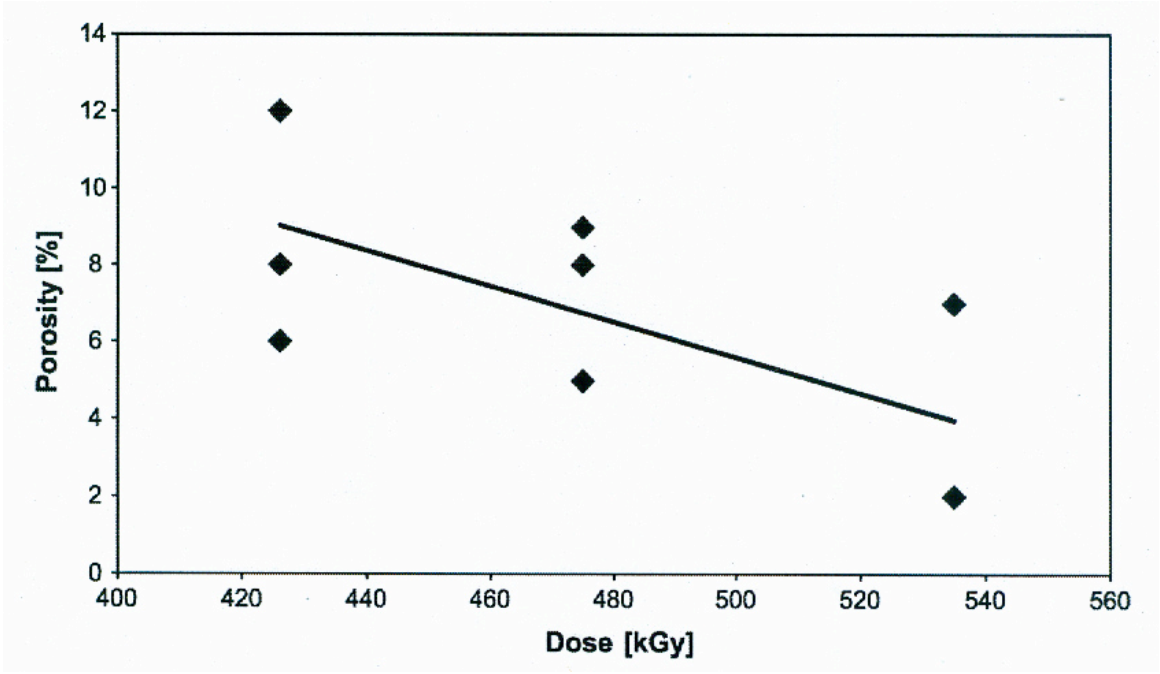

Figure 5.2. The porosity of concrete vs dose of gamma radiation. (Vodák et al. 2005.)

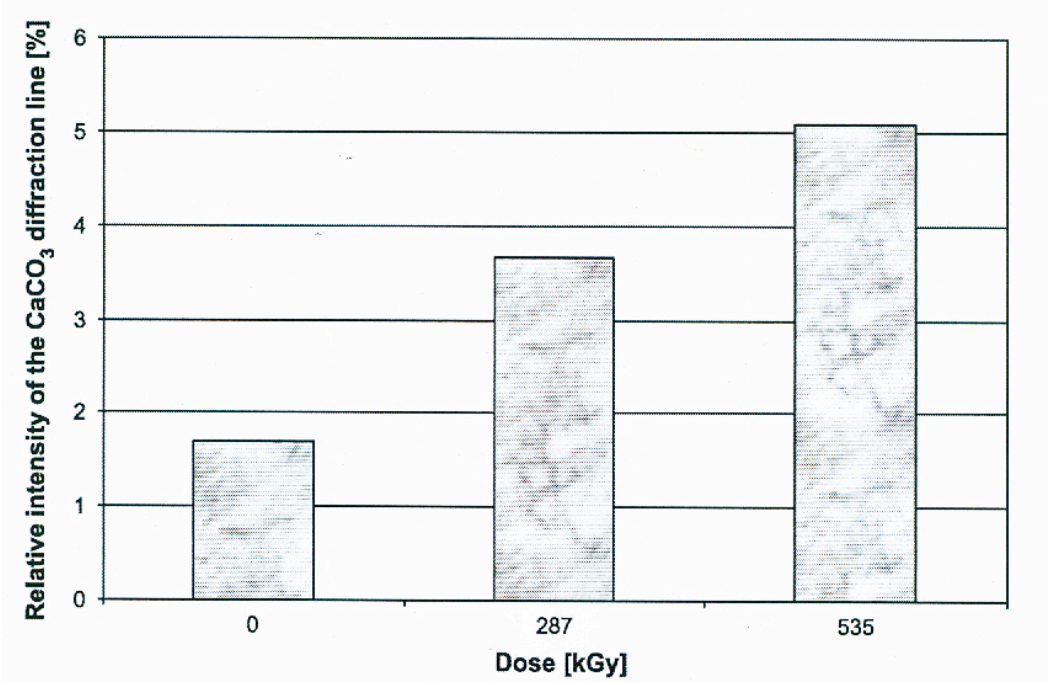

Figure 5.3. The intensity of $CaCO_3$ vs dose of gamma radiation. (Vodák et al. 2005)

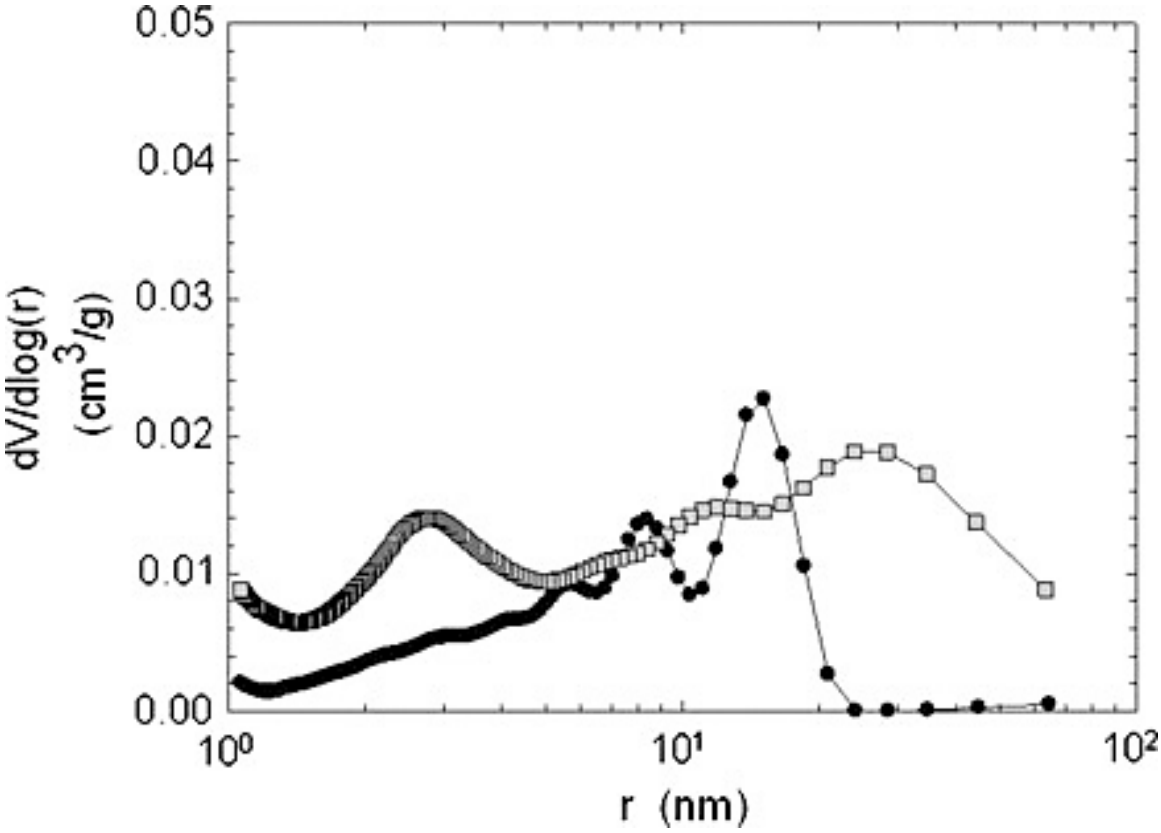

Figure 5.4. The pore size distributions of irradiated (1 MGy) and unirradiated concrete specimens in the surface of concrete. Filled circles are unirradiated samples. Open squares are irradiated samples. (Vodák et al. 2011)

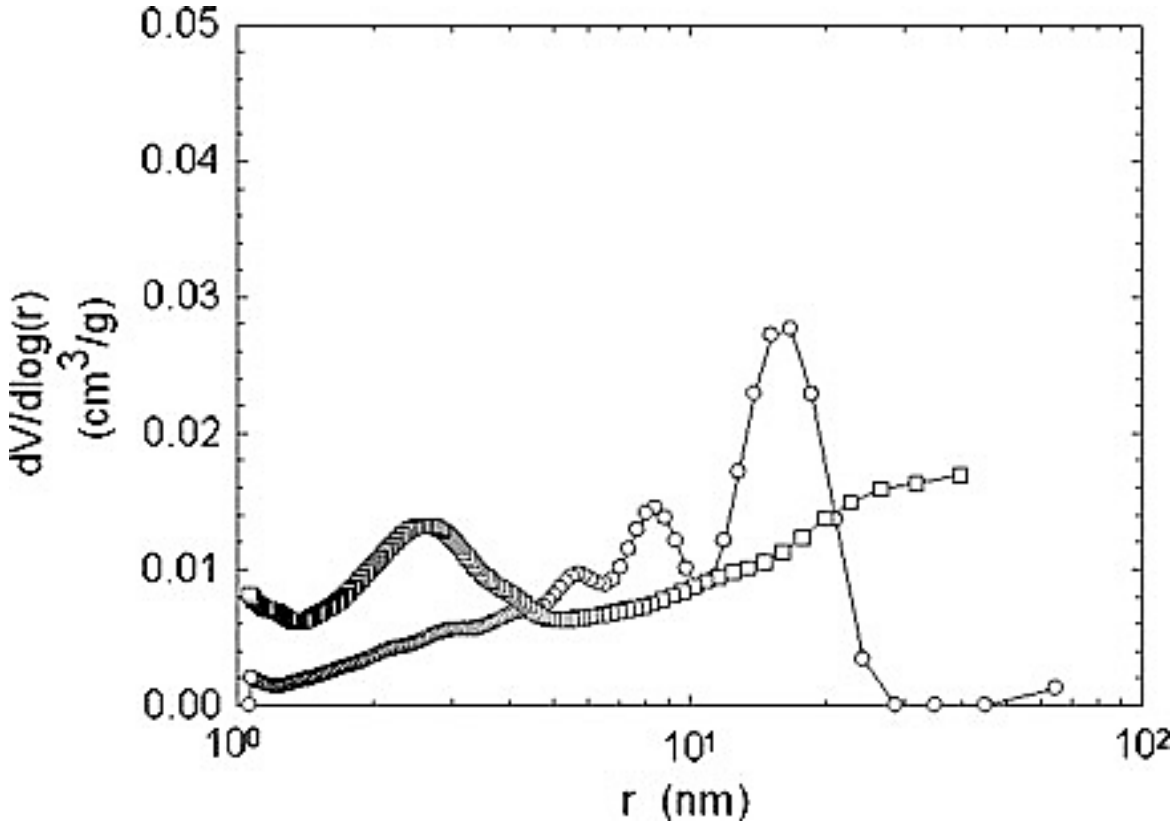

Figure 5.5. The pore size distributions of irradiated (1 MGy) and unirradiated concrete specimens in the center of concrete. Open circles are unirradiated samples. Open squares are irradiated samples (Vodák et al. 2011).

Kontani et al. (2010) provided a very good summary of the interactions of gamma and neutron radiation with cement paste and aggregates and of the deterioration mechanisms of concrete under nuclear irradiation. Table 5.1 summarizes the interactions of gamma rays with cement paste and aggregate. Table 5.2 summarizes the interactions of neutrons with cement paste and aggregate.

The effects of radiation on the components of concrete (aggregate and cement paste) translate to effects on properties of concrete itself, such as compressive strength, tensile strength, modulus of elasticity, and thermal expansion. Table 5.3 summarizes the deterioration mechanisms of concrete due to neutron radiation.

Table 5.1. The interactions of gamma rays with cement paste and aggregate (Kontani et al. 2010)

	Water phase	Solid phase	
Cement paste	• Water may be decomposed by radiolysis to generate hydrogen and hydrogen peroxide, which in turn decomposes into water and oxygen. • Gamma heating may cause additional hydration of unhydrated cement and transformation to hydrated cement. • Hydrogen peroxide generated in radiolysis process may react with cement paste.	• SiO bond of calcium silicate hydrate in cement paste may be slightly decomposed due to the covalent nature of the bond.	• Electrons are ejected by scattering of gamma rays and collide with the solid phases of cement paste or aggregates.
Aggregate	• Small amount of water may be released by the radiolysis in the form of hydrogen and oxygen gases as well as by gamma heating in the form of vapor.	• Siliceous aggregate may be slightly decomposed.	

Table 5.2. The interactions of neutrons with cement paste and aggregate (Kontani et al. 2010)

	Water phase	Solid phase
Cement paste	Molecular products from water may be the same as those for gamma rays, but the yields are different due to the different LET*	Although dislocation of atoms in solid cement particles may take place, the lattice defect by the distortion may not be accumulated, and the deformation of the paste may be negligible due to the porosity of the paste and the fineness of the cement particles
Aggregate	Interaction with water is the same as that in cement paste	Lattice constants are increased due to the dislocation of atoms, and lattice defects are accumulated

*LET = Linear Energy Transfer, which is the amount of radiation energy deposited in matter per unit particle path length in Joules per meter or keV/μm (Hala and Navratil 2003).

Table 5.3. Deterioration of concrete due to neutron radiation (Kontani et al. 2010)

Water phase	Solid phase
• Drying of cement paste reduces its stiffness. Drying of cement paste produces microcracks to reduce its strength or increases surface energy of cement paste to increase strength. • Additional hydration may increase the stiffness and the strength of concrete • Hydrogen peroxide generated in the radiolysis process may react with cement paste. • Neutrons have some effects on water phase of cement paste.	• Neutrons may have some effects on solid phases of cement paste, but the details are not understood very well. • Volume expansions of aggregates may introduce microcracking in cement paste and decrease stiffness and strength of concrete, but the details are not understood very well. • Concrete containing siliceous aggregates seems to crack more severely than those made with nonsiliceous aggregates, even if the expansions of aggregate alone are the same, but the mechanisms causing the difference is not understood.

5.2 COMPRESSIVE STRENGTH

A general assessment is that compressive strength of concrete decreases under gamma and neutron radiation exposure. Experimental studies in the literature have focused on specific strength reduction levels at specific radiation intensity (Hilsdorf et al. 1978). The purpose is to find the critical radiation intensities for gamma and neutron irradiation beyond which severe strength reduction will occur.

Many compressive strength tests were performed on concrete cubes of various compositions to study the effects of thermal-neutron radiation (Kaplan 1989). The tests showed insignificant changes in the compressive strength of irradiated concrete compared with that of heated unirradiated concrete. The results indicate that most of the strength degradation comes from the increased temperature and not from the thermal-neutron radiation itself at those levels.

Compressive strength tests have been performed on samples subjected to both neutron and gamma radiation, but few focus on gamma radiation alone (e.g., neutron radiation frequently occurs with gamma radiation).

In assessing the reduction of concrete strength under nuclear irradiation, 1×10^{19} n/cm^2 for fast neutrons and 2×10^{10} rad (2×10^{8} Gy) for gamma rays have been used as the critical levels of nuclear radiation. Concrete structures have been regarded to be sound as long as the levels of radiation do not exceed the critical levels, even if the NPPs were operated for more than 30 years. The critical levels were based on experimental data collected by Hilsdorf et al. (1978).

Figure 5.6 presents a plot, prepared by Kontani et al. (2010) of the test data collected by Hilsdorf et al. (1978), showing the effect of neutron radiation on the residual compressive strength of concrete (i.e., residual equals ratio of radiated to unirradiated strength). The change in compressive strength is insignificant for neutron fluence below 2×10^{19} n/cm^2. Above that limit, the compressive strength of concrete appears to decline as the radiation level increases. The threshold fluence value proposed by Hilsdorf et al. (1978) was 1×10^{19} n/cm^2, not 1×10^{20} n/cm^2 as shown in Figure 5.6.

Figure 5.7 presents a plot, prepared by Kontani et al. (2010) of the test data collected by Hilsdorf et al. (1978), showing the effect of gamma rays on the residual compressive and tensile strengths of concrete. In the figure, the threshold value is shown as 2.0×10^{10} rad (2.0×10^{8} Gy). In an Electric Power Research Institute (EPRI) report (EPRI 2012), the threshold value was considered as 10^{10} rad. In the original paper of Hilsdorf et al. (1978), no threshold value was proposed for gamma rays (only the 1×10^{19} n/cm^2 was proposed for neutrons).

Most experimental studies of radiation effects on concrete were carried out from the 1960s into the 1970s in support of development of prestressed concrete reactor vessels for high-temperature gas-cooled reactors and radioactive waste storage facilities. More recently, Vodák et al. (2005) conducted an experimental study of the effect of gamma radiation on the strength of concrete. The concrete specimens were exposed to various levels of gamma irradiation. Based on their results, presented in Figure 5.8(a), the authors indicated that the compressive strength of concrete exposed to a gamma radiation of 5×10^{5} Gy was reduced by about 10% compared to unirradiated samples. In fact, they noted that the strength reduction started from 3×10^{5} Gy. As stated by the authors, their results were not consistent with others, such as the commonly accepted reference value of 2×10^{8} Gy. One possible problem of the test was that no method of shielding neutron radiation was mentioned, and therefore, the reduction in strength may be due to the combined effect of neutron and gamma radiation instead of only gamma

radiation. Also, the data scatter was relatively large and the data set relatively small so that statistically valid conclusions could not be derived.

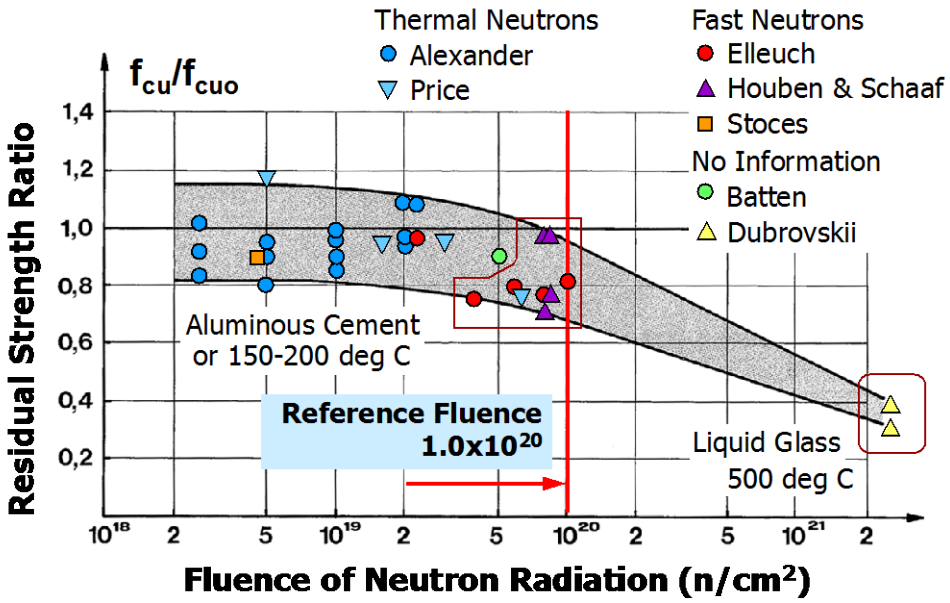

Figure 5.6. Effect of neutron radiation on the residual compressive strength of concrete. (Kontani et al. 2010)

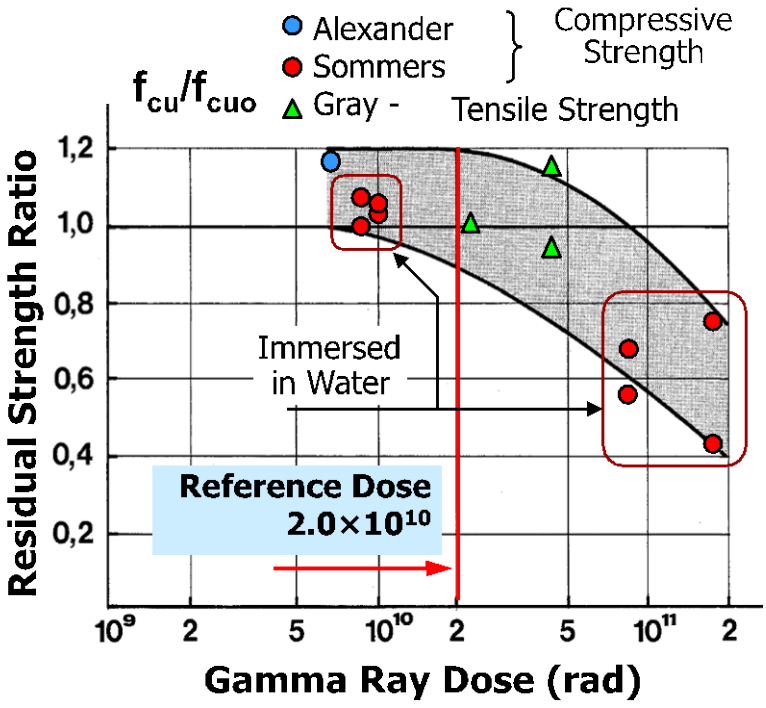

Figure 5.7. Effect of gamma radiation on the residual compressive strength of concrete. (Kontani et al. 2010)

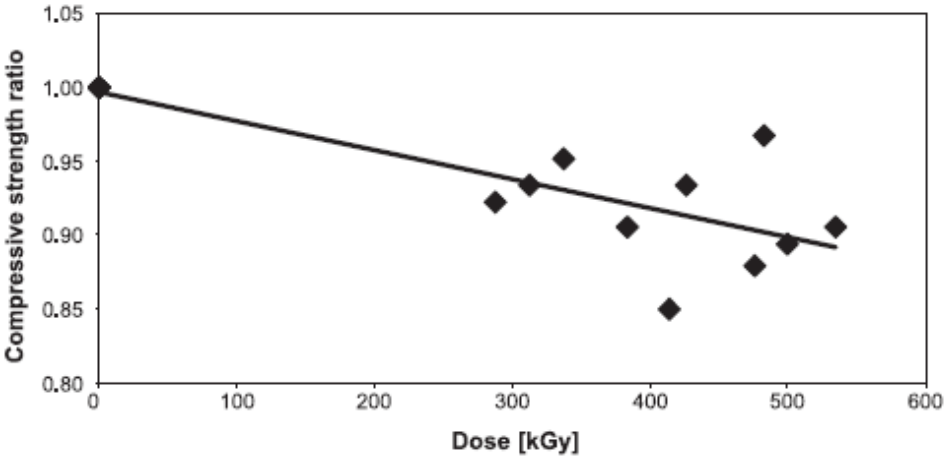

(a)

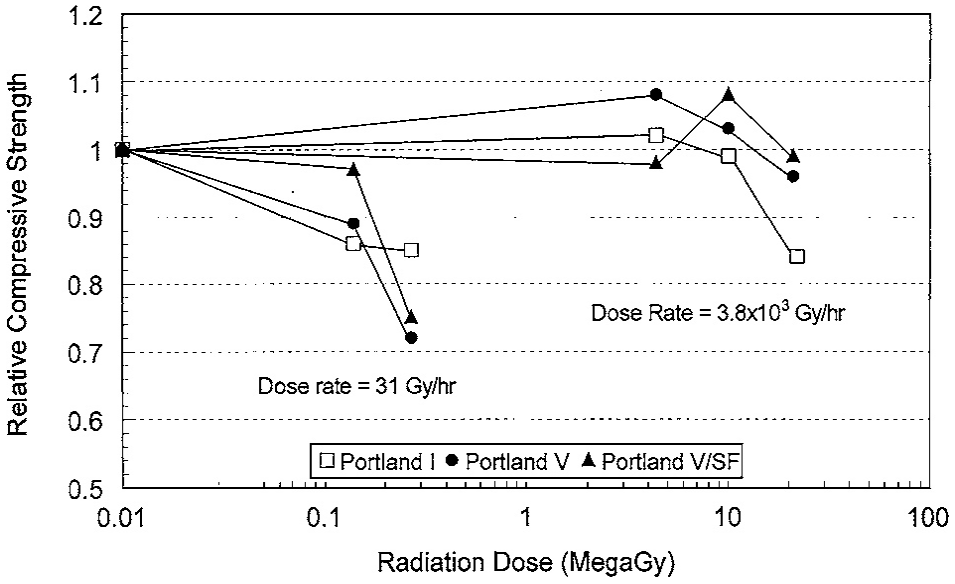

(b)

Figure 5.8. Effect of gamma radiation on the compressive strength of concrete and mortar: (a) test data by Vodák et al. (2005) and (b) text data by Soo and Milian (2001).

The data shown in Figure 5.8(b) are from tests by Soo and Milian (2001) on Portland cement mortars. The data are similar to the test data from Vodák et al. (2005). Soo and Milian found that loss of compressive strength could occur at gamma doses that are much less than the threshold dose of 2 x 10^8 Gy (2 x 10^{10} rad) noted in Kontani et al. (2010). They postulated that the loss of strength could be connected with the radiolysis of the water of hydration in the cement as well as pore water. A loss of hydrogen and oxygen radiolytic species during irradiation would decrease the level of cement hydration and thus the strength of the cement. In Figure 5.8(b), the strength of the materials irradiated at the low dose rate (Co-60 gamma flux of 31Gy/hr) falls rapidly once the dose exceeds about 10^5 Gy, but the strength for the higher dose

rate (Co-60 gamma flux of 3.8 x 10^3 Gy/hr) does not decrease until the dose exceeds about 10^7 Gy (Soo and Milian 2001). There was no explanation provided for this phenomenon.

Fujiwara et al. (2009) conducted carefully designed compressive strength tests on neutron-irradiated concrete samples and found no significant reduction of the compressive strength due to neutron radiation. In the study, the irradiation temperature was kept lower than 65ºC, which is the limiting value stipulated in the design standard for nuclear power stations in Japan (and in the United States). The specimens were 50 mm diam × 100 mm long cylinders. Table 5.4 presents neutron fluence levels for each step in the tests as well as the number of irradiation cycles.

Table 5.4. The neutron fluence level in each step in the test
(Fujiwara et al. 2009)

Step	**Fast neutron fluence, n/cm^2 (E > 0.1 MeV)**	**Irradiation cycles**
1	0.5×10^{18}	1
2	3.0×10^{18}	6
3	2.0×10^{18}	4

The maximum fast neutron fluence used in the study was 12.0×10^{18} n/cm^2 (E > 0.1MeV), which sufficiently exceeds the total fast neutron fluence levels for the concrete located at the exterior of a reactor pressure vessel for a typical BWR after 60 years of operation. Test results presented in Figure 5.9 show that compressive strength of the irradiated concrete specimens was roughly equivalent to that of concrete specimens cured for the same duration under the basic environment of 20ºC and 60% relative humidity. Therefore, their test data indicated that the radiation exposure at levels below 12×10^{18} n/cm^2 did not significantly affect the compressive strength of concrete.

Because Professor Hilsdorf's paper was very important in determining the critical radiation values, Fujiwara et al. (2009) analyzed in detail the test data collected by Hilsdorf et al. (1978). They studied the original papers, compared the test specimens and conditions, and found the following:

- The temperatures in some of the specimens during irradiation reached 100ºC or higher (approximately 140ºC to 550ºC). Thus the strength reduction could very well be induced by the elevated temperatures and not by the radiation, as shown in Figure 5.10 by red circles.

- The sizes of some specimens were very small (some were as small as 8 to 15 mm), which did not characterize the compressive strength of concrete, as shown in Figure 5.10 by green circles.

- Some specimens were tested for bending strength but not for compressive strength. Specimens tested for bending strength are shown as blue circles in Figure 5.10.

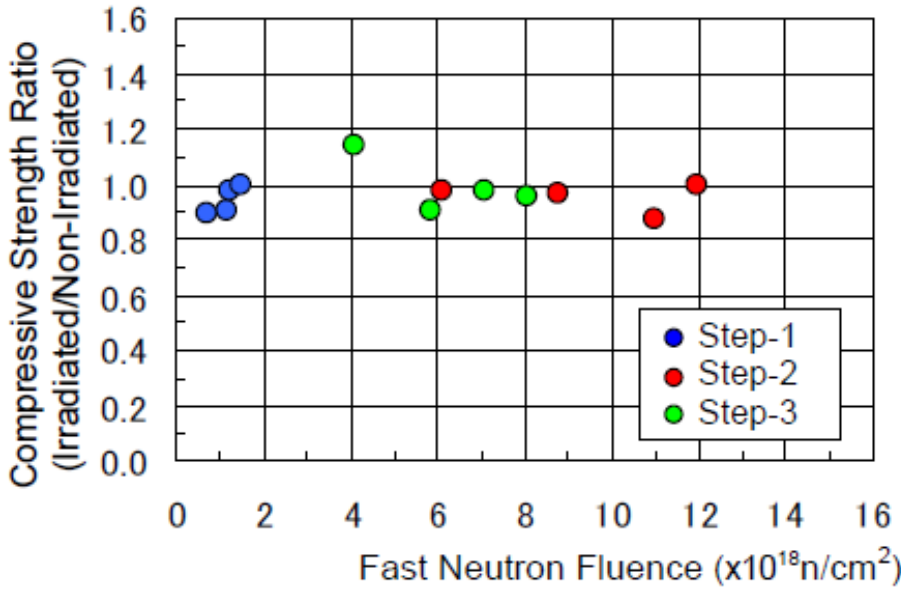

Figure 5.9. Compressive strength of concrete under different levels of neutron radiation. (Fujiwara et al. 2009)

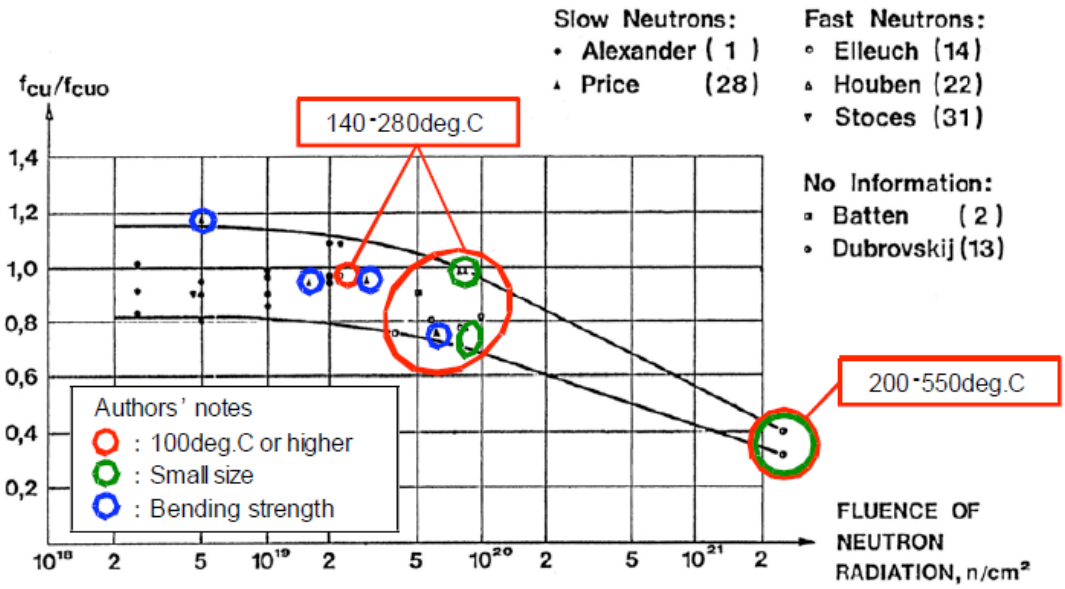

Figure 5.10. The problems in the test data collected by Hilsdorf et al. (1978) on compressive strength of concrete. (Fujiwara et al. 2009)

Similar problems with the test data collected by Hilsdorf et al. were also pointed out by Kontani et al. (2010), as shown in Figs. 5.6 and 5.7 and summarized in Table 5.5. With these observations, Fujiwara et al. (2009) designed their test specimens and testing conditions carefully to avoid those problems. As noted in Figure 5.9, the Fujiwara et al. data indicated that fast neutron fluences up to 12 x 10^{18} did not significantly affect concrete strength.

Fujiwara et al. (2009) also compared their test data with those collected by Hilsdorf et al. (1978). They took out the test data shown in Figure 5.10 in the red, green, and blue circles because of the reasons listed above (temperature, specimen size, and noncompressive strength). The comparisons are shown in Figure 5.11, in which the purple circles are Fujiwara's test data and the blue circles are selected compressive strength results using data screened from that presented by Hilsdorf et al.

Table 5.5. The experimental conditions found in papers referenced. (Hilsdorf et al. 1978, Kontani et al. 2010) (screened) from Hilsdorf's collection. One can see that a clear decrease in concrete

Author*	Property Measured	Cement Type†	Specimen Size (mm)	Irradiation Conditions	
				Temperature (°C)	Neutron Energy Level & Fluence (n/cm^2)
Alexander[8]	Compress.	OPC	51 × 51 × 51	20 to 100	Thermal neutron 0.29×10^{19} to 2.3×10^{19}
Batten[9]	Compress.	OPC	51 × 51× 203	Not available	No information 5.0×10^{19}
Dubrovskii[2]	Compress.	Liquid glass	ϕ15 × 15 cylinder	200 to 550	No information 2.0×10^{21} to 2.4×10^{21}
Elleuch[3]	Compress.	Aluminous cement	25 × 25 × 50	210	Fast neutron 2.6×10^{20} to 11.1×10^{20}
Houben[4] Schaaf[5]	Compress.	OPC	8 × 8 × 70	15 to 200	Fast neutron 3.0×10^{19} to 8×10^{19}
Price[6]	Bending	OPC	51 × 51× 203	50	Thermal neutron 0.5×10^{19} to 7×10^{19}
Stoces[10]	Compress.	OPC	ϕ50 × 70 cylinder	<80	Fast neutron 4.2×10^{18}

* The numbers shown in [ ] in the first column are the reference numbers in Kontani et al. 2010.

† OPC: ordinary Portland cement

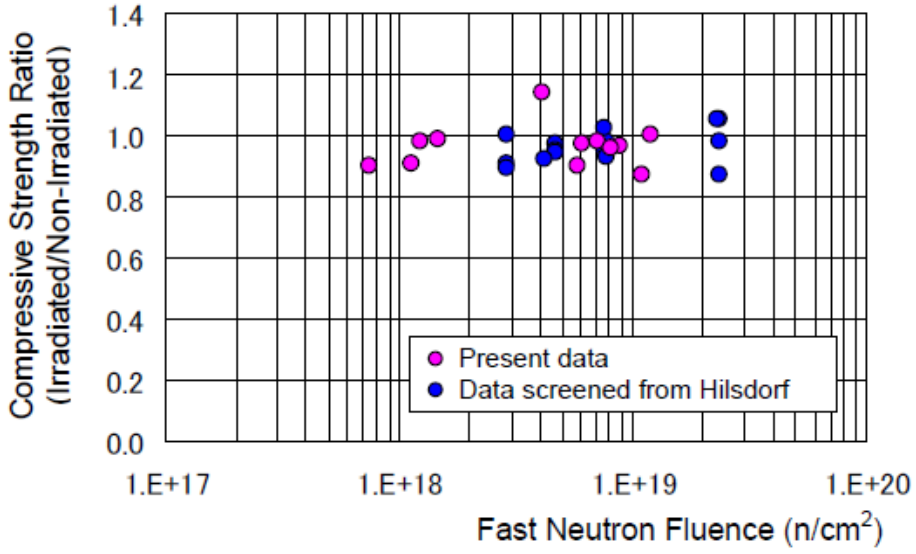

Figure 5.11. Comparisons of the test data collected. [Hilsdorf et al. 1978 (shown as "Data screened from Hilsdorf") and Fujiwara et al. 2009 (shown as "Present data").

So far, the highest neutron radiation level used in the experimental studies was from 2.0 to 2.4×10^{21} n/cm^2, which was used by Dubrovskii et al. (1966) as shown in Figure 5.6, Figure 5.10, and Table 5.5. Their test results are very important because the test data are the only data set that showed the trend of strength reduction with increasing neutron radiation beyond 1.0×10^{20} n/cm^2. Therefore, the experimental conditions used by Dubrovskii et al. (1966) have been carefully reexamined and the following four important findings resulted:

- Two binders were used in the study, as shown in Table 5.6, one was Portland cement and the other was liquid water glass. This is different from the information shown in Table 5.5 by Kontani et al. (2010), which only lists the liquid water glass information noted by Hilsdorf et al. The samples made of Portland cement were relevant to studying the effect of nuclear radiation on compressive strength of concrete.

- The samples were 15 mm diam cylinders with 15 mm height. Only fine aggregate (chromite filler) was used. Although the size of sample was small as indicated in Figures 5.6 and 5.10, it is an adequate size for studying the strength of Portland cement mortar (which is related to Portland cement concrete) under nuclear irradiation.

- The mean neutron energy level used in the study was 0.23 MeV; 30% of neutrons had an energy greater than 0.7 MeV. Thus the neutron energy level is in the energy level for fast neutrons [the energy level of fast neutrons is greater than 0.1 MeV according to Hilsdorf et al. (1978)].

- The radiation tests were conducted under high temperatures, in the range between 200 ºC and 550ºC. However, the temperature effect was considered by using hot (heated) samples that underwent the same temperature history as irradiated samples and cold (unheated) samples that were maintained under standard laboratory conditions. The differences between the hot and cold samples accounted for the temperature effect,

and the difference between the hot and irradiated (irradiated and heated) samples showed the radiation effect. As marked in Table 5.6, about 26% of the fall in strength must be attributed to the radiation, and 34% must be attributed to the thermal effect (Dubrovskii et al. 1966). Therefore, assuming there was no synergistic effect, in the papers by Hilsdorf et al. (1978), Fujiwara et al. (2009), and Kontani et al. (2010, 2011), the test data from Dubrovskii et al. (1966) should be shown with the 26% reduction, not with the 60% reduction. The 60% reduction was due to the combined effect of high temperature and neutron radiation.

Dubrovskii et al. conducted more studies on the effect of nuclear radiation on concrete (Dubrovskii et al. 1967, 1968). In the studies, "ordinary concrete" samples were used, which was defined as concrete made with Portland cement and aggregates of nonmetallic materials such as limestones, sandstones, granites, and serpentine. In their previous study (Dubrovskii et al. 1966), chromite filler was used as the aggregate. The test data from the studies in 1967 and 1968 were not included in the collection of test data by Hilsdorf et al. (1978).

Table 5.6. Strength and stiffness of concrete samples (Dubrovskii et al. 1966)*

Samples of chromite concrete using Portland cement binder			**Samples of chromite concrete using liquid glass binder**		
Irradiated	**Hot**	**Cold**	**Irradiated**	**Hot**	**Cold**
56.6 / 0.64	110.4 / 0.77	124.6 / 0.817	82.1 / 0.615	90.6 / 0.682	209.5 / —
62.3 / 0.68	95.1 / 0.725	126.3 / 0.885	71.3 / 0.545	134.8 / —	262.7 / 0.885
41.3 / 0.68	81.5 / 0.725	94 / 0.68	74.7 / 0.58	141.6 / 0.853	286.5 / 0.885
53.8 / 0.68	78.1 / 0.634	126.3 / 0.885	—	141.6 / 0.767	207.2 / 0.885
37.4 / 0.612	35.1 / —	126.3 / 0.817	—	—	—
37.4 / 0.68	101.9 / —	78.1 / —	—	—	—
—	51 / 0.578	163.1 / —	—	—	—
Average value					
78.1 / 0.665	79 / 0.686	119.8 / 0.816	76.1 / 0.58	127.9 / 0.767	241.5 / 0.885
Relative value %					
40 / 82	66 / 84	100 / 100	32 / 66	53 / 87	100 / 100

*Numerator of the fraction gives the strength of the sample in kg/cm^2; denominator gives the slope of the strain curve on the compression diagram.

In one study by Dubrovskii et al. (1967), the concrete samples were cylinders measuring 40 mm in height and diameter. The temperature variation during irradiation was from 20°C to 220°C. The test data showed that for radiation to a neutron fluence less than 5×10^{19} n/cm^2, the changes in strength and stiffness of concrete were insignificant. When the neutron fluence was increased to 1.45×10^{20} n/cm^2, noticeable changes were observed. Compressive strength of the concrete was reduced by 10% to 20%. However, the level of fluence used in this study did not reach 2.0 to 2.4 × 10^{21} n/cm^2, which was used for the study on the concrete with chromite filler (Dubrovskii et al. 1967). Part of the reason for this was that concrete samples expanded considerably during the irradiation process up to a neutron fluence level of 1.45×10^{20} n/cm^2. At higher levels, the samples were damaged in the steel container due to the excessive expansion.

The expansion of concrete came from the expansion of the aggregates that were 80% to 95% silicon oxide in the form of crystalline quartz; the quartz becomes amorphous during neutron irradiation with associated expansion.

In another study by Dubrovskii et al. (1968), the properties of serpentine concrete under neutron irradiation were studied. Finely ground serpentine was used in the concrete mixture. Large changes were observed when the neutron fluence was increased to 1.3 to 1.7 × 10^{21} n/cm^2. Compressive strength of the concrete was reduced by 60%, and linear expansion reached 1.3% to 1.7%, with these changes considered to be due to microcracks that formed in concrete.

Based on results presented in this section, it is very difficult to deduce from these studies the extent of reduction of compressive strength due to nuclear irradiation and the mechanism of concrete deterioration by nuclear radiation. The experimental conditions of some of the data collected by Hilsdorf et al. (1978) were very different from the testing conditions of Fujiwara et al. (2009) and Vodák et al. (2005). They were also not representative of the operating conditions of NPPs (for example, operation temperature is no higher than 65ºC). More importantly, there has been a lack of experimental studies under high levels of irradiation, and the studies conducted by Dubrovskii et al. (1966, 1967, 1968) were each for one type of concrete. Therefore, Kontani et al. (2010, 2011) noted that there is a pressing need to conduct new and more systematic radiation tests to study the critical levels of gamma and neutron radiation corresponding to noticeable strength reduction. Systematic experimental studies are needed for determining appropriate reference levels of nuclear radiation for assessing the integrity and soundness of NPP concrete structures. Interactions between radiation effects and temperatures need to be investigated as well as the effects of neutron and gamma ray radiation on cement paste and aggregates in concrete.

5.3 TENSILE STRENGTH

Tensile strength of concrete can be tested by different methods, such as splitting-tension, flexural-tension, and direct-tension testing. The tensile strength measured by the flexural tension test is usually higher than the value obtained from the splitting-tension test because of nonuniform stress distribution in the concrete beam. As a result, the tensile strength test data exhibit large scattering, especially when tensile strengths have been obtained by different testing methods and compared together. This is apparent in the paper by Hilsdorf et al. (1978) that summarized tensile test data for concrete subjected to irradiation. The results indicate that for a neutron fluence of 5 × 10^{19} n/cm^2, the tensile strength of irradiated specimens can be 20% to 80% less than the strength of unirradiated and unheated specimens, as shown in Figure 5.12. Thus, depending on the test conditions and the radiation level, the tensile strength of concrete can be reduced significantly.

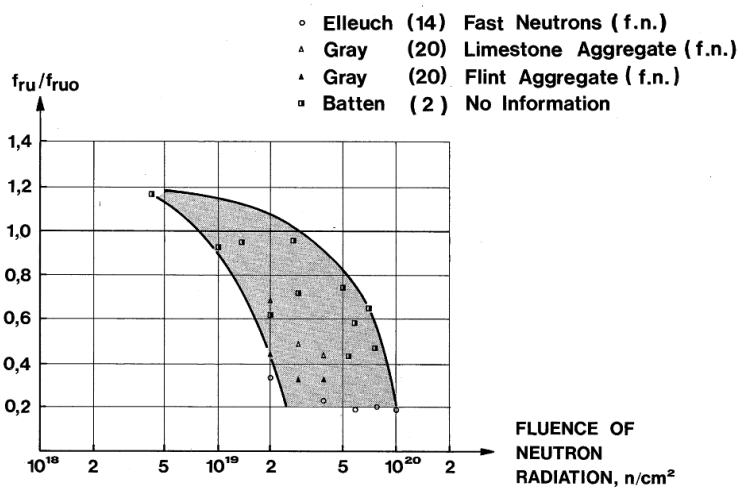

Figure 5.12. Effect of neutron radiation on tensile strength of concrete. (Hilsdorf et al. 1978)

For evaluation of the effect of gamma radiation, Vodák et al. (2005) performed tensile-strength tests on samples similar to those described in Section 5.2 for compressive strength of concrete. Their results are shown in Figures 5.13 and 5.14 for splittingtensile strength and flexural tensile strength, respectively. Although the authors indicated that there was a trend in tensile-strength reduction due to increasing gamma radiation similar to that in Figure 5.8(a) for the compressive strength, statistically valid conclusions cannot be derived because the data scatter was relatively large and the data set relatively small. It was noted that a reduction in tensile strength for some specimens had started to occur by the time the dose to the specimens reached approximately 3×10^5 Gy (i.e., an amount corresponding to approximately 40 years of operation at the Temelin NPP).

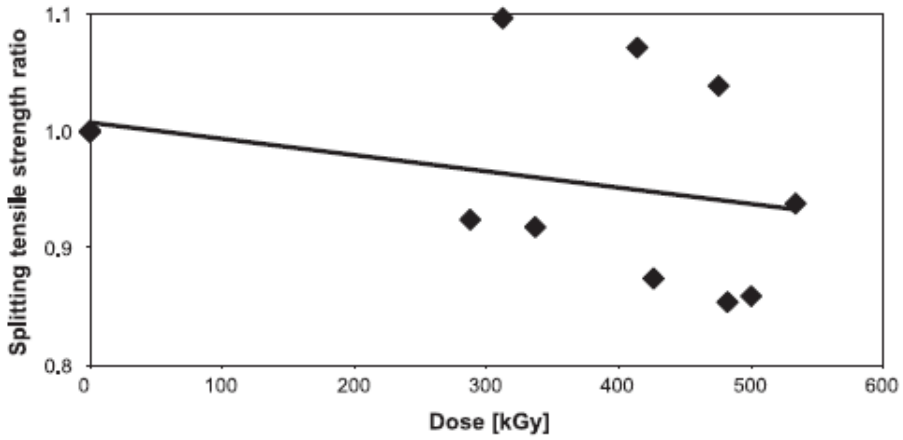

Figure 5.13. Effect of gamma radiation on splitting tensile strength of concrete. (Vodák et al. 2005)

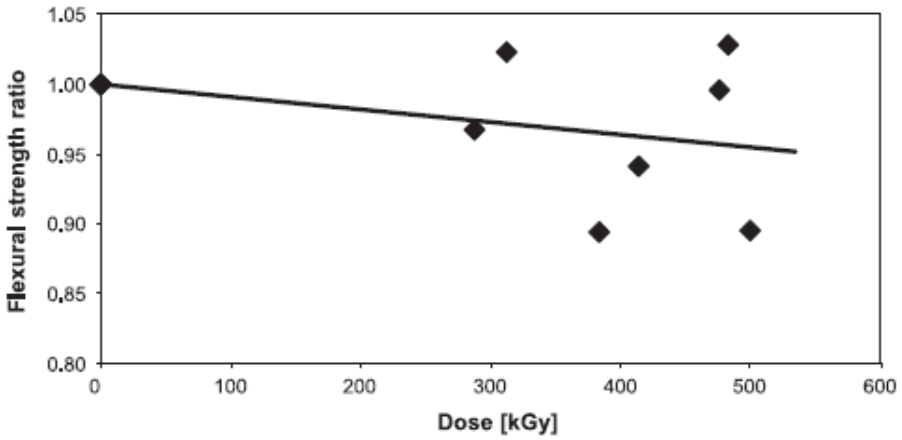

Figure 5.14. Effect of gamma radiation on flexural tensile strength of concrete. (Vodák et al. 2005)

Because the tensile strength test data are very limited and available results exhibit significant data scatter, it is difficult to obtain a definite reference level of radiation that leads to a significant reduction of the tensile strength of concrete. Kaplan (1989) summarized that in general neutron fluences greater than 10^{19} n/cm^2 will lead to a reduced tensile strength.

5.4 MODULUS OF ELASTICITY

Similar to the strengths of concrete, the stiffness, or modulus of elasticity, of concrete is reduced under nuclear radiation, as shown in Figure 5.15 (Hilsdorf et al. 1978). In the figure, "E_c/E_{co}" is the ratio of the modulus of elasticity after irradiation and heating to the modulus of elasticity before irradiation and heating. A neutron fluence in the range of 1 × 10^{19} n/cm^2 leads to a slight decrease of the modulus of elasticity. When the fluence was larger than 5 × 10^{19} n/cm^2, the reduction can be as high as 30% of the original stiffness.

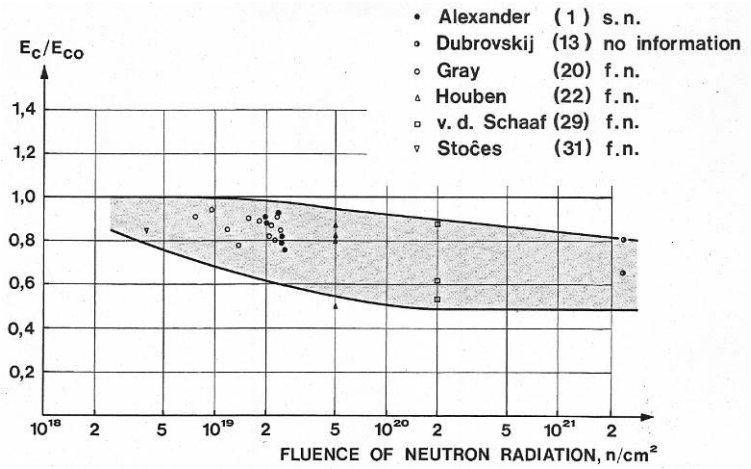

Figure 5.15. The effect of neutron radiation on the modulus of elasticity of concrete: E_c = after neutron radiation and E_{co} = untreated. (Hilsdorf et al. 1978)

Fujiwara et al. (2009) reported test data in which the static modulus of elasticity of irradiated specimens was not significantly different from that of nonirradiated specimens at the levels of fast neutron fluence expected on the reactor pressure vessel exterior of a typical BWR over a 60 year period [3.0×10^{18} n/cm^2 (E > 0.1 MeV)]. There was a tendency for the values to decrease slightly at levels above 6.0×10^{18} n/cm^2, but the decrease was not significant, as shown in Figure 5.16.

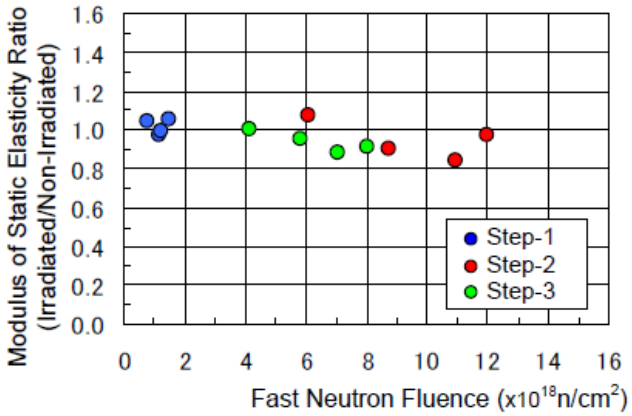

Figure 5.16. Static modulus of elasticity of concrete after different levels of neutron radiation. (Fujiwara et al. 2009)

The test data presented in this section showed the combined effect of neutron radiation and thermal effect. Available test data are therefore not sufficient to separate the effects of radiation and temperature, which is one of the main goals of the ongoing study by Kontani et al. (2010, 2011).

5.5 CREEP, SHRINKAGE, AND VOLUMETRIC VARIATION

The effect of gamma radiation on the creep and shrinkage of concrete was investigated using a limestone aggregate concrete representative of that used in the concrete pressure vessel of the Oldbury Nuclear Power Station (McDowall 1971). Cylindrical specimens, 105 mm in diameter by 305 mm long were subjected to a load of 10 N/mm^2 at an average sample temperature of 30°C. Figure 5.17 presents shrinkage and creep results obtained from specimens subjected to an average gamma dose rate of 11.4×10^3 rad/h as well as those for unirradiated control specimens. In the figure, the creep of untreated (i.e., unirradiated and unheated) concrete is shown to be higher than that of irradiated concrete. As indicated earlier, the modulus of elasticity of irradiated concrete is expected to be lower than that of regular concrete, and thus the creep of irradiated concrete would be expected to be higher. However, the results in Figure 5.17 show an opposite trend. One theory for creep being opposite of what was expected was that results for the irradiated concrete at any point in time were obtained from specimens that were drier than the control specimens.

Figure 5.18 shows the effect of neutron radiation on volume expansion of concrete (Gray 1972, Kelly et al. 1968; also see Hilsdorf et al. 1978). The cement paste undergoes shrinkage while the aggregate expands under neutron radiation. Thus, the amount of shrinkage of cement paste

and the amount of expansion of aggregate determine the overall volumetric variation of the concrete. It is clearly shown in Figure 5.18 that the concrete made of flint aggregate expands much more than the concrete made of limestone aggregate; the cement paste in the two types of specimens would be expected to have similar shrinkage.

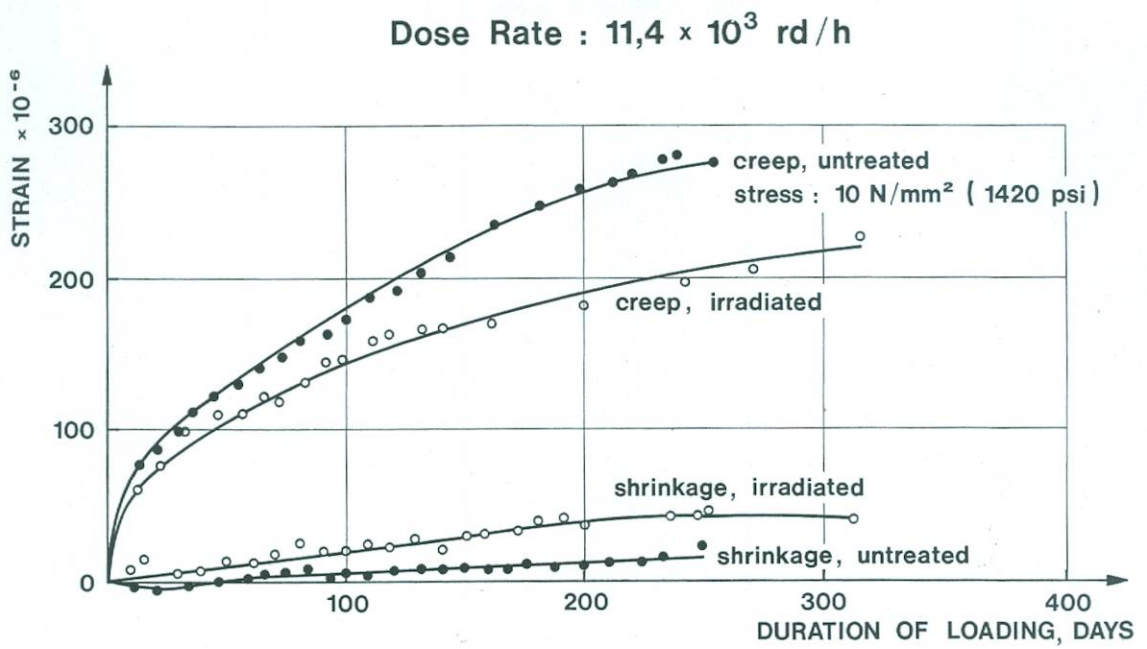

Figure 5.17. The effect of gamma radiation on creep and shrinkage of concrete. (McDowall 1971) (Note: rad = 0.01 Gy).

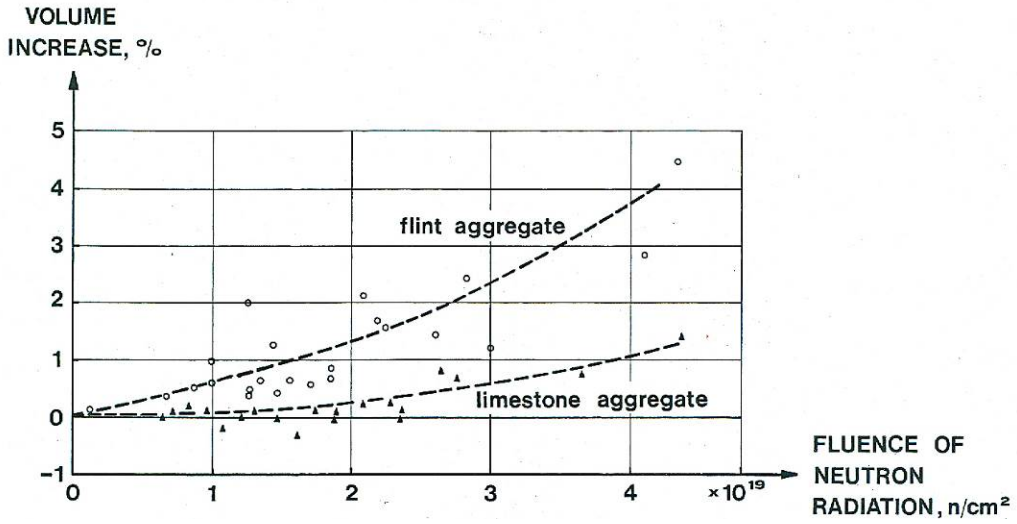

Figure 5.18. The effect of neutron radiation on the volume of concrete. (Gray 1972, Kelly et al. 1968)

Hilsdorf et al. (1978) pointed out that, for the volumetric expansion shown in Figure 5.18, concrete specimens that were only exposed to elevated temperatures but not irradiated did not show such a volume increase; rather, they showed the expected shrinkage. The shrinkage was of the cement paste, resulting from loss of water. This means that the volume expansion was mainly from the volume expansion of aggregates due to the neutron irradiation, and the volume expansion of aggregate under neutron irradiation can be very significant. Hilsdorf et al. (1978) compared the test data shown in Figure 5.18 for volumetric expansion with tensile strength test data given in the research reports (Gray 1972, Kelly et al. 1968) and further concluded that tensile strength of concrete is lower when the volume increase during neutron irradiation is larger.

With increasing age of nuclear reactors in service in the United States and around the world, deformation properties of concrete, such as creep and shrinkage, have increased importance for long-term performance evaluation of the concrete structures. Brooks (2005) conducted a long-term study (i.e., 30 years) to test the creep and shrinkage of various concretes. These tests were conducted without nuclear irradiation, but the results are very important for long-term evaluation of concrete structures in NPPs.

The creep test data in Figure 5.19 indicate that (1) the creep rates (the slopes of the curves) of dry-stored concrete samples decreased at about one year after loading, the rates remained the same all the way to 30 years, and there was no sign for the asymptotic trend of the ultimate creep; and (2) the rates of wet-stored concrete samples started to increase after about 10 years. The range of the measured 30 year creep coefficient was from 1.2 to 9.2, depending on the water/cement ratio (or strength) and aggregate type. For those test data, specific creep and creep compliance were underestimated by all methods of prediction.

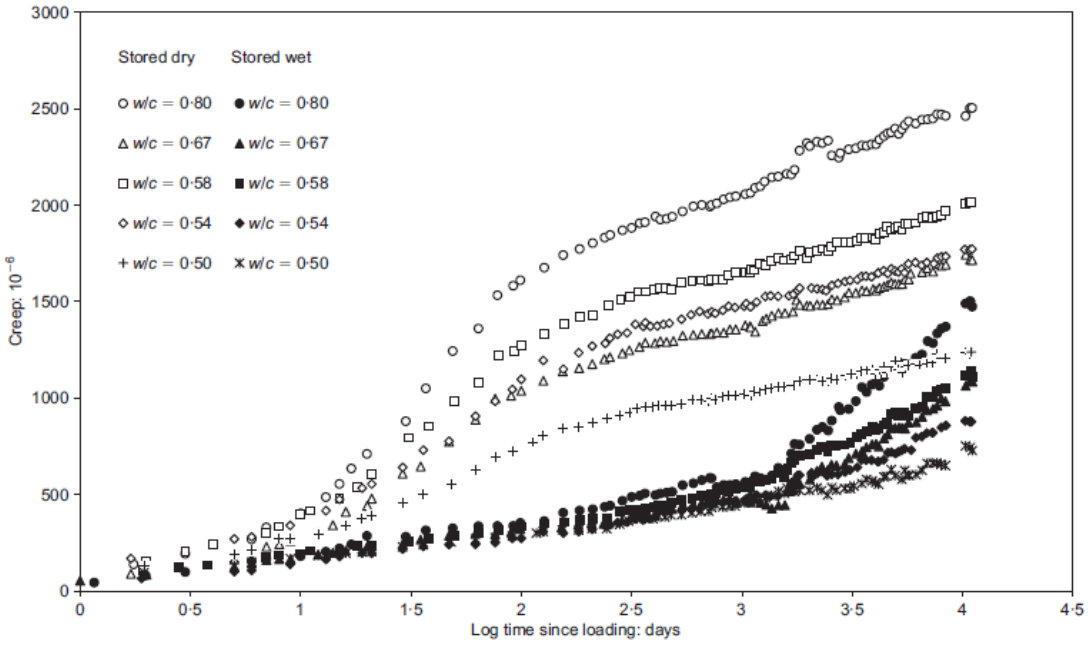

Figure 5.19. Creep of concrete made with North Notts coarse aggregate stored under dry conditions (T = 20ºC – 22ºC, relative humidity = 65%) and wet conditions (under water at T = 20 ºC - 22°C) (creep in m/m)(Brooks 2005)

The shrinkage test data in Figure 5.20 indicate that (1) the drying shrinkage of concrete started to level off after 1 year because the internal moisture state of the concrete reached equilibrium, and (2) the swelling appeared to increase after about 1 year; however, the total amount of swelling was quite small, 200 to 300 microstrain.

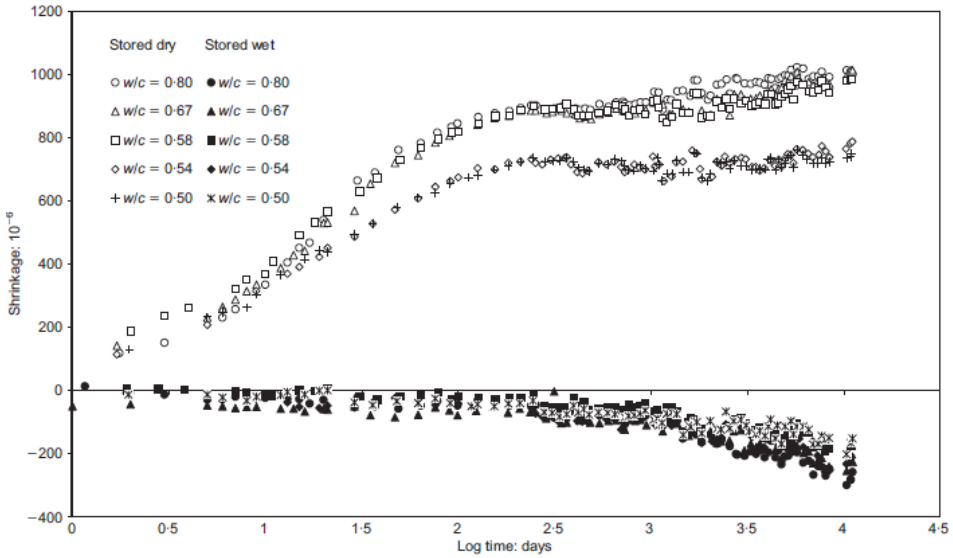

Figure 5.20. Shrinkage of concrete made with North Notts coarse aggregate stored under dry conditions (T = 20ºC –22ºC, relative humidity = 65%) and wet conditions (under water at T = 20 ºC to 22ºC) (shrinkage in m/m). (Brooks 2005)

5.6 EFFECT OF HIGH TEMPERATURE ON THE NUCLEAR SHIELDING CAPACITIES OF CONCRETE

Yousef et al. (2008) conducted an experimental study related to the effect of high temperature on the strength and gamma-ray and neutron shielding properties of four types of concrete. The samples were exposed to temperatures between 20ºC and 800ºC. Only the temperature effects on shielding properties are discussed here. Figure 5.21(a) shows the test data on attenuation coefficients of gamma rays. Results indicate small losses in attenuation coefficients for gamma rays at temperatures up to 100ºC, with no significant loss in attenuation resulting for temperatures between 100ºC and 400ºC. From 400ºC and 500ºC, there also was no significant loss in gamma rays attenuation except for one of the concretes (D-mix), which suffered a higher loss in gamma-ray attenuation as the temperature was increased from 350ºC to 500ºC. The F and D mixes lost their integrity between 500ºC and 550ºC. The effect of temperature on neutron attenuation index, noted in Figure 5.21(b), exhibited a similar trend to that for the gamma attenuation coefficient at temperatures to 500ºC. Although the hematite coarse-aggregate concrete performed best, the shielding capacities of all the concrete mixes exhibited only small reductions at temperatures almost up to 400ºC.

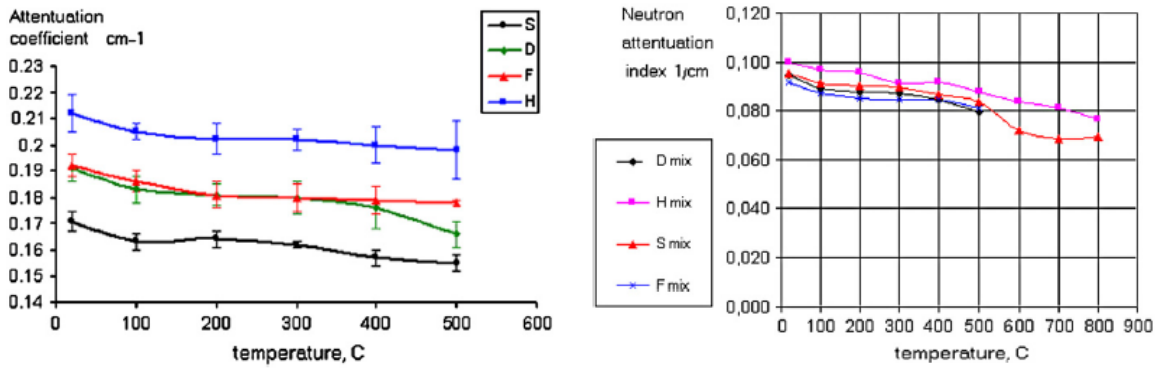

(a) **(b)**

Figure 5.21. (a) Gamma-ray attenuation coefficients vs temperature and (b) attenuation index of neutron vs temperature for the four concretes: D mix (dolomite crushed coarse aggregate), F mix (river natural coarse aggregate), H mix (hematite crushed coarse aggregate), and S mix (serpentine crushed coarse aggregate). (Yousef et al. 2008)

Sakr and El-Hakim (2005) conducted an experimental study of the effect of high temperature on attenuation capacities of concretes made with different types of aggregates. Three types of aggregates were used in the study: gravel, baryte, and ilmenite. The effect of different durations (1, 2, and 3 h) of high temperatures (250ºC, 500ºC, 750ºC and 950ºC) on the physical, mechanical, and shielding properties of heavyweight concretes were studied. Some of the test data are shown in Table 5.7. The table presents the attenuation coefficient percentage (μ%) of Co^{60} and Cs^{137} gamma sources for different types of concrete heated for 2 h to different temperatures. The table shows that the attenuation coefficient depends on temperature and that it decreases by about 16% for gravel concrete, 17% for baryte concrete, and 16% for ilmenite concrete at 750ºC, compared with the respective attenuation coefficients at room temperature (25ºC) for different energy levels (1330, 1170, and 660 keV). The attenuation coefficient of ilmenite concrete was higher than that of gravel concrete for Co^{60} by 31% and for Cs^{137} by 34%, respectively, at 750ºC. Similar results were obtained for the baryte concrete. This can be attributed to the fact that ilmenite concrete had a higher density than either the gravel or baryte concretes.

Table 5.7. Attenuation coefficient percentages of tested concrete at different temperatures (Sakr and El-Hakim 2005)

Type of concrete	Temperature (°C)	Attenuation coefficient percent (μ%)		
		Co^{60}		Cs^{137}
		1330 keV	1170 keV	(660 keV)
Gravel	25	12.72	12.21	7.33
	250	11.53	11.16	6.67
	500	11.01	10.55	6.28
	750	10.69	10.31	6.15
	950	9.55	9.18	5.50
Baryte	25	15.79	15.54	9.73
	250	14.53	14.14	8.94
	500	13.89	13.52	8.54
	750	13.25	12.91	8.15
	950	12.61	12.27	7.76
Ilmenite	25	16.59	16.22	9.81
	250	14.61	14.27	8.66
	500	14.27	13.95	8.46
	750	13.93	13.62	8.26
	950	13.61	13.31	8.1

5.7 EFFECT OF LOW TEMPERATURE ON THE NUCLEAR SHIELDING CAPACITIES OF CONCRETE

Under a low temperature, ice may form in concrete and the volume expansion associated with the ice formation may cause damage in concrete. The damage induced by low temperatures will have an impact on the shielding capacity of concrete. Basyigit et al. (2006) conducted an experimental study on the shielding capacity of two types of concretes after the concretes were subjected to freeze-thaw cycles (see Figure 5.22). When normal weight coarse aggregate was used, the concrete was called A, if the coarse aggregate was barite, it was called B. The indices of 2, 3, and 4 represent w/c ratios of 0.65, 0.51, and 0.43, respectively. Figure 5.22(a) and Figure 5.22(b) present linear attenuation coefficient results for the A- and B-type concretes, respectively, and indicate that the linear attenuation coefficient of both concretes decreased with an increasing number of freeze-thaw cycles.

Comparing the two figures, one can see that the attenuation coefficient of B-type concretes (with barite aggregates) is much higher than that of the A-type, which is due to the contribution of barite aggregate (heavyweight aggregate). For A-type concrete, the effect of w/c was not as significant as it was for the B-type concrete. Although the biological shield of an NPP in all likelihood will not be subjected to freeze-thaw cycles, the results are important from the perspective of indicating the potential impact of damage (i.e., cracking) on the attenuation of shielding concretes.

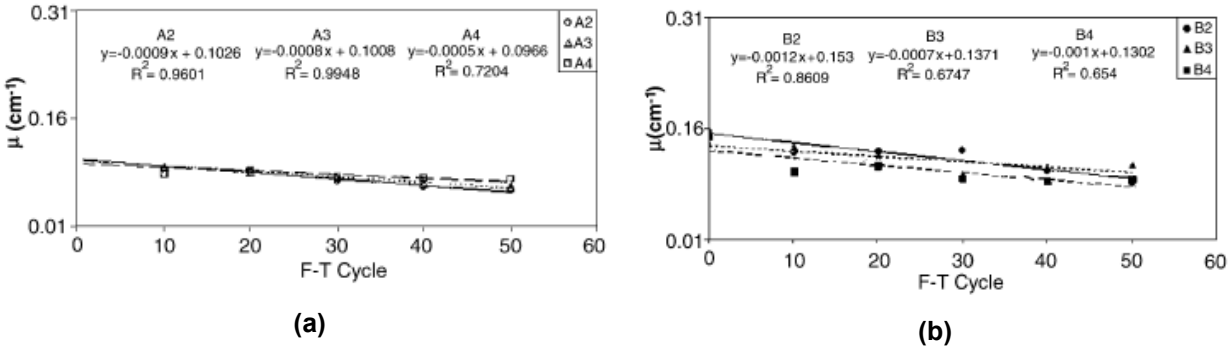

Figure 5.22. (a) Linear attenuation coefficient μ of A-type concretes as a function of freeze-thaw cycles; and (b) Linear attenuation coefficient μ of B-type concretes as a function of freeze-thaw cycles. (Basyigit et al. 2006)

6. INTERACTION OF NUCLEAR RADIATION, DURABILITY, AND SHIELDING EFFECTIVENESS

In theory, radiation can have significant effects on durability of concrete. In practice, limited research has been conducted on the durability of concrete under the influence of nuclear radiation. In this chapter, the interaction of nuclear radiation, durability, and shielding effectiveness will be addressed in four areas: (1) alkali-silica reaction, (2) carbonation, (3) radiolysis and evaporation of water, and (4) concrete cracking/spalling.

6.1 ASR AND THE COUPLING EFFECT BETWEEN ASR AND RADIATION

Ichikawa and Koizumi (2002) and Ichikawa and Kimura (2007) showed that ASR nonreactive aggregates can become reactive (or ASR-sensitive) under irradiation, depending on the intensity of the radiation, the reactivity of the aggregate, and the alkali content of the cement. Therefore, ASR and the possible coupling effect between ASR and nuclear radiation have become important research topics.

6.1.1 ASR of Concrete

The alkali-silica reaction (ASR) in concrete can be described as a chemical reaction involving alkali cations and hydroxyl ions from concrete pore solutions (Hobbs 1987). ASR will produce a gel that swells with the absorption of moisture. The amount of ASR gel and the swelling pressure vary depending on the reaction temperature, type and proportions of the reacting materials, gel composition, gradation of aggregates, and other factors. Sometimes the pressure generated by ASR gel in concrete is sufficient to generate and propagate microcracks in the concrete. The chemical reactions occurring in ASR-affected concrete structures are slow and complex. In a simplified manner, it can be described as a two-step reaction between alkalis (sodium and potassium) in cement and reactive silica aggregates. The first step is the chemical reaction between the reactive silica in the aggregate with the alkali present in cement paste to produce alkali-silica gel:

$$\underset{[xSiO_2]}{\text{Reactive silica in aggregate}} + \underset{[yNa(K)OH]}{\text{Alkali in cement paste}} \rightarrow \underset{[Na(K)_ySi_xO_z \text{ aqueous}]}{\text{Alkali-silica gel}} \quad (6.1)$$

The second step is the expansion due to the alkali-silica gel interacting with sufficient moisture:

$$\underset{[Na(K)_ySi_xO_z \text{ aqueous}]}{\text{Alkali-silica gel}} + \underset{[H_2O]}{\text{Moisture}} \rightarrow \underset{[Na(K)_ySi_xO_z\ wH_2O]}{\text{Expanded alkali-silica gel}} \quad (6.2)$$

The silica content and the internal structure of aggregate are very important. In a more sophisticated description for ASR, it has been considered as four fundamental reactions (Kurtis et al. 2002). These reactions are the dissolution of silica by hydroxyl attack, the reaction of surface silanol groups with OH^-, the binding of cations to the silicate, and the reaction to form calcium silicate hydrates. It should be pointed out that for understanding the exact nature of ASR, detailed information on the reactions and kinetics at microscale and nanoscale are needed, for which there are some experimental results available in the literature (Jennings 1986, Glasser 1992, Zanni et al. 1994, Monteiro et al. 1997).

From the abovementioned chemical equations, one can see two important conditions for the expansive ASR to occur in a concrete structure. One is the high concentration of alkalis, which results in an equally high concentration of OH^- ions (to maintain charge equilibrium). It is this high OH^- concentration, and thus high pH, that leads to the initial breakdown of reactive silica components in the aggregates, as shown in Eq. (6.1). The other is the presence of moisture in the concrete structure. Usually, the structures that have a high risk of ASR are the ones exposed to wet environments because, as shown in Eq. (6.2), one of requirements for expansive ASR to occur is moisture. As such, many concrete dams have experienced ASR problems (Saouma and Xi 2004). ASR has also been identified in one NPP in the United States (i.e., the Seabrook NPP), where the intrusion of moisture into sections of walls in certain below-grade structures resulted in indications of ASR degradation as evidenced by pattern cracking (see http://www.nrc.gov/info-finder/reactor/seabrook/concrete-degradation.html). After cracking occurs in a concrete structure, the cracking can expose the interior of the concrete to aggressive agents such as chlorides or sulfates. This can then lead to further deterioration through other mechanisms, such as corrosion of steel reinforcement.

Many different types of aggregates that have been used in concrete have caused ASR. All of the reactive aggregates contain silicon dioxide (SiO_2). Some are crystalline, such as tridymite, cristobalite, and strained quartz; others, such as opal, chert, and glassy volcanic materials, are glassy. Other types of reactive aggregates are composites having both crystalline and glassy components, including graywackes and phyllites.

6.1.2 ASR and Radiation of Concrete

When an aggregate is subjected to neutron irradiation, the degree of expansion of the aggregate strongly depends on the type of aggregate. The expansion at a fluence of 5×10^{19} n/cm^2 is about 1% for limestone and flint, and about 0.1% for serpentine. However, when these aggregates were used to make concrete, the resulting concrete exhibited expansions differing from the estimated expansion based on expansion of the aggregates. For example, limestone and flint showed the same degree of expansion under neutron radiation. The expansion of concrete with flint is about five times larger than that with limestone; moreover, the concrete with quartzite sand showed severe expansion, but the crystalline quartz itself showed only small expansion. These results suggest that the aggregates may react with surrounding cement paste in concrete to generate greater expansion due to neutron radiation than that experienced by the aggregate alone. Ichikawa and Koizumi (2002) considered this additional expansion as possibly occurring as a result of a coupling effect between ASR and radiation.

The experimental study by Ichikawa and Koizumi (2002) showed that the reactivity of silica-rich quartz to alkali may be significantly increased by nuclear radiation. Samples used for their experiment were 2 × 2 cm crystalline and amorphous quartz plates. A part of the plates was irradiated with 200 keV Ar ions to different dosages, and the plates were then immersed in an aqueous solution of NaOH (to simulate the high-alkali pore solution in concrete). The height of the terraces generated at the boundary of the irradiated and unirradiated areas was measured, which is an indication of the increased reactivity of quartz to the alkali. Irradiation of the plate to less than 2×10^{14} Ar/cm^2 does not generate a terrace, which means that the reactivity to NaOH was not changed, however, when increased to 6×10^{14} Ar/cm^2, the reactivity was significantly increased, with a plateau forming as shown in Figure 6.1(a). Figure 6.1(b) shows the evolution of the plateau under three different temperatures, the higher the temperature, the higher the height of the terrace. Because the irradiation used in the study, 6×10^{14} Ar/cm^2, was close to

that for amorphization of crystalline quartz, it can be concluded that the amorphization of crystalline quartz significantly increases the reactivity of crystalline quartz to the alkali.

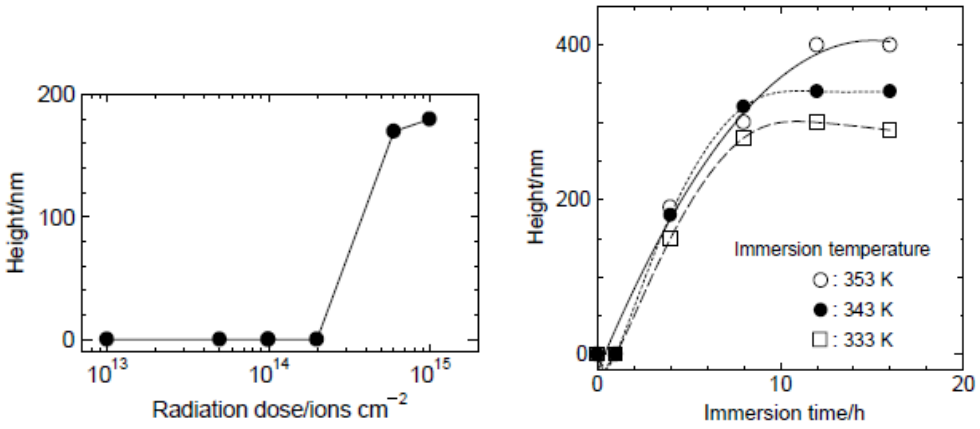

(a) **(b)**

Figure 6.1. (a) The height of terrace emerged at the boundary of irradiated and unirradiated areas of crystalline quartz after being immersed in 1 mol/dm^3 NaOH solution at 353 K for 4 h. (b) Evolution of a terrace on 1 × 10^{15} Ar/cm^2 irradiated crystalline quartz in 1 mol/dm^3 NaOH solution at different temperatures. (Ichikawa and Koizumi 2002)

Such an increase in the reactivity does not necessarily induce ASR; the rate of ASR development depends not only on the reactivity of aggregate but also on the chemical composition of Portland cement. When the combination of aggregate and cement is quite close to the critical condition for a detrimental ASR, then the increase in aggregate reactivity due to nuclear radiation could become a very important factor, making a nonreactive aggregate ASR-sensitive.

The experimental study by Ichikawa and Kimura (2007) showed that the reactivity of plagioclase, one of the major minerals composing volcanic rocks, can be increased by nuclear radiation. Irradiation of plagioclase with a 30 keV electron beam at a dose of more than 0.9×10^8 Gy converts a crystalline plagioclase to an amorphous form that is 35 times more reactive to alkali than the crystalline form. The high reactivity of the irradiated plagioclase indicates that irradiation can induce ASR in aggregate materials that are not normally susceptible to ASR.

In addition to the amount of its free expansion, the stiffness of ASR gel is also very important in determining the extent of damage due to ASR. When the ASR gel is soft and its stiffness is low, it is able to permeate into the surrounding porous cement paste, and thus the swelling pressure is not high and the cracking potential is low. In that case, a large amount of ASR gel formation may not create severe damage and cracking in concrete. On the other hand, when the ASR gel is stiff, a small amount of ASR can generate significant damage. The stiffness of ASR gel depends mainly on its chemical composition, such as the ratio of Na_2O to SiO_2. Struble and Diamond (1981a, 1981b) conducted a study to investigate the swelling pressure of ASR in terms of ASR chemical composition. Table 6.1 presents examples of maximum swelling capacity and pressure for different ASR gel chemical compositions.

Table 6.1. Swelling capacity and swelling pressure of ASR gel. (Struble and Diamond 1981a)

	Mole Ratios				Total Free Swelling, %	Maximum Swelling Pressure, MPa
	Na_2O	CaO	SiO_2	H_2O		
1	0.27		1.00	1.93	81.6	0.40
2	0.27	0.17	1.00	1.16	8.0	0.30
3	0.28		1.00	1.32	3.6	0.14
4	0.30		1.00	1.77	2.5	0.27
5	0.33		1.00	1.98	0.5	0.06
6	0.34		1.00	2.24	1.3	10.89
7	0.35	0.18	1.00	1.57	3.1	0.51
8	0.42		1.00	1.99	63.2	3.09
9	0.46		1.00	1.84	2.0	0.09
10	0.53		1.00	2.1	69.8	2.22

From Table 6.1, it is evident that sample No. 6 has the highest swelling pressure (10.89 MPa) and only 1.3% free-swelling. Thus the stiffness of ASR gel in sample No. 6 must be high. On the other hand, sample No. 9 has a low swelling pressure (0.09 MPa) and higher free-swelling capacity (2%). Therefore, the stiffness of ASR gel in sample No. 9 must be low.

The test data of Ichikawa and Koizumi (2002) showed that nuclear irradiation may change the ASR expansion potential of aggregate. A similar question may be asked about whether the stiffness of ASR gel can change under nuclear irradiation. If it can, then ASR coupled with nuclear irradiation can generate more severe damage than the ASR alone.

6.2 CARBONATION

Carbonation is the chemical reaction of portlandite, $Ca(OH)_2$, in the cement matrix with carbon dioxide gas leading to calcite ($CaCO_3$). Radiation-induced carbonation was discussed in Section 5.1, which is similar to the natural carbonation reaction in concrete. One of the main consequences of the carbonation reaction is the reduction of the pH value in the pore solution of concrete from an initial range of 12.5 and 13.5 to a value below 9 in the carbonated zones (Van Gerven et al. 2004). In the presence of radiation, the carbonation reaction is accelerated as shown by Vodák et al. (2005, 2011).

Bar-Nes et al. (2008) conducted an experimental study on the combined effect of carbonation and gamma irradiation on concrete. Carbonation tests were performed on (a) samples that were irradiated at atmospheric conditions to a dose of 10^7 Gy during a 6 month period, (b) reference samples that were nonirradiated and left in free atmospheric conditions during the same period, and (c) sealed samples that were not subjected to either free atmospheric conditions or irradiation during the whole period. All samples were prepared with a constant w/c ratio of 0.45. No carbonation was detected for the samples in group (c). The reference samples, exposed to free atmospheric conditions but not irradiated, showed an average carbonation depth of

approximately 0.5 to 0.6 mm. For the irradiated samples, a much larger carbonation depth was detected (average of around 3 mm), reaching, in some cases, depths of up to 6 mm.

The effects of carbonation on the properties of concrete are quite complicated. Consumption of portlandite during the reaction increases the porosity while deposition of calcite decreases the porosity. As a result, the strength and transport properties of concrete depend more on other parameters than on radiation-induced carbonation. For instance, the leaching rate of heavy metals such as Sr and Cs in nuclear waste was studied by Bar-Nes et al. (2008). Although the carbonation depth was increased by the nuclear irradiation, the diffusion coefficients of Sr and Cs were affected differently as noted below.

Figure 6.2(a) shows the leaching test data of Sr from cement paste (w/c = 0.3), in which the cumulative fraction of Sr leached from the irradiated sample is lower than that from the nonirradiated sample. For the Sr ions, irradiation reduces the diffusion coefficient by a factor of 28 early in the experiment for the w/c = 0.3 pastes, probably due to increased carbonation. For the w/c = 0.45 pastes, the apparent diffusion coefficient has been reduced due to irradiation by a factor of 9 (not shown). With a reduced diffusion coefficient, the leaching rate of Sr is lower.

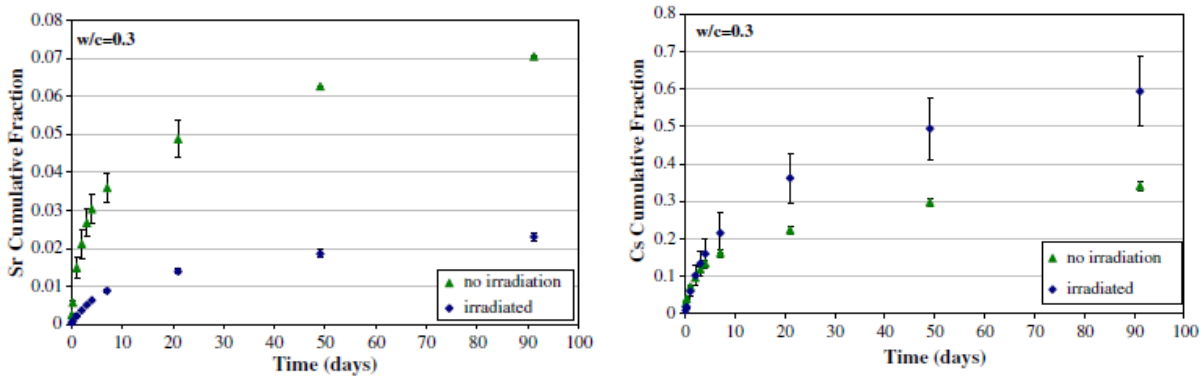

Figure 6.2. (a) Leaching of Sr from samples with w/c = 0.3. (b) Leaching of Cs from samples with w/c = 0.3. (Bar-Nes et al. 2008)

For Cs ions, the diffusion coefficient of the irradiated sample increased slightly, which is different from the effect of radiation on the diffusion coefficient of Sr. As shown in Figure 6.2(b), the cumulative fraction of Cs leached from the irradiated sample is higher than that from the nonirradiated sample. This may be caused by the high solubility of Cs in the paste. Cs ions do not precipitate as a carbonate phase, and the carbonation has no effect on the Cs ion diffusivity. The small increase in Cs diffusivity due to irradiation might originate from the formation of microcracks in the product due to the radiolysis process.

6.3 RADIOLYSIS AND EVAPORATION OF WATER

The decomposition of water under radiation is called radiolysis. It is different from vaporization of water under elevated temperature, as shown in Figure 6.3. Both interstitial water and water in the pore structure of concrete may participate in the radiolysis process. One of the products of radiolysis is hydrogen gas, H_2. In addition to the effects of radiolysis resulting from radiation noted in Chapter 2, water radiolysis is important for dry storage facilities and for radioactive waste conditioning. For long-lived wastes, concrete materials are used as an immobilization matrix undergoing mixed irradiation (i.e., a combination of alpha, beta, and gamma radiation)

(Bouniol and Aspart 1998, Bouniol 2011). The two main outcomes resulting from water radiolysis are (1) buildup of internal overpressure that may lead to cracking of the waste form and (2) the accumulation of hydrogen gas in a storage area, hence, the buildup of an explosive gas mixture when mixed with atmospheric oxygen (Bar-Nes et al. 2008). Therefore, radiolysis of water is more of a safety problem related to those applications than to the damage of concrete.

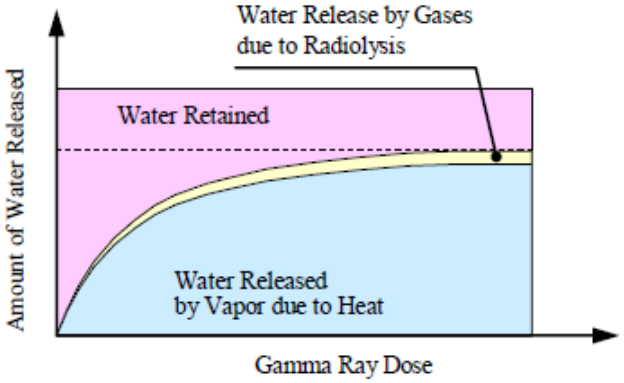

Figure 6.3. Gamma ray dose vs water retained in concrete. (Kontani et al. 2011)

Kontani et al. (2011) conducted a carefully designed test to study the water released by concrete during irradiation. Figure 6.4(a) and (b) show the experimental setup. The radiation level was controlled by the distance from the concrete samples to the radiation source. Figure 6.5(a) shows temperature changes of containers at the first and second rows and changes of irradiation room temperatures. The temperatures of containers in the second row were 15ºC higher than the room temperatures, and the temperatures of the containers in the first row were 30ºC higher than the room temperatures. Figure 6.5(b) shows the water released vs irradiation periods due to the heat of radiation. After 40 to 50 days of irradiation, release of water vapor due to the heat of gamma rays reached the maximum. The amount of water released was greater in the first row than in the second row because of differences in temperatures.

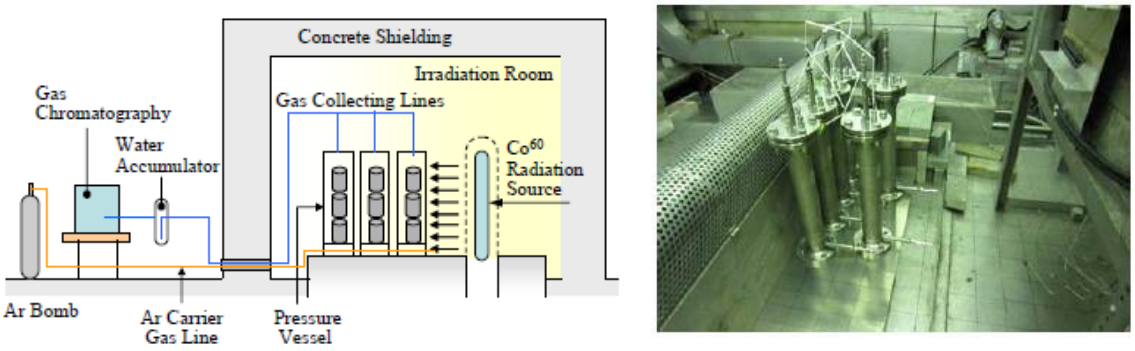

Figure 6.4. (a) Test configurations of gamma irradiation tests; and (b) arrangement of containers. (Kontani et al. 2011)

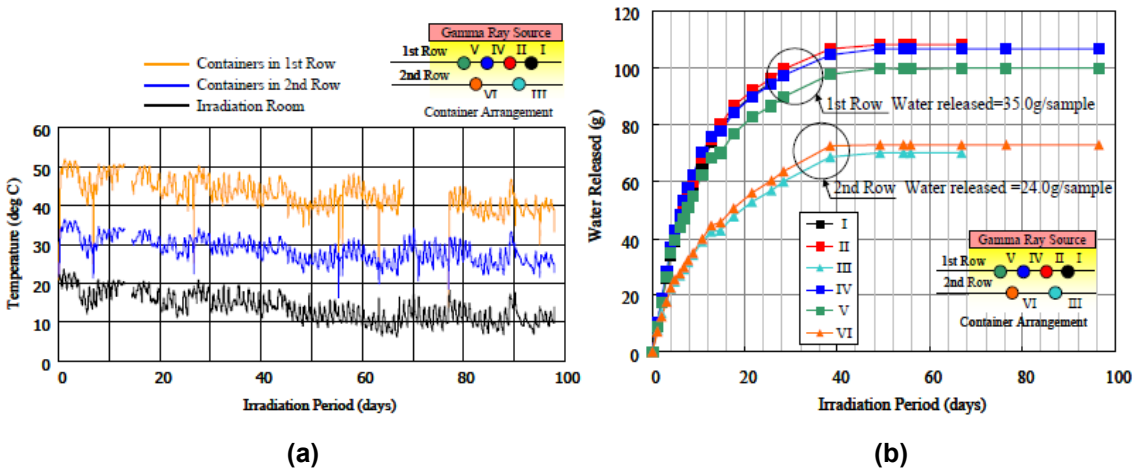

(a) (b)

Figure 6.5. (a) Temperature in the room and in the specimens and (b) water released vs irradiation duration. (Kontani et al. 2011)

Figure 6.6 shows the rates of hydrogen generation from each container. Those from containers in the first row showed maximum values of 8.5 x 10^{-5} mol/h just after the start of irradiation and then started to reduce rapidly. Those from containers in the second row showed maximum values of 3.0 x 10^{-5} mol/h 2 days after the start of irradiation and then reduced very slowly. After 60 days of irradiation, the generation rates of hydrogen were greater in the second row than in the first row although the temperatures in the first row were higher. This means that the radiolysis of water in the concrete at the second row could occur more easily than that in the concrete in the first row, which is unexpected.

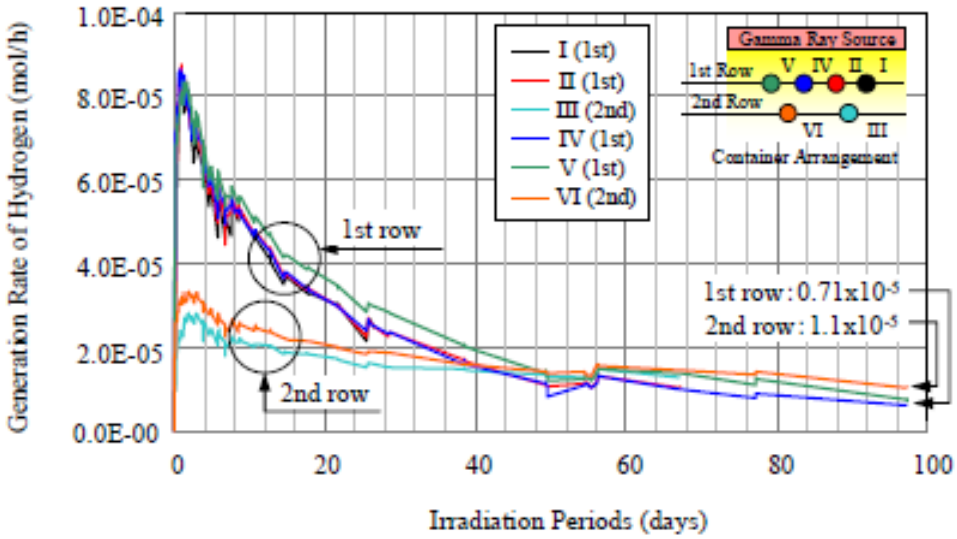

Figure 6.6. Generation of hydrogen vs irradiation period. (Kontani et al. 2011)

6.4 THE EFFECT OF CONCRETE CRACKING/SPALLING ON SHIELDING

The rust formation during rebar corrosion generates a high interface pressure between the rebar and the surrounding concrete. The level of pressure depends on many factors, such as the volume ratio of rust to steel and the thickness of the concrete cover. If the pressure is high enough, cracks may form in the concrete and the concrete cover may spall. Because applied loads to shielding structures are relatively low, the formation of cracks may not be a problem for the load-carrying capacity of the structure, but may have an impact on the radiation shielding capacity of the concrete.

Lee et al. (2008) conducted a numerical study on the effect of corrosion cracks on shielding capacity of a concrete wall. The interface pressure and the crack pattern due to rebar corrosion are shown schematically in Figure 6.7. The results of finite-element simulation of the crack growth are shown in Figure 6.8. Assuming that the wall thickness is 100 cm and the cover thickness is 10 cm, and that the spalling of the cover will occur due to the rebar corrosion, it is estimated that the radiation safety standards will be maintained under any conditions related to the effect of cracking. The analysis can also be used for other geometries of the wall and cover thickness. Results indicated that as long as the wall thickness minus cover thickness is more than 90 cm, radiation safety standards will be maintained.

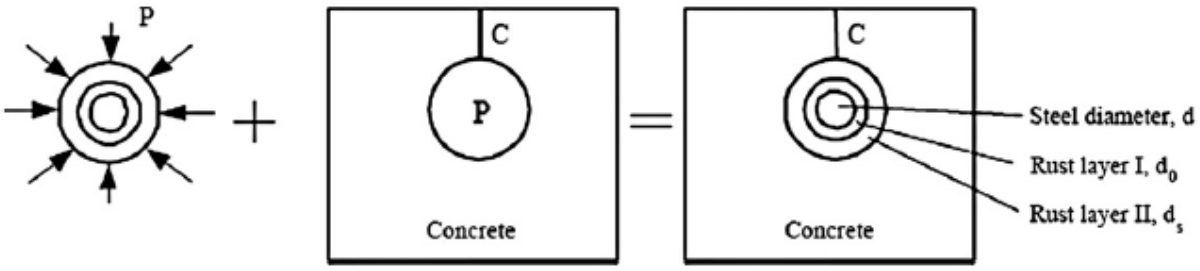

Figure 6.7. The interface pressure and the crack pattern due to rebar corrosion. (Lee et al. 2008)

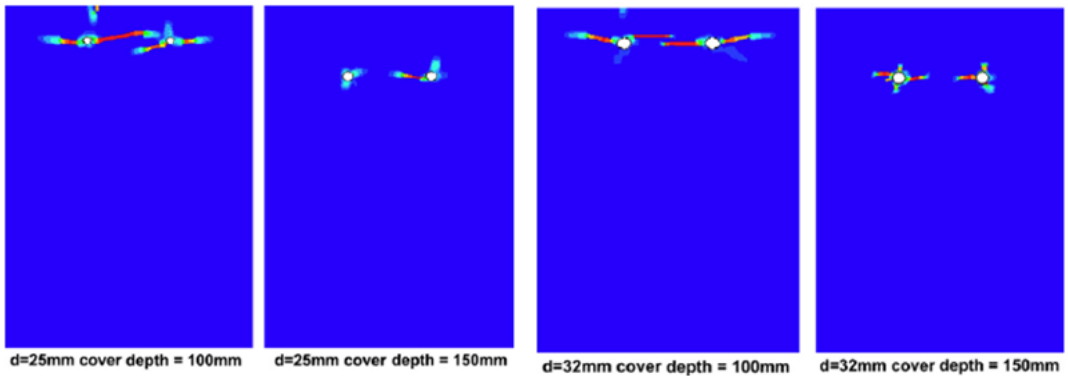

Figure 6.8. Crack growth around steel bars due to the rust formation. (Lee et al. 2008)

Lee et al. (2007) proposed a testing system for quantifying the effect of cracks on shielding performance in a concrete body. The correlation between crack width and shielding performance is deduced through experiments. The measuring system has a collimator, and it can be mounted on a concrete sample with collinear cracking. Schematics of the experimental setup and the concrete sample are shown in Figure 6.9. A photograph of the experimental setup is shown in Figure 6.10. Figure 6.11 presents the relationship between crack width, concrete thickness, and the relative intensity of radiation.

Lee et al. (2007) noted that if the thickness of the shielding material exceeds 20 cm and the crack width is $\leq$ 0.4 mm, the estimated effect of the crack on shielding performance will not be greater than 10%. They also noted that the cracks were straight; in an actual structure the crack formation would be irregular, and the irregularity would have an additional effect.

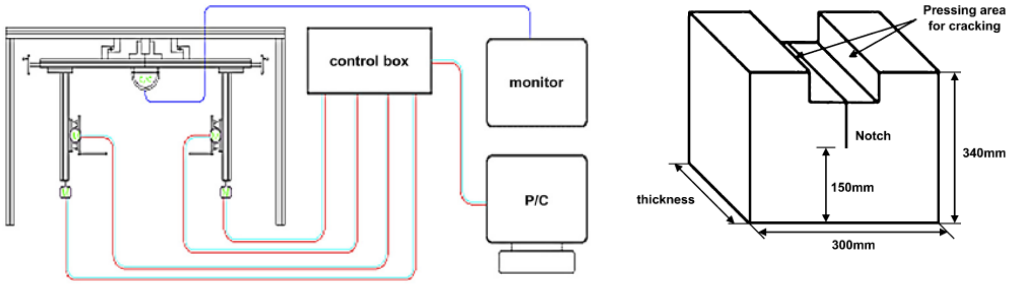

Figure 6.9. Schematic of the positioning system and the concrete sample. (Lee et al. 2007)

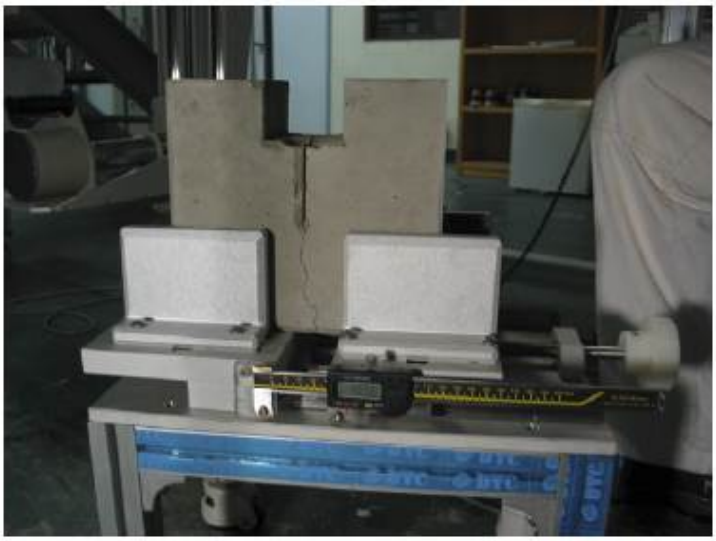

Figure 6.10. Experimental setup of the testing system for cracks in concrete. (Lee et al. 2007)

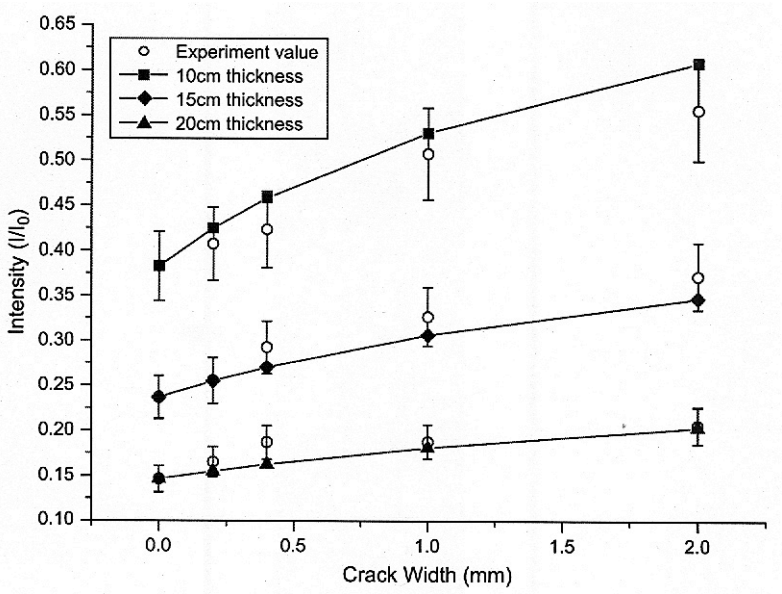

Figure 6.11. The relationships between crack width, material thickness, and shielding performance. (Lee et al. 2007)

7. COMPUTATIONAL MODELS FOR RADIATION DAMAGE OF CONCRETE

There are very few computational publications in the open literature addressing radiation damage to concrete (Hora and Patzak 2007). Most papers consider the shielding properties of concrete and its constituents under gamma and fast neutron irradiation as described in the previous sections. However an integrated approach to a computational assessment of thermal and irradiation damage of structural concrete in NPPs is still missing.

An understanding of the transport of thermonuclides in reinforced and prestressed concrete members and structures is within reach if we consider recent computational advances in hygrothermal analysis of concrete spalling under rapid heating and drying (Xotta et al. 2013a) and the multiphysics area of durability of aging dry cask structures under sustained creep and shrinkage and transient environmental conditions. In fact, decomposing structural concrete into plain concrete and steel members and further decomposing plain concrete into swelling aggregate and shrinking cement paste at the mesoscale of observations are scenarios that have been and are still being pursued by several research teams at different scales of observation. However integration into a consistent multiscale analysis procedure for the thermonuclide transport and for the associated temperature and moisture transport and the resulting mechanical damage is still a lofty goal when full-scale concrete dry casks, biological shields, reactor pressure vessel support structures, and containment structures in NPPs are to be considered. For illustration, the recent papers by Pomaro et al. (2011a, 2011b) that address many of the underlying issues in a fairly pragmatic way will be reviewed.

7.1 INTRODUCTION

Irradiation in the form of fast and thermal neutrons, primary gamma rays, or gamma rays produced as a result of neutron capture affects concrete. Changes in the properties of concrete depend primarily on the behavior of concrete aggregates that can undergo a volume change when exposed to radiation. Radiation damage in concrete aggregates is caused by changes in the lattice structure of the minerals in the aggregates. Fast neutrons are mainly responsible for the growth caused by atomic displacements; such growth has been measured in certain aggregates. Quartz aggregates, made of crystals with covalent bonding, seem to be more affected by radiation than calcareous aggregates, which contain a weaker ionic bonding. Neutron fluences on the order of 1×10^{19} n/cm^2 and gamma doses of 10^{10} rad have been noted in the literature as critical values for concrete strength degradation.

7.2 NUMERICAL MODELS FOR RADIATION DAMAGE EVOLUTION

An example of a computational model for evaluating radiation damage in concrete is the recent study by Pomaro et al. (Pomaro et al. 2011a, 2011b). Their research originated from a partnership between the Department of Civil, Environmental and Architectural Engineering of the University of Padova and the National Institute of Nuclear Physics (INFN) of Legnaro (Padova), aimed at the design of the Selective Production of Exotic Species (SPES) project. The work was related to construction of a next-generation nuclear facility dedicated to the production of special kinds of radioactive ion beams called “exotic species.” The overall objective of that activity was to investigate the behavior of concrete when exposed to nuclear radiation and to evaluate the consequent effects on its response by means of a proper definition of radiation damage in relation to the mechanical properties of the concrete.

Specifically, the subject of Pomaro's study was the concrete shielding surrounding a next-generation nuclear facility; the purpose was to develop a full understanding of the physical aspects involved in the radiation exposure of concrete to nuclear radiation generated by the fission reactions due to a primary proton beam impinging a uranium-carbide target.

In that work, the available finite-element research code NEWCON3D (Salomoni et al. 2009) for fully coupled hygro-thermo-mechanical analyses of cementitious materials was upgraded to take into account the effects of nuclear radiation on the material via the introduction of a new damage variable. In particular, the required damage law was based on the experimental evidence of stiffness degradation (Hilsdorf 1978), as shown in Figure 7.1. The lower bound to data in Figure 7.1 was used to indicate the impact of neutron fluence on modulus. The elastic degradation acts in conjunction with the already-implemented chemo-thermo-mechanical damage formulation.

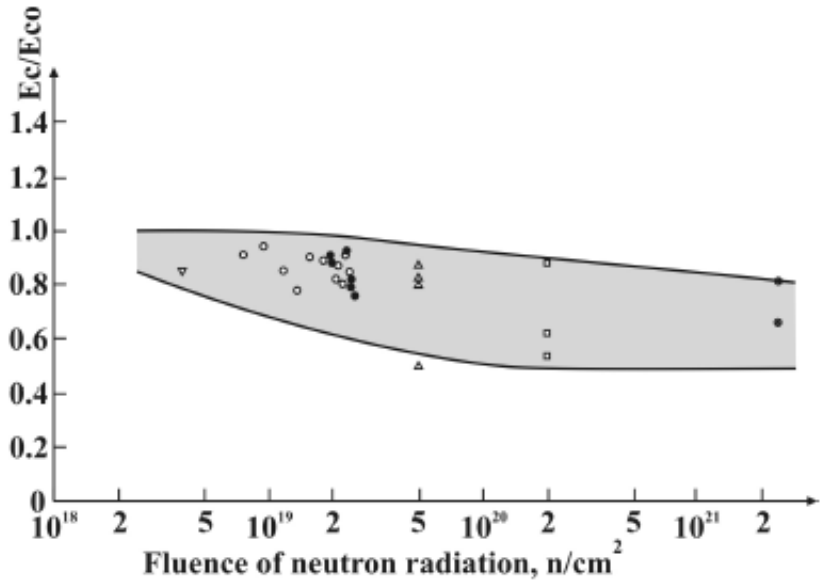

Figure 7.1. Modulus of elasticity of concrete after neutron irradiation (E_c) related to modulus of elasticity of untreated concrete (E_{co}) (See Figure 5.15 for key to data points). (Hilsdorf et al. 1978)

The effect of the mechanical and thermo-chemical damage is taken into account in a multiplicative way:

$$D = 1 - (1 - Dm)\,(1 - Dtc) \tag{7.1}$$

where Dm is the mechanical damage parameter, and Dtc is the thermo-chemical damage parameter that describes thermo-chemical material degradation at elevated temperatures, mainly due to microcracking and cement dehydration.

The extended damage model was developed by assuming that the nuclear radiation damage can activate a damage process that may be combined with the mechanical and thermochemical

ones. Hence the multiplicative damage relationship is maintained when the total damage is redefined as,

$$D = 1 - (1 - Dm)\,(1 - Dtc)\,(1 - Dr) \tag{7.2}$$

where Dr accounts for radiation damage, whose evaluation is empirically based on the stiffness degradation shown in Figure 7.1.

The implementation within the numerical code NEWCON3D results in a coupled system of finite element equations of linear momentum, mass, and energy balance:

$$\begin{bmatrix} \mathbf{K} & \mathbf{HU} & \mathbf{TU} \\ \mathbf{L}^T & \mathbf{I} & \mathbf{TP} \\ \mathbf{0} & \mathbf{TH} & \mathbf{TS} \end{bmatrix} \begin{Bmatrix} \dot{\mathbf{u}} \\ \dot{\mathbf{h}} \\ \dot{\mathbf{T}} \end{Bmatrix} + \begin{bmatrix} \mathbf{0} & \mathbf{0} & \mathbf{0} \\ \mathbf{0} & \mathbf{Q} & \mathbf{0} \\ \mathbf{0} & \mathbf{0} & \mathbf{TR} \end{bmatrix} \begin{Bmatrix} \mathbf{u} \\ \mathbf{h} \\ \mathbf{T} \end{Bmatrix} = \begin{Bmatrix} \dot{\mathbf{f}} + \dot{\mathbf{c}} \\ \dot{\mathbf{HG}} \\ \dot{\mathbf{TG}} \end{Bmatrix} \tag{7.3}$$

where

u, **h,** and **T** bar are the nodal values of the basic variables (displacement, relative humidity, and temperature;
HU and **TU** account for shrinkage and thermal dilation;
L and **TP** are coupling matrices representing the influence of the mechanical and thermal field on the hygral field;
Q is the diffusivity matrix;
TH the coupling matrix between the hygral and thermal field;
TS is the matrix of heat capacity;
TR is the matrix of thermal conductivity;
c accounts for creep;
HG represents the humidity variation load due to drying;
TG accounts for heat fluxes.

Additional analyses were performed with the Monte Carlo code FLUKA (Fassò et al. 2005), developed at CERN and INFN of Milan. FLUKA was used to describe the radiation and the temperature field for the design specifics of the SPES facility. Use of the Monte Carlo technique and the finite-element code were upgraded to take into account the radiation exposure effects on concrete and the thermal aspect (i.e., the temperature rise in the shielding due to the deposition of radiation energy).

The results of the 3D simulations are summarized in Figure 7.2, which illustrates the change of humidity and temperatures during drying and cooling. Figure 7.3 depicts the evolution of temperatures after five irradiation cycles at three locations of the shielding structure.

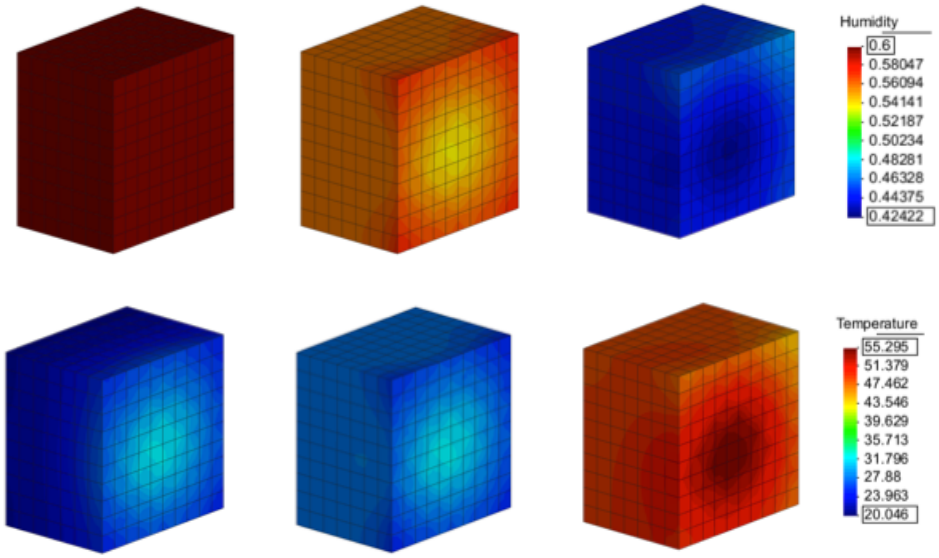

Figure 7.2. Contour maps of relative humidity and temperature after 1 h, 1 week, and 6 months. (Pomaro et al. 2011b)

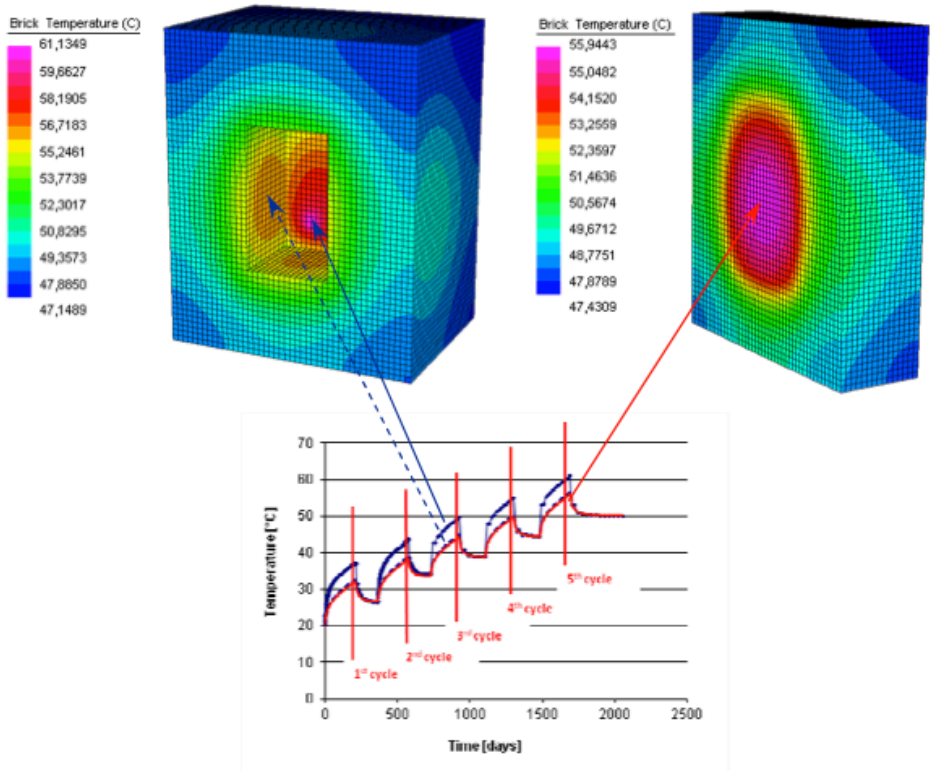

Figure 7.3. Contours after the fifth irradiation cycle and evolution of temperature at three points of the target bunker. (Pomaro et al. 2011b).

Numerical analyses were also conducted to investigate radiation damage (i.e., the impact on concrete modulus of elasticity) and its progression in the concrete structure at ages up to 50 years, assuming a neutron flux density of 10^{12} n cm^{-2} s^{-1}, which is nearly twice that expected at SPES (Pomaro et al. 2011a). Two extreme situations were considered for neutron energies: the case in which the entire integrated flux is prescribed by fast neutrons and the one that develops from thermal neutrons. This enabled the minimum and maximum threshold for radiation damage to be predicted under realistic neutron spectrum.

The sample analyzed was a 3.5 m long prism with a square cross section of 1 m^2. Both ordinary Portland cement concrete and heavyweight concretes were considered in the analyses. Results were developed in terms of damage parameter versus distance, with damage considered as being totally due to radiation. Following the diffusion theory for thermal neutrons and the two-group theory for fast neutrons, the resulting damage behavior evolves as a function of depth for ordinary Portland cement concrete as presented in Figure 7.4 for times to 50 years. These results indicate that when fast neutrons are impinging, the damaged thickness is more pronounced and the level of damage induced by fast neutrons exceeds the one induced by thermal neutrons. Figure 7.5 summarizes damage versus thickness results obtained for heavyweight and ordinary Portland cement concretes for a fast and thermal neutron flux of 10^{12} n cm^{-2} s^{-1} integrated over a 1 year exposure. The heavyweight concretes exhibited improved shielding properties relative to the ordinary (normal weight) Portland cement concrete.

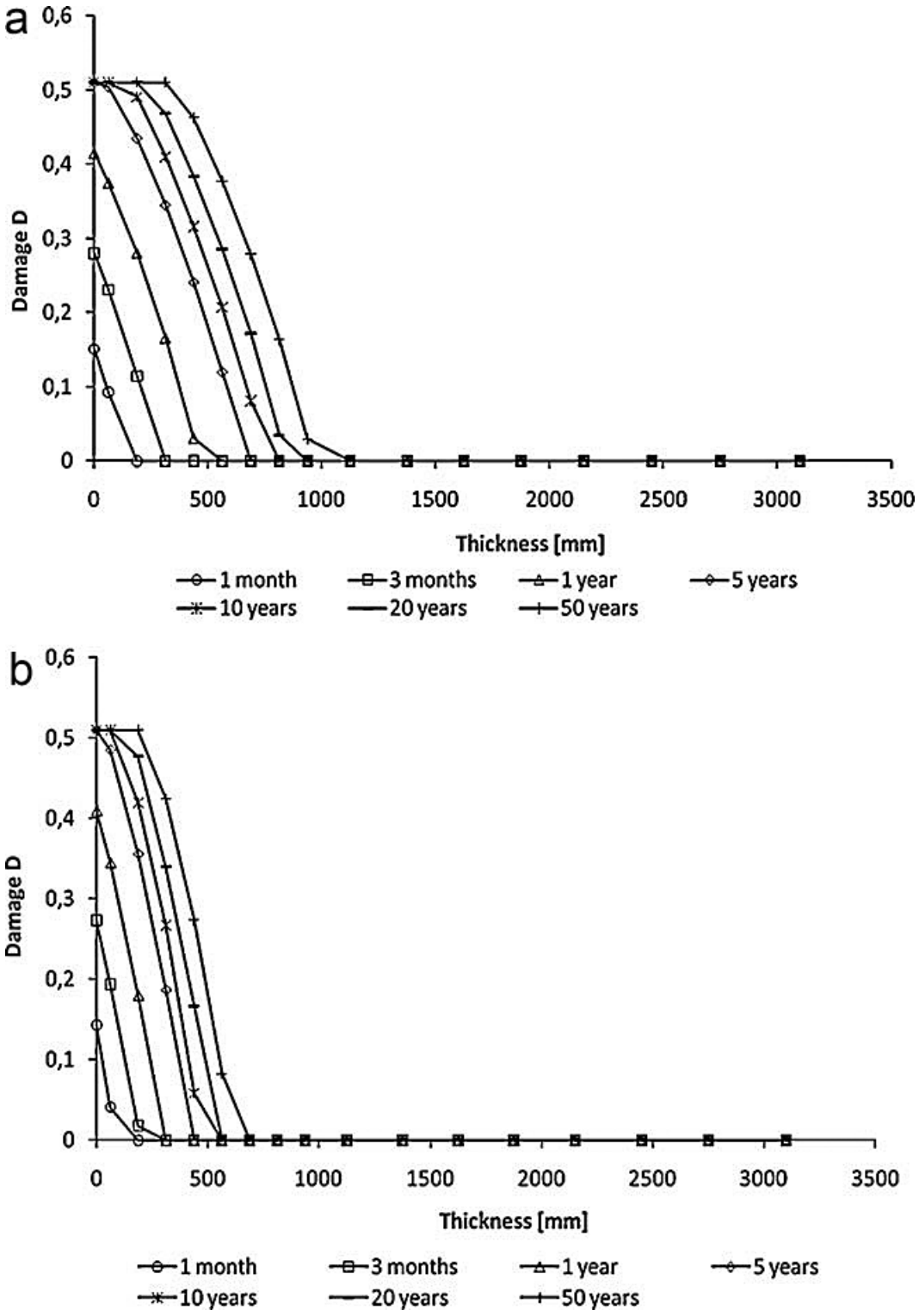

Figure 7.4. Radiation damage progression with depth for ordinary Portland cement concrete under radiation fluence for up to 50 years: (a) fast neutrons, (b) thermal neutrons. (Pomaro 2011a)

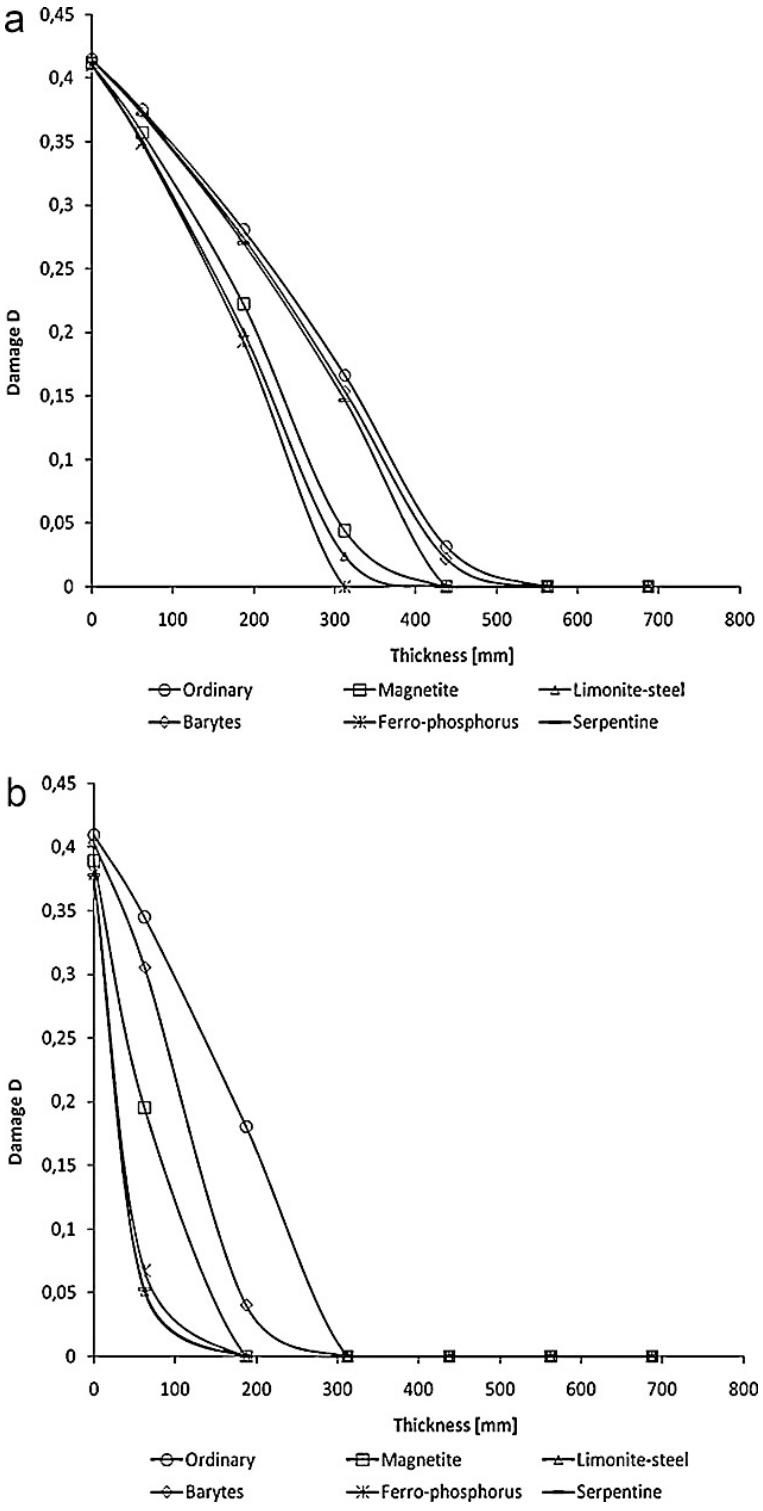

Figure 7.5. Radiation damage progression with depth for ordinary Portland cement and heavyweight concretes under radiation fluence up to 1 year: (a) fast neutrons, (b) thermal neutrons. (Pomaro, 2011a)

7.3 DAMAGE-PLASTICITY MODELS FOR CONCRETE

The Pomaro continuum damage model (Pomaro et al. 2011) raises the question of whether the mechanical characterization properly captures the main material features of concrete. In the earlier discussion it was observed that both radiation and temperature affect the aggregates of the composite material. In other terms, the granular nature of concrete is an important feature that is the basis of the so-called “Reynolds effect of volume dilatancy” under shearing. A brief review of the limitations of continuum damage models follows.

Surveys of recent concrete literature indicate an increasing number of proposals to combine plasticity and continuum damage mechanics to characterize the mechanical behavior of concrete materials (Lee and Fenves 1998; Carol et al. 2001; Grassl et al. 2002; Salari et al. 2004; Tao and Phillips 2005; Grassl and Jirasek 2006; Voyiadjis et al. 2008). Thereby, it is understood that both formulations are dissipative in nature, even though they start from very different constitutive concepts. Irrespective of the thermodynamic setting, continuum damage mechanics resorts to reduction of the initial elastic stiffness properties in the form of a Cauchy-type elastic secant relationship. In contrast, plasticity is understood in terms of strength and with reference to a description of an evolving yield surface separating elastic behavior from plastic behavior. Before examining the main shortcomings and limitations of the two dissipation models for concrete materials, let us briefly report the main relations for the different constitutive models:

1. Scalar Damage Models (Mazars 1984, Mazars and Hamon 2013):

$$\dot{\boldsymbol{\sigma}} = (1 - \mathrm{D})\mathbf{E}_0 : \dot{\boldsymbol{\varepsilon}} - \dot{\mathrm{D}}\mathbf{E}_0 : \boldsymbol{\varepsilon} \tag{7.4}$$

2. Plasticity Models (Drucker and Prager 1952,

$$\dot{\boldsymbol{\sigma}} = \left(\mathbf{E}_0 - \frac{1}{\mathrm{h_p}}\mathbf{m} \otimes \mathbf{n}\right) : \dot{\boldsymbol{\varepsilon}} \tag{7.5}$$

3. Scalar Damage-Plasticity Models (Lee and Fenves 1998; Grassl and Jirasek 2006; Vojiadjis 2009):

$$\dot{\boldsymbol{\sigma}} = (1 - \mathrm{D})\mathbf{E}_0\left[\dot{\boldsymbol{\varepsilon}} - \dot{\boldsymbol{\lambda}}\mathbf{m}\right] - \dot{\mathrm{D}}\mathbf{E}_0 : \boldsymbol{\varepsilon} \tag{7.6}$$

In the case of scalar damage, the entire isotropic stiffness tensor is reduced by the scalar valued (1-D) factor, which retains the fundamental construct of the undamaged reference (e.g., linear isotropic scalar-valued). Consequently, the main deficiency of scalar damage models is the initial reference stiffness, which does not change during progressive damage when frictional materials such as concrete exhibit strongly dilatant behavior near the maximum load resistance in uniaxial compression. Therefore, the concrete behavior exhibits a transition from compaction to dilatation under increasing axial compression. This transition of volume change is missing in scalar-valued damage models when the initial elastic Poisson’s ratio remains fixed. The other deficiency of continuum damage models is the reversibility of deformations under load-unload cycles, which does not account for permanent deformations. In the case of elastoplasticity, it is the question of the flow rule (and hence the plastic potential) whether the elastic reference stiffness is sufficiently modified by plastic dilatancy(i.e., the volumetric plastic strains). In fact, most pressure-sensitive plasticity formulations for granular materials resort to nonassociated flow rules to monitor the plastic dilatation of concrete. Clearly, the main attribute of plasticity is the irreversible nature of the plastic deformations under load cycles. Therefore, one may

conclude that the main shortcoming of scalar damage models may be corrected by their combination with plasticity.

Figures 7.6 and 7.7 illustrate the results of three simple benchmark tests comparing the triaxial response of three material models, (i) the classic elastic damage model of Mazars in its latest manifestation (2013), (ii) the associated plasticity model of Drucker and Prager (1952), and (iii) the so-called damage plasticity model of Lee and Fenves (1998) that has been implemented in Abaqus Unified FEA (DASSALT SYSTEMS 2013). Starting from identical elastic stiffness and strength properties in uniaxial tension and compression, and assuming linear softening of the tensile strength, the uniaxial calibration response in tension and compression are compared in Figure 7.6 together with the ensuing prediction of the volumetric behavior in simple shear. The results of the uniaxial tension test in the right of Figure 7.6 show similar behavior for all three material models; there is a slight difference in the postpeak branch, which may be attributed to the exponential rather than the linear softening assumption used in the damage model.

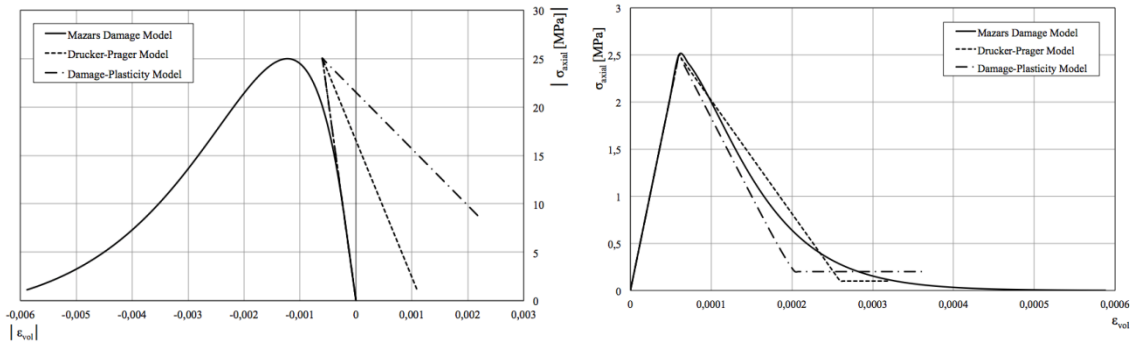

Figure 7.6. Comparison of Damage and Plasticity Models in Uniaxial Compression and Tension. (Xotta et al. 2013b)

Comparing Mazars' Damage Model with the associated DP Model and the Damage-Plasticity Model in uniaxial compression results in the response diagrams shown on the left side of Figure 7.6. The post- peak dilatancy of the two plasticity-based models is in stark contrast to the volumetric compaction of Mazars' Damage model. In short, the scalar damage model does not capture the well-known transition of volumetric concrete behavior from compaction to expansion under axial compression. Moreover, the slightly different dilatations of the DP model and Combined-Damage-Plasticity (CDP) models may be explained by the different plastic flow rules used: the associated DP flow rule is used in the DP model; nonassociated flow is used in the "Barcelona" model proposed by Lubliner (1989) for the CDP model in Abaqus.

For the case of simple shear, the three predictions are shown in the left part of Figure 7.7. There is a fundamental difference between Mazars damage model and the two plasticity models; specifically the right part of Figure 7.7 shows no volume change whatsoever for Mazars' damage model, but the two plasticity models exhibit significant volume dilatation in shear. Moreover a slight difference between DP and CDP models due to the different yield functions used in the DP and the CDP models may be noticed in the peak strength and the postpeak behavior.

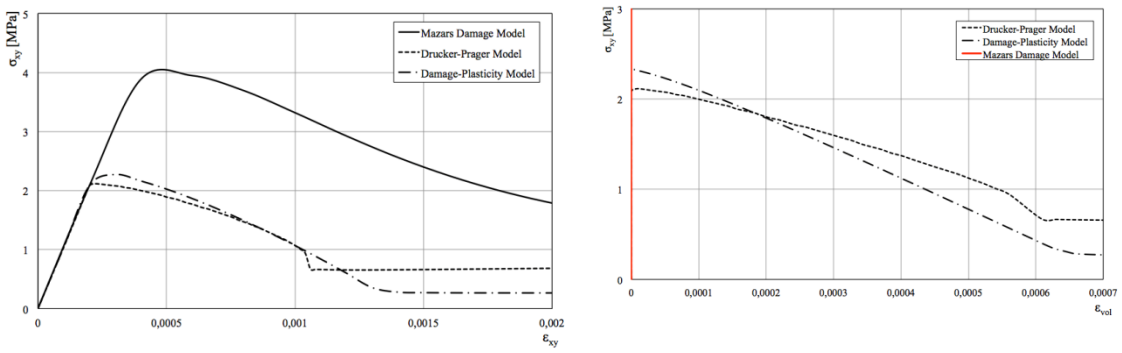

Figure 7.7. Comparison of Shear Response Predictions of Damage and Plasticity Models under Simple Shear. (Xotta et al. 2013b)

In conclusion, the brief study illustrates the drastic difference between scalar damage and pressure-sensitive plasticity models when the shear dilatancy is considered. In fact, the comparison demonstrates the need to combine damage with pressure-sensitive plasticity when dilatancy effects of frictional materials are to be captured. In summary, the lack of dilatancy of scalar damage models may be compared with the lack of dilatancy in pressure–insensitive von Mises plasticity.

8. DETECTION AND EVALUATION OF RADIATION DAMAGE IN NPP CONCRETE STRUCTURES

All commercial NPPs in the United States contain concrete structures whose performance and function are necessary for protection of the safety of plant operating personnel and the general public as well as the environment. A myriad of concrete-based structures are contained as a part of a light-water reactor (LWR) plant to provide foundation, support, shielding, and containment functions. Typical safety-related concrete structures contained in LWR plants may be grouped into four general categories: primary containments, containment internal structures, secondary containments/reactor buildings, and other structures.

The primary containment is a vital engineered safety feature of an NPP that is subjected to various operating and environmental stressors (e.g., ambient pressure fluctuations, temperature variations, and earthquakes). Concrete containments are metal-lined, reinforced concrete pressure-retaining structures that in some cases may be post-tensioned. The concrete containment includes the concrete shell and shell components, shell metallic liners, and penetration liners that extend the containment liner through the surrounding shell concrete. The reinforced concrete shell, which generally consists of a cylindrical wall with a hemispherical or ellipsoidal dome and flat base slab, provides the necessary structural support and resistance to pressure-induced forces. Leak tightness is provided by a steel liner fabricated from relatively thin plate material (e.g., 6 mm thick) that is anchored to the concrete shell by studs, structural steel shapes, or other steel products. In addition to the containment, a number of other concrete structures are contained as part of a light-water plant to support and protect safety-related systems and components. The other structures are primary, secondary, and biological shield walls as well as floors and supporting structures in the containments, reactor buildings, auxiliary (or intermediate) buildings, diesel generator buildings, intake structures, and service-water pump houses. The exterior walls and roofs, shield walls and buildings, interior floors that support heavy equipment and piping, and foundation mats are constructed of reinforced concrete. Some of the interior walls of these structures are constructed of (reinforced or unreinforced) masonry blocks. Beams and columns that support the floors are either of structural steel or reinforced concrete. Of these concrete structures, the structures most susceptible to the potential effects of radiation exposure would be those that provide biological shielding and support for the reactor pressure vessel. The presence of concrete degradation in these structures resulting from nuclear radiation could be determined through visual examination for signs of distress (e.g., cracking, volume change, and misalignment), application of nondestructive test methods, or removal and evaluation of concrete samples. However, prior to any assessments of concrete that has been subjected to nuclear radiation, precautions need to be taken to ensure that exposure of the personnel performing the assessments poses no risk to their health and safety.

8.1 NONDESTRUCTIVE TEST METHODS FOR CONCRETE AND REINFORCED CONCRETE STRUCTURES

Nondestructive testing (NDT) is a branch of materials science that utilizes noninvasive techniques to determine the integrity of a material, component, or structure or to quantitatively measure some characteristic of an object. Objectives of NDT are to:

- determine material properties;
- detect, characterize, locate, and size discontinuities/defects;

- determine the quality of manufacturing or fabrication of a component or structure; and
- check for deterioration after a period of service for a component or structure.

With respect to application of NDT methods to concrete, they can indicate strength, density and quality; locate and characterize voids or cracks; locate steel reinforcement and indicate depth of concrete cover; and indicate corrosion of reinforcing materials. Tables 8.1 and 8.2 present NDT methods to determine structural properties and to assess conditions of concrete and to determine material properties of hardened concrete in existing structures, respectively.

Table 8.1. Nondestructive test methods to determine structural properties and assess conditions of concrete (ACI 2013)

Property	Methods		Comment
	Primary	Secondary	
Reinforcement location	Covermeter; Ground-penetrating radar (GPR) (ASTM D4748)	X-ray and γ-ray radiography	Steel location and distribution; concrete cover
Concrete component thickness	Intrusive probing impact-echo (I-E) (ASTM C1383); GPR (ASTM D4748)		Verify thickness of concrete; provide more certainty in structural capacity calculations; I-E requires knowledge of wave speed, and GPR of dielectric constant in place of specific calibration to known thickness on site
Steel area reduction	Intrusive probing; ultrasonic thickness gage (requires direct contact with steel)	Radiography	Observe and measure rust and area reduction in steel; observe corrosion of embedded post-tensioning components; verify location and extent of deterioration; provide more certainty in structural capacity calculations
Local or global strength and behavior	Load test, deflection or strain measurements	Acceleration, strain, and displacement measurements	Ascertain acceptability without repair or strengthening; deterrmine accurate load rating
Corrosion potentials	Half-cell potential (ASTM C876)		Identification of likely-hood of corrosion activity
Corrosion rate	Linear polarization (SHRP-S-324 and SHRP-S-330)		Corrosion rate of embed-ded steel; rate influenced by environmental conditions

Table 8.1. (continued)

Property	Methods		Comment
	Primary	Secondary	
Location of delaminations, voids, and other hidden defects	Impact-echo; infrared thermography (ASTM D4788); impulse-response; radiography; GPR (ASTM D6087); sounding (ASTM D4580)	Pulse-echo; UPV; intrusive drilling, and borescope	Assessment of reduced structural properties; extent and location of internal damage and defects; sounding limited to shallow delaminations

ACI = American Concrete Institute
ASTM = American Society for Testing and Materials
SHRP = Strategic Highway Research Program

Table 8.2. Nondestructive test methods for determining material properties of hardened concrete in existing structures (ACI 2013)

Property	Possible Methods		Comment
	Primary	Secondary	
Compressive strength (ACI 228.1R)	Cores for compression testing (ASTM C42/C42M and C39/C39M); pullout testing (post-installed) (ASTM C900)	Penetration resistance (ASTM C803/C803M)	Strength of in-place concrete; comparison of strength in different locations.
Relative compressive strength	Rebound number (ASTM C805/C805M); UPV (ASTM C597)	In-place pulloff test (ACI 503.1R: BS 1881-207) with appropriate calibration	Rebound number influenced by near surface properties; UPV gives average result through the thickness
Tensile strength	Splitting-tensile strength of core (ASTM C496/C496M)	In-place pulloff test (ACI 503.1R; ACI 228.1R; BS 1881-207)	Assess tensile strength of concrete
Density	Relative density (specific gravity) of samples (ASTM C642)	Nuclear gage (ASTM C1040/C1040M)	
Moisture content	In-place moisture probes (ASTM F2170) Preinstalled fiber optic relative humidity sensors	Nuclear gage (ASTM C1040/C1040M); moisture content by drying (ASTM C642)	
Static modulus of elasticity	Compression test of cores (ASTM C469/C469M)		

Table 8.2. (continued)

Property	Possible Methods		Comment
	Primary	Secondary	
Dynamic modulus of elasticity	Resonant frequency testing of sawed specimens (ASTM C215)	Ultrasonic pulse velocity (ASTM C597); impact-echo; spectral analysis of surface waves	Requires knowledge of density and Poisson's ratio (except ASTM C215); dynamic elastic modulus is typically greater than static elastic modulus
Shrinkage/expansion	Length change of drilled or sawed specimens (ASTM C341/C341M)		Measure of incremental potential length change
Resistance to chloride penetration	90-day ponding test (AASHTO T259); ASTM C1543) permit ion migration test	Electrical indication of concrete's ability to resist chloride ion penetration (ASTM C1202)	Establishes relative susceptibility of concrete to chloride ion intrusion; assess effectiveness of chemical sealers, membranes, and overlays
Air content; cement content; and aggregate properties (scaling, alkali-silica reactivity, freezing and thawing susceptibility)	Petrographic examination of concrete samples removed from structure (ASTM C856 and ASTM C457/C457M); cement content (ASTM C1084)	Petrographic examination of aggregates (ASTM C294, ASTM C295/C295M)	Assist in determination of cause(s) of distress; degree of damage; quality of concrete when originally cast and current
Alkali-silica reactivity	Cornell/SHRP rapid test (SHRP-C-315); petrography		Establish in field if observed deterioration is due to ASR
Carbonation, pH	Phenolphthalein (qualitative indication); pH meter; Fiber optic pH sensors embedded in concrete	Other pH indicators (e.g., litmus paper)	Assess corrosion protection value of concrete with depth and susceptibility of steel reinforcement to corrosion; depth of carbonation
Fire damage	Petrography; rebound number (ASTM C805/C805M)	SASW; UPV; impact-echo; impulse-response	Rebound number permits demarcation of damaged surface
Freezing-and-thawing damage (in-place)	Petrography	SASW; Impulse-response; UPV	
Chloride ion content	Acid-soluble (ASTM C1152/C1152M) and water soluble (ASTM C1218/C1218M)	Specific ion probe (SHRP-S-328)	Chloride ingress increases susceptibility of steel reinforcement to corrosion
Air permeability	SHRP surface airflow method (SHRP-S-329); Torrent (1992) and autoclam air-permeability tests		Measure in-place permeability index of the near-surface concrete: within 0.6 in. (15 mm)

Table 8.2. (continued)

Property	Possible Methods		Comment
	Primary	Secondary	
Electrical resistance of concrete	AC resistance using four-probe resistance meter (FSTM 5-578)	SHRP surface resistance test (SHRP-S-327)	AC resistance useful for evaluating effectiveness of admixtures and cementitious additions; SHRP method useful for evaluating effectiveness of sealers
Water absorprion (sorptivity)	ISAT, Figg, covercrete, or autoclam sorptivity tests		In-place moisture content considered for interpreting the data

AASHTO = American Association of State Highway and Transportation Officials
AC = alternating current
ACI = American Concrete Institute
ASTM = American Society for Testing and Materials
BS = British Standard
SHRP = Strategic Highway Research Program

Visual and NDT methods are effective in identifying areas of concrete exhibiting distress but often cannot quantify the extent or nature of the distress. Quantifying and determining the nature of distress in concrete are generally accomplished through removal of cores or other samples using an established procedure. When core samples are removed from areas exhibiting distress, a great deal can be learned about the cause and extent of deterioration through property determinations and petrographic studies. Additional uses of concrete core samples include calibration of NDT devices, conduct of chemical analyses, visual examinations, determination of steel reinforcement corrosion, and detection of the presence of voids or cracks. Information on methods for examining hardened concrete to characterize materials and to identify and quantify degradation is available (Walker et al. 2006). Qualitative or quantitative characterization of the microstructure can be done using techniques such as nanoindentation, mercury intrusion porosimetry, XRD, thermal gravimetric analysis, nuclear magnetic resonance, SEM, and energy-dispersive spectroscopy.

8.2 SPECIFIC CONDITIONS RELATED TO THE EFFECT OF RADIATION ON CONCRETE

NPP concrete structures, particularly those related to the biological shield or support for the reactor pressure vessel, can be subjected to neutron and gamma radiation during their service lives. As the service lifetimes of these plants are being extended, the impact of radiation on the concrete structures may have increased significance that can affect their functional and performance requirements. Irradiation of concrete has the potential to impact the concrete's microstructure as well as its mechanical and physical properties. An assessment of the impact of radiation on the concrete microstructure and properties would require removal of concrete samples from the areas of interest and application of techniques such as identified in Tables 8.1 and 8.2.

In addition to the impacts of radiation on the microstructure and properties of concrete, radiation can contribute to elevated temperatures in the concrete as well as increased potential for ASR and concrete carbonation to occur. Techniques associated with identification of concrete that has experienced or is experiencing elevated temperatures, ASR, or carbonation may also provide indications that the concrete has been affected by radiation.

8.2.1 Temperature effects

Gamma and neutron radiation can produce elevated temperatures and thermal gradients in concrete structures. Thermal loading of reinforced concrete can result in damage ranging from cosmetic blemishes to more serious effects (e.g., misalignment and distortions). Heating of concrete may result in a variety of structural changes such as cracking, spalling, debonding of aggregate, expansion, and mineralogical or chemical changes such as discoloration, dehydration, and dissociation. With respect to the cement paste, evaporation may occur as well as dissolution, dehydration, and dissociation of ettringite, gypsum, calcium hydroxide, calcium carbonate, and other phases, such as calcium silicate hydrates.

Information related to thermal effects on concrete structures generally is obtained through a condition assessment that involves a general visual inspection of the structure for signs of distress (e.g., cracking, spalling, deflections, distortions, misalignment, and exposed steel). Nondestructive approaches identified for application to fire-damaged concrete can also be utilized as part of the assessment process. Table 8.3 presents a listing of possible NDT approaches. Examples of approaches that have been used in the field include: rebound hammer, impact echo, indirect ultrasonic pulse measurements based on refraction of longitudinal waves to identify depth of damage, and drilling resistance based on measurement of either the thrust exerted to drill the material at constant feed rate or the work to drill a unit deep hole (Colombo and Felicetti 2007). Detailed information is obtained by removal of cores and conduct of laboratory tests to provide information on the mechanical properties or internal condition of the concrete.

Table 8.3. Listing of possible nondestructive approaches for use in assessment of fire-damaged concrete (Columbo and Felicetti 2007)

Average response of cover concrete	Point-by-point response of small samples	Special interpretation techniques
Hammer tapping Schmidt rebound hammer Windsor probe Capo test Building Research Establishment internal fracture Ultrasonic pulse velocity	Small-scale mechanical testing Differential thermal analysis Thermogravimetric analysis Dilatometry (thermomechanical analysis) Thermoluminescence Porosimetry Microcrack density analysis Colorimetry Petrographic analysis Chemical analysis	Ultrasonic pulse velocity method Impact echo Sonic tomography Modal analysis of surface waves Ground-penetrating radar Electric resistivity

8.2.2 ASR potential of existing concrete and detection

ASR has been identified at one U.S. NPP (i.e., Seabrook). It was noted in Section 6.1 of this report that there may be a coupling effect between radiation and ASR that can potentially accelerate ASR activity or cause ASR to occur with aggregates that are not normally reactive. As plants age, the potential of ASR to occur in structures forming the biological shield or support for the reactor pressure vessel may increase as these structures are located in areas in which they are subjected to moderate elevated temperature in combination with radiation.

The primary method utilized for detection of ASR is through visual examinations indicating evidence of expansion, relative movements between structural elements, and cracking. ASR capable of being detected visually, however, is probably in a fairly advanced stage of development. Removal, examination, and testing of concrete samples from suspect areas can be used to confirm the presence of ASR. Petrographic examinations of thin sections of aggregate materials, and tests developed for identification of ASR reactivity products (e.g., use of sodium cobalt nitrite solution to detect potassium and uranyl acetate to detect sodium) are examples of examination and testing methods (Walker et al. 2006).

Testing methods are available for evaluating the potential for new concrete to undergo ASR expansion; however, there is no standard testing method for existing concrete. Therefore it is desirable to develop a reliable testing protocol to evaluate the ASR potential and its occurrence for concrete in the existing structures.

Since ASR requires the participation of both alkali in cement paste and reactive silica in aggregate in the presence of moisture, tests need to be performed to examine the remaining reaction potentials of the two components. This is necessary because alkali in cement paste may be exhausted at a certain age of a structure, but at a later time more alkali may be supplied from the environment. In that case, the ASR will resume and continue if there is sufficient reactive silica in the aggregate.

Two specific tests can be conducted to examine the remaining reaction potential. One is to measure the expansion of concrete specimens from an existing structure in 100% relative humidity (e.g., at 40°C); the other is to measure the expansion of the concrete specimens submerged in NaOH solutions (e.g., 1M concentration, at 40°C). Comparing the difference in the two measured expansions will show the remaining ASR expansion potential of the existing concrete. In these two tests, the first one (the 100% relative-humidity test) is to determine whether the concrete still has sufficient alkali left to form ASR gel; the second one (the NaOH test) investigates the remaining reaction potential of the aggregate used in the concrete. Both tests would require the removal of samples from the concrete structures of interest.

8.2.3 Carbonation

In Section 5.1, it was indicated that radiation can produce carbonation of concrete that is internal to the concrete (i.e., it does not start at exposed concrete surface). The extent of concrete carbonation can be easily determined either in situ or in a laboratory by treating the surface of a freshly removed concrete sample with phenolphthalein. The carbonated portion will be uncolored. Incrementally drilled concrete powder samples also can be extracted and sprayed with phenolphthalein. In addition, acid etching or microscopic analysis of thin sections cut from the concrete can assess the presence of carbonation.

9. RADIATION EXPOSURE LIMITS FOR NPP CONCRETE

In assessing the reduction of concrete strength under nuclear radiation, several threshold values were used for neutron and gamma radiation. For instance, 1×10^{20} n/cm^2 for fast neutrons and 2×10^{10} rad (2×10^8 Gy) for gamma rays have been used as the reference levels of nuclear radiation in concrete [Section III, Division 2 of the American Society of Mechanical Engineers (ASME) *Boiler and Pressure Vessel Code* (ASME 2010)*, also see* Fillmore 2004]. Concrete structures have been regarded to be sound as long as the levels of radiation do not exceed the reference levels. IAEA-TECDOC-1025 (IAEA 1998) lists 1×10^{19} n cm^{-2} for fast neutrons and 10^{10} rad (10^8 Gy) for gamma rays.

According to the available data (Mirhosseini 2010, Fillmore 2004), primary shields may experience neutron radiation fluence beyond 5×10^{19} n cm^{-2}. Concrete reactor vessels may be exposed to thermal neutron, fast neutron, and gamma radiation with the estimated values of 6×10^{19} n cm^{-2}, 2-3 $\times 10^{18}$ n cm^{-2} and 1×10^{11} rad (1×10^9 Gy), respectively, after 30 years. The tests results from the British Experimental Pile "0" Reactor by United Kingdom Atomic Energy Authority show a constant flux around 3×10^{11} n cm^{-2} s^{-1}, which is equivalent to a fluence of 3.78×10^{20} n cm^{-2} after 40 years (Alexander 1963).

Thresholds were set by various national standards for radiation exposure in 1960s, 1970s, and 1980s to reduce risk of shielding concrete property degradation due to radiation.

- The ASME *Pressure Vessel and Piping Code* (Section III, Division 2) (ASME 2010) provides a limit for neutron exposure of 1×10^{20} n cm^{-2}.

- The British *Specification for Prestressed Concrete Pressure Vessels for Nuclear Reactors* (British Standards Institute 1973) notes that although it was not possible to quantify precisely the effects of neutron radiation on the properties of concrete, it was noted that for radiation fluence less than 5×10^{19} n cm^{-2} the effects of radiation on concrete properties is not considered to be significant.

- According to American National Standards Institute (ANSI/ANS 2006a), compressive strength and modulus of elasticity are degraded for neutron exposure > 1×10^{19} n cm^{-2} or to a gamma radiation dose exceeding 10^{10} rad (10^8 Gy).

- In the *Engineering Compendium on Radiation Shielding* (Jaeger 1975) it is stated that damage to concrete by nuclear heating is more important than the effects of radiation damage. It was recommended that the incident neutron flux density should be limited to 5×10^{19} n cm^{-2} s^{-1} and for 1 MeV gamma rays it should be limited to 4×10^{10} gamma photons cm^{-1} s^{-1}.

In Japan, Ichikawa and Kimura (2007) considered that γ-rays do not affect the nature of concrete up to a dose of 1×10^{10} Gy. Irradiation by fast neutrons at a fluence of more than 5×10^{19} n cm^{-2} causes the deterioration of concrete due to the expansion of aggregates and the shrinkage of cement paste.

In an Electric Power Research Institute (EPRI) report (EPRI 2012), the threshold value for gamma radiation was considered as 10^{10} rad (10^8 Gy).

10. SUMMARY AND CONCLUSIONS

The current understanding of the effects of irradiation on concrete materials is summarized in this document. Much of the research related to this topic was conducted from the 1960s into 1970s in support of development of prestressed concrete reactor vessels for high-temperature gas-cooled reactors and radioactive waste storage facilities. Concrete structures used as biological shields and as support for the reactor pressure vessel in current LWR plants are subjected to two types of radiation, gamma and neutron.

Gamma radiation refers to electromagnetic radiation of high frequency; high energy per photon. Gamma rays typically have energies above 100 keV and wavelengths less than 10 picometers. The absorbed dose in a small volume element is equal to the energy imparted by ionizing radiation to the material in a volume element divided by the mass of the material in the volume element. The unit of absorbed dose is a gray having units of joule kg^{-1}: 1 Gy = 100 rad. The photons interact with the shielding concrete in different ways: photoelastic effect, Compton scattering, and pair production. Gamma rays have an insignificant effect on solid materials composed of ionic and metallic bonds, but they can result in the destruction of anisotropic chemical bonds such as covalent bonds. Water in the concrete can be decomposed by gamma rays by a process called radiolysis and can be converted to hydrogen, oxygen, and hydrogen peroxide. Water can also be removed from the concrete by evaporation due to heat generated by gamma radiation. Because most of the water in concrete is contained in the cement paste, gamma radiation has a greater effect on the cement paste than it has on the aggregate materials.

In the instance of neutron irradiation, the neutrons do not interact with the electrons but with the nuclei of atoms. The amount of neutron radiation absorbed is typically expressed by fluence, which is a measure of the total number of neutrons that penetrate a unit area expressed as n cm^{-2}. Because neutrons interact with the nuclei of atoms, the lattice spacing within the material may change after the collisions. Therefore, the neutrons have a more significant effect on dense and well-crystallized materials (e.g., aggregates) than on randomly structured materials with high porosity (e.g., cement paste). Under nuclear radiation, the internal structure of some aggregates can be converted from an ordered crystalline structure to a disordered structure, resulting in a decrease in specific gravity and an increase in volume.

Interactions between nuclear radiation and the internal structure of concrete produce geometric changes of the structure resulting from displacements of atoms from their lattice sites and phase transformations of the concrete constituents resulting in a reduction in porosity and/or formation of microcracks. These interactions result in changes in the various concrete properties. As the gamma radiation dose increases, the specific pore surface and the porosity of the Portland cement paste have been shown to decrease. It also has been shown that as the gamma radiation dose increases the concentration of calcite increases resulting in carbonation of the concrete. Experimental studies have shown that the reactivity of silica-rich quartz to alkali can be significantly increased by exposure to nuclear radiation. As a result, irradiation can produce ASR in concretes containing aggregates that are typically nonreactive.

Results indicating the effect of irradiation on the mechanical and physical properties of concrete are very limited. The impact of neutron and gamma radiation on concrete properties is dependent on the concrete mix proportions, type of cement, and type of aggregate. Tests presenting the effect of gamma dose on the compressive strength of mortar and concrete indicated that the compressive strength of concrete that had received a dose of 5×10^5 Gy was approximately 10% less than that of unirradiated specimens. However, the data scatter

exhibited by these results was relatively large and the data set relatively small so that statistically valid conclusions could not be derived. More recent results indicate that the compressive strength of concrete is relatively unaffected by fast neutron irradiation at exposures up to fluences of 2×10^{19} n cm^{-2}. Flexural- and splitting-tensile strength results obtained from specimens that had been subjected to gamma radiation exhibited a trend for the tensile strength to decrease with increasing dose, with the reduction on the order of 10% or less at a gamma dose of 5×10^5 Gy relative to results obtained from unirradiated specimens. However, the data scatter exhibited by these results was relatively large and the data set relatively small so that statistically valid conclusions could not be derived. It was noted by one researcher that, in general, neutron fluences greater than 1×10^{19} n cm^{-2} will lead to a reduction in the tensile strength of concrete. The static modulus of elasticity has been shown to start decreasing slightly at a fast neutron fluence of 0.6×10^{19} n cm^{-2}; however, at 1.2×10^{19} n cm^{-2} it was still within 20% of the modulus values obtained by testing unirradiated specimens. Relatively short term (i.e., approximately 300 day) creep (load = 10 N/mm^2) and shrinkage test results obtained from a limestone aggregate concrete representative of that used for the Oldbury Power Station concrete pressure vessel subjected to an average gamma dose rate of 11.4×10^3 rad hr^{-1} indicated that the creep of the irradiated concrete was less and that the shrinkage was more than results obtained from the unirradiated specimens. The effect of radiation on the coefficients of thermal expansion and thermal conductivity of concrete was reported in the literature to be similar to that obtained from unirradiated temperature-exposed concrete. Results indicated that the thermal conductivity of concrete subjected to neutron radiation decreased to about 60% of the value for unirradiated concrete and that it remained relatively constant at neutron radiation fluences up to about 3.7×10^{19} n cm^{-2}.

The combination of mechanical loading, thermal effect, moisture content, radiation effect, and time determines the response behavior of concrete in nuclear environments. However, the coupling effects among the physical and chemical driving forces need to be studied. Although limited, theoretical methods are available that can be used to model the effect of nuclear radiation on concrete. A few multiscale modeling methods exist that can address the deterioration mechanisms taking place, ranging from the micrometer-level for the internal structure of concrete to the meter-level for concrete containment structures. A computational model for evaluating radiation damage in concrete has been used related to the design of a next-generation nuclear facility for the Selective Production of Exotic Species Project in Italy. A finite-element code for fully coupled hygro-thermo-mechanical analyses of cementitious materials was upgraded in this study to include the effects of nuclear radiation through a thermochemical damage parameter (i.e., empirically based on resulting stiffness degradation). The resulting damage law accounts for the coupling of moisture, heat transfer, and the mechanical field in concrete that was treated as a fully coupled porous medium. This enabled the development of the damage front in the concrete shielding wall of the facility under neutron irradiation and provided results within the wall thickness for long-term radiation spans and several concrete mixtures to evaluate shielding properties. Contour maps of damage relative to 1 month, 1 year, 5 years, and 50 years of irradiation were developed.

In-service testing and inspection programs for U.S NPP concrete structures have the primary goal of ensuring that the structures have sufficient structural margins to continue to perform in a reliable and safe manner. A secondary goal is to identify environmental stressors or aging factors before they reach sufficient intensity to potentially degrade structural components. Nondestructive examination methods having application to reinforced-concrete structures are identified. Candidate inspection and testing methods having potential application to detection of the effects of radiation on concrete materials are noted (e.g., temperature, ASR, and carbonation).

Limitations on radiation exposure contained in several codes are identified. The limitations are placed on exposure to ensure that the concrete properties, notably strength, do not deteriorate as a result of exposure to neutron and gamma radiation. Reference levels provided in the ASME *Boiler and Pressure Vessel Code* of 1×10^{20} n cm^{-2} for fast neutrons and 2×10^{10} rad (2×10^{8} Gy) were based primarily on a paper published by Professor Hilsdorf et al. summarizing available data. Revisiting the data used by Professor Hilsdorf et al. indicates that all of the data at the higher exposure levels (i.e., fast neutron fluence > 1×10^{19} n cm^{-2}) were obtained using materials or test conditions that were not representative of LWRs.

Results presented in this report indicate that data related to the effect of gamma and neutron radiation on concrete mechanical and physical properties are very limited, particularly data representative of conditions associated with LWR plants. There is a need to improve and expand the database on irradiated concrete degradation and to develop an improved understanding of the basic mechanisms causing radiation damage. Expansion of the database can occur through laboratory studies as well as through testing concrete samples obtained from aged NPPs. In parallel with this, calculations should be performed to identify the neutron and gamma fields that develop in the concrete structures of interest, biological shield and support for the reactor pressure vessel, after various periods of operation (e.g., 40, 60, 80, and 100 years). The estimated exposure levels for the various plant designs can then be compared to exposure limits for neutron and gamma radiation that have been developed from data in the database to determine whether exposure levels are high enough to degrade the concrete, or at what period of operation an exposure limit will be exceeded.

11. REFERENCES

1. Abdo, A.E., and Amin, E. (2001) “Distribution of Temperature Rise in Biological Shield due to Thermal Neutrons”, *Annals of Nuclear Energy*, 28, 275-283.

2. Abdo, A.E., Kansouh, W.A., and Megahid, R.M. (2002) “Investigation of Radiation Attenuation Properties for Baryte Concrete”, *Jpn. J. Appl. Phys.,* 41, 7512-7517.

3. Acevedo C.E., and Serrato, M.G. (2010) “Determining the Effects of Radiation on Aging Concrete Structures of Nuclear Reactors – 10243”, WM2010 Conference Proc., March 7-11, Phoenix, AZ.

4. ACI (12013) “Report on Nondestructive Test Methods for Evaluating Concrete in Structures, ACI 228.2R-13, American Concrete Institute”, Farmington Hills, MI.

5. Alexander, S. C. (1963) “Effects of irradiation on concrete: Final results”, United Kingdom Atomic Energy Authority.

6. Alhajali, S., Kharita, M.H., Naoom, B., Yousef, S., and AlNassar, M. (2009) “Estimation of the Activation of Local Reactor Shielding Concretes”, *Progress in Nuclear Energy*, 51, 374-377.

7. ANSI/ANS (1987) “Program for Testing Radiation Shields in Light Water Reactors (LWRS)”, ANSI/ANS-6.3.1-1987, American Nuclear Society, La Grange Park, Illinois.

8. ANSI/ANS (1999) “Neutron and Gamma-Ray Cross Sections for Nuclear Radiation Protection Calculations for Nuclear Power Plants”, ANSI/ANS-6.1.2-1999, American Nuclear Society, La Grange Park, Illinois.

9. ANSI/ANS (2006a) “Nuclear Analysis and Design of Concrete Radiation Shielding for Nuclear Power Plants”, ANSI/ANS-6.4-2006, American Nuclear Society, La Grange Park, Illinois.

10. ANSI/ANS (2006b) “Specification for Radiation Shielding Materials”, ANSI/ANS-6.4.2-2006, American Nuclear Society, La Grange Park, Illinois.

11. ASME (2010) “ASME Boiler and Pressure Vessel Code”, American Society of Mechanical Engineers, New York.

12. Bar-Nes, G., Katz, A., Peled, Y., and Zeiri, Y. (2008) “The Combined Effect of Radiation and Carbonation on the Mobilization of Sr and Cs Ions in Cementitious Pastes”, *Materials and Structures,* 41, 1563-1570.

13. Bashter, I.I. (1997) “Calculation of Radiation Attenuation Coefficients for Shielding Concretes”, *Ann. Nucl. Energy*, 24(7), 1389-1401.

14. Basyigit, C., Akkurt, I., Altindag, R., Kilincarslan, S., Akkurt, A., Mavi, B., and Karaguzel, R. (2006) “The Effect of Freezing-Thawing (F-T) Cycles on the Radiation Shielding Properties of Concretes”, *Building and Environment*, 41, 1070-1073.

15. Bouniol, P., and Aspart, A. (1998) “Disappearance of Oxygen in Concrete under Irradiation: The Role of Peroxides in Radiolysis”, *Cement and Concrete Research*, 28(11), 1669-1681.

16. Bouniol, P. (2011) “Radiation Effects in Concrete”, ppt presentation, SFEN L’irradiation dans les matériaux des réacteurs nucléaires, 22 Novembre 2011.

17. Brooks, J.J. (2005) “30-year Creep and Shrinkage of Concrete”, *Magazine of Concrete Research*, 57(9), 545-556.

18. Callan, E. J. (1953) “Concrete for Radiation Shielding”, *Journal of the American Concrete Institute ,* Title No. 50-2, 17-44.

19. Carol, I., Rizzi, E., and Willam, K. (2001) “On the Formulation of Anisotropic Elastic Degradation. Part I: Theory based on a Pseudo-logarithmic Damage Tensor Rate”, *Int. J. Solids and Struct.,* 38, 491–518.

20. CEMENBUREAU (2004) “Improving Fire Safety in Tunnels: The Concrete Pavement Solution,” Brussels, Belgium (http://www.efca.info/downloads/Improving_Fire_Safety_In_Tunnels.pdf).

21. Colombo. M. and Felicetti (2007) “New NDT Techniques for the Assessment of Fire-Damaged Concrete Structures,” *Fire Safety Journal*, 42, 461-472.

22. DASSALT SYSTEMS (2013) “Abaqus Unified FEA,” Waltham, MA (http://3ds.com/products/simulia/portfolio/abaqus/overview)

23. Dubrovskii, V.B., Ibragimov, S.S., Ladygin, A.Y., and Pergamenshchlk, B.K. (1966) “Effect of Neutron Irradiation on Some Properties of Heat-Resistant Concretes”, *Atomnaya Energiya*, 21(2), 108-112.

24. Dubrovskii, V.B., Ibragimov, S.S., Kulakovskii, M.Y., Ladygin, A.Y., and Pergamenshchlk, B.K. (1967) “Irradiation Damage in Ordinary Concretes”, *Atomnaya Energiya*, 23(4), 310-316.

25. Dubrovskii, V.B., Ibragimov, S.S., M.Y., Ladygin, A.Y., Kulakovskii, M.Y., and Pergamenshchlk, B.K. (1968) “Radiation Stability of Serpentine Concrete”, *Atomnaya Energiya*, 25(6), 515.

26. Drucker, D.C., and Prager, W. (1952) “Soil Mechanics and Plastic Analysis for Limit Design”, *Quarterly of Applied Mathematics*, 10(2), 157–165.

27. El-Khayatt, A.M. (2011) “NXcom - A Program for Calculating Attenuation Coefficients of Fast Neutrons and Gamma-rays”, *Ann. Nucl. Energy*, 38 (1), 128–132.

28. EPRI (2012) “Effect of Radiation on Concrete – A Literature Survey and Path Forward”, *Final Report 1025584, Electric Power Research Institute*, Palo Alto, CA.

29. Eskandari-Ghadi, M., Zhang, W.P., Xi, Y., and Sture, S. (2013) “Modeling of Moisture Diffusivity of Concrete at Low Temperatures”, *Journal of Engineering Mechanics, ASCE*, 139(7), 1-13.

30. Fassò A., Ferrari A., Ranft J., Sala P.R. (2005) “FLUKA: A Multi-particle Transport Code”, CERN-2005- 10, INFN/TC_05/11, SLAC-R-773.

31. Feldman, R.F., and Sereda, P.J. (1968) "A Model for Hydrated Portland Cement Paste as Deduced from Sorption-Length Change and Mechanical Properties", *Materials and Structures*, RILEM, Paris, 1(6), 509-519; (1969), 2(8), 155-162.

32. Fillmore, D.L. (2004) “Literature Review of the Effects of Radiation and Temperature on the Aging of Concrete”, INEEL/EXT-04-02319, Idaho National Engineering and Environmental Laboratory, Bechtel BWXT Idaho, LLC.

33. Fujiwara, K., Ito, M., Sasanuma, M., Tanaka, H., Hirotani, K., Onizawa, K., Suzuki, M., and Amezawa, H. (2009) “Experimental Study of the Effect of Radiation Exposure to Concrete”, Proc. of 20th Int. Conf. on Stru. Mech. In Reactor Tech. (SMiRT 20), Espoo, Finland, Aug. 9-14, SMiRT 20 – Division I, Paper 1891.

34. Gerward, L., Guilbert, N., Jensen, K.B., Levring, H. (2004) “WinXCom – A Program for Calculating X-ray Attenuation Coefficients”, *Radiat. Phys. Chem.* 71, 653–654.

35. Glasser, F.P. (1992) “Chemistry of the Alkali-Aggregate Reaction”, The Alkali-silica Reaction in Concrete. Ed. R.N. Swamy, Van Nostrand Reinhold, New York, 30-54.

36. Grassl, P., Lundgren, K., and Gylltoft, K. (2002) “Concrete in Compression: a Plasticity Theory with a Novel Hardening Law”, *International Journal of Solids and Structures*, 39, 5205-5223.

37. Grassl, P., and Jirasek, M., (2006) “Damage-plastic Model for Concrete Failure”, *International Journal of Solids and Structures,* 43(22-23), 7166-7196.

38. Gray, B.S. (1972) “The Effect of Reactor Radiation on Cements and Concrete”, Commission of the European Communities, Luxembourg, 17-39.

39. Granata, S. and Montagnint, A. (1972) “Studies on Behavior of Concrete under Irradiation”, ACI Special Publication SP-34: Concrete for Nuclear Reactors, Vol. II, 1163-1172.

40. Hala, J., and Navratil, J.D. (2003) “Radioactivity, Ionizing Radiation, and Nuclear Energy”, Konvoj, Spol. S.R.O. (Ltd.), Brno, Czech Republic.

41. Hilsdorf, H.K. (1967) “A Method to Estimate the Water Content of Concrete Shields”, *Nuclear Engineering and Design*, 6, 251-263.

42. Hilsdorf, H. K., Kropp, J., and Koch, H. J. (1978) “The Effects of Nuclear Radiation on the Mechanicals Properties of Concrete”, *American Concrete Institute Special Publication SP-55*, 223-251.

43. Hobbs, D.W. (1987) “Deleterious Expansion of Concrete due to ASR,” *Magazine of Concrete Research*, 38(137), 191-205.

44. Hora, Z., and Patzak, B. (2007) “Analysis of Long-Term Behavior of Nuclear Reactor Containment”, *Nuclear Engineering and Design*, 237, 253-259.

45. IAEA (1998) “Assessment and Management of Ageing of Major Nuclear Power Plant Components Important to Safety: Concrete Containment Buidings”, *IAEA-TECDOC-1025, International Atomic Energy Agency*, p. 162,

46. Ichikawa, T., and Koizumi, H. (2002) “Possibility of Radiation-Induced Degradation of Concrete by Alkali-Silica Reaction of Aggregates*”, Journal of Nuclear Science and Technology*, 39(8), 880-884.

47. Ichikawa, T., and Kimura, T. (2007) “Effect of Nuclear Radiation on Alkali-Silica Reaction of Concrete*”, Journal of Nuclear Science and Technology*, 44(10), 1281-1284.

48. Jaeger, R.G. (Ed.) (1968) “Engineering Compendium on Radiation Shielding”, Vol. I, Heat Generation by Neutrons, Springer-Verlag, New York.

49. Jaeger, R.G. (Ed.) (1975) “Engineering Compendium on Radiation Shielding, Vol. II, Shielding Materials, Springer-Verlag, Berlin.

50. Jennings, H.M., and Xi, Y. (1992) "Relationships Between Microstructure and Creep and Shrinkage of Cement Paste", *Material Science of Concrete*, III, Ed. J. Skalny, The Amer. Cer. Soc., Westerville, OH, 37-69.

51. Jennings, H.M., (1986) "Aqueous Solubility Relationships for Two Types of Calcium Silicate Hydrate," *Journal of American Ceramic Society*, 69, 614-618.

52. Jennings, H.M., and Bullard, J.W. (2011) “From Electrons to Infrastructure: Engineering Concrete from the Bottom Up”, *Cement and Concrete Research*, 41, 727-735,

53. Kaplan, M. F. (1989) *Concrete Radiation Shielding: Nuclear Physics, Concrete Properties, Design and Construction.* Essex: Longman Scientific & Technical.

54. Kelly, B.T., Brocklehurst, J.E., Mottershead, D., McNearney, S., and Davidson, I. (1968) “The Effect of Reactor Radiation on Concrete”, United Kingdom Atomic Energy Authority, G.R.D., Rislay, Nr. Warrington, Lancs, Nr. 8, 237-265.

55. Kharita, M.H., Takeyeddin, M., Alnassar, M., and Yousef, S. (2008) “Review on the Addition of Boron Compounds to Radiation Shielding Concrete”, *Progress in Nuclear Energy*, 53, 207-211.

56. Kharita, M.H., Yousef, S., and AlNassar, M. (2010) “The Effect of the Initial Water to Cement Ratio on Shielding Properties of Ordinary Concrete”, *Progress in Nuclear Energy*, 52, 491-493.

57. Kharita, M.H., Yousef, S., and AlNassar, M. (2011) “Development of Special Radiation Shielding Concretes using Natural Local Materials and Evaluation of their Shielding Characteristics”, *Progress in Nuclear Energy*, 50, 33-36.

58. Kontani, O., Ichikawa, Y., Ishizawa, A., Takizawa, M., & Sato, O. (2010) “Irradiation Effects on Concrete Structures*”,* Proc. of International Symposium on the Ageing Management & Maintenance of Nuclear Power Plants, 173-182.

59. Kontani, O., Ichikawa, Y., and Ishizawa, A. (2011) “Irradiation Effects on Concrete Durability of Nuclear Power Plants”, Proceedings of ICAPP 2011, Nice, France, May 2-5, Paper 11361.

60. Kurtis, K.E., Collins, C.L., Monteiro, P.J.M. (2002) “The Surface Chemistry of the Alkali-Silica Reaction: A Critical Evaluation and X-ray Microscopy”, *Concrete Science and Engineering*, 4.

61. Lee, J., and Fenves, G.L. (1998) “Plastic-Damage Model for Cyclic Loading of Concrete Structures”, *Journal of Engineering Mechanics*, ASCE, 124(8), 892–900.

62. Lee, C.M., Lee, K.J., and Cho C.H. (2008) “Spalling Effect on Gamma-ray Shielding Performance in MACSTOR-400 (Korean CANDU spent fuel storage module), *Prog. Nucl. Energy*, doi:10.1016/j.pnucene.2008.02.007.

63. Lee, C.M., Lee, Y.H., and Lee, K.J. (2007) “Cracking Effect on Gamma-ray Shielding Performance in Concrete Structures”, *Progress in Nuclear Energy*, 49, 303-312.

64. Lee. S.Y., Daugherty, A.M. and Broton, D.J. (2013) “Assessing Aggregates for Radiation-Shielding Concrete,” *Concrete International*, 35(5), 31-38.

65. Lowinska-Kluge, A., and Piszora, P. (2008) “Effect of Gamma Irradiation on Cement Composites Observed with XRD and SEM Methods in the Range of Radiation Dose 0 – 1409 MGy”, *Acta Physica Polonica* A, 114, 399 – 411.

66. Lubliner, J., Oliver, J., Oller, S., and Oñate, E. (1989) “A Plastic-Damage Model for Concrete”, *International Journal of Solids and Structures*, 25, 299–329.

67. Martinez-Barrera, G., Urena-Nunez, F., Gencel, O., and Brostow, W. (2011) “Mechanical Properties of Polypropylene-fiber Reinforced Concrete after Gamma Irradiation”, *Composite: Part A*, 42, 567-572.

68. Mazars, J. (1984) “Application de la mécanique de l’endommagement au comportement non linéaire et à la rupture du béton de structure”, Thèse de Doctorat d’Etat, Université Paris VI, France.

69. Mazars, J. and Hamon, F. (2013) “A New Model to Forecast the Response of Concrete Structures under Severe Loadings: the μ Damage Model”, FramCOS-8 International Conference on Fracture Mechanics of Concrete and Concrete Structures, March 10-14, Toledo, Spain.

70. McDowall, D.C. (1971) “The Effect of Gamma Irradiation on the Creep Properties of Cncrete”, Commission of the European Communities, Luxembourg, 55-69.

71. Mehta, P.K., and Monteiro, P.J.M. (1993) “Concrete, Structure, Properties, and Materials”, Prentice Hall, Englewood Clifs, New Jersey.

72. Mirhosseini, S.S. (2010) “The Effect of Nuclear Radiation on Aging Reinforced Concrete Structures in Nuclear Power Plants”, MS Thesis, University of Waterloo, Ontario, Canada.

73. Monteiro, P.J.M.; Wang, K.; Sposito, G.; dos Santos, M.C.; and de Andrade, W.P. (1997) "Influence of Mineral Admixtures on the Alkali-Aggregate Reaction", *Cement and Concrete Research*, 27(12), 1899.

74. Pellenq, R.J.M., Kushima, A., Shahsavari, R., Van Vliet, K.J., Buehler, M.J., Yip, S., and Ulm, F,-J. (2009) "A Realistic Molecular Model of Cement Hydrates", Proc. National Academy of Science, U.S.A., 106, 16102-16107.

75. Powers, T.C., and Brownyard, T.L. (1948) "Studies of the Physical Properties of Hardened Portland Cement Paste", *PCA Res. Bull. 22*, Chicago.

76. Pomaro, B., Salomoni, V.A., Gramegna, F., Prete, G., and Majorana, C.E. (2011a) "Radiation Damage Evaluation on Concrete within a Facility for Selective Production of Exotic Species (SPES Project), Italy", *J. of Hazardous Materials*, 194, 169-177.

77. Pomaro, B., Salomoni, V.A., Gramegna, F., Prete, G., and Majorana, C.E. (2011b) "Radiation Damage Evaluation on Concrete Shielding for Nuclear Physics Experiments", *Ann. Solid Struct. Mech*., 2, 123-142.

78. Sahin, R., Polat, R., Icelli, O., and Celik C. (2011) "Determination of Transmission Factors of Concretes with Different Water/Cement Ratio, Curing Condition, and Dosage of Cement and Air Entraining Agent", *Annals of Nuclear Energy*, 38. 1505-1511.

79. Sakr, K., and El-Hakim, E. (2005) "Effect of High Temperature or Fire on Heavy Weight Concrete Properties", *Cement and Concrete Research*, 35, 590-596.

80. Salari, M.R., Saeb, S., Willam, K.J., Patchet, S.J., and Carrasco, R.C. (2004) "A coupled Elastoplastic Damage Model for Geomaterials", *Comput. Methods Appl. Mech. Engrg*., 193 (27-29), 2625-2643.

81. Salomoni, V., Majorana, C., Mazzucco, G. Xotta, G. and Khoury, G.A. (2009) "Multiscale Modelling of Concrete as a Fully Coupled Porous Medium," Ch. 3 in *Concrete Materials: Properties, Performance and Applications,* NOVA Science Publishers Inc., ISBN: 978-1-60741-250-2, 171-231, 2009.

82. Saouma, V., and Xi, Y. (2004) "Literature Review of Alkali Aggregate Reactions in Concrete Dams", Project report to Swiss Federal Office for Water and Geology FOWG, 78p.

83. Schmidt, F.A.R. (1969) "Analytical Radiation Shielding Calculations for Concrete – Formulas and Parameters", *Nuclear Engineering and Design*, 10, 308-324.

84. Shultis, J.K., and Faw, R.E. (2000) "Radiation Shielding", American Nuclear Society, Inc., La Grange Park, IL.

85. Silberberg, M.S. (2007) "Principles of General Chemistry", McGraw-Hill, New York, New York.

86. Soo, P., and Milian, L.M. (2001) "The Effect of Gamma Radiation on the Strength of Portland Cement Mortars", *Journal of Materials Science Letters* 20, 1345-1348.

87. Struble, L., and Diamond, S. (1981a) “Swelling Properties of Synthetic Alkali Silica Gels”, *Journal of the American Ceramic Society*, 64(11), 652-655.

88. Struble, L., and Diamond, S. (1981b) “Unstable Swelling Behavior of Alkali Silica Gels”, *Cement and Concrete Research*, 11, 611-617.

89. Tao, X. Y., and Phillips, D. V. (2005) "A Simplified Isotropic Damage Model for Concrete under Bi-axial Stress States," *Cement & Concrete Composites*, 27(6), 716-726.

90. Taylor, H.F.W. (1986) "Proposed Structure of Calcium Silicate Hydrate Gel", *J. Amer. Cerem. soc*., 69(6), 464-467.

91. Taylor, H.F.W. (1997) “Cement Chemistry”, 2nd Edition, Tomas Telford.

92. Timoshenko, S. and Goodier, J. N. (1970) “Theory of Elasticity”, New York, McGraw-Hill.

93. USNRC (2009) “Concrete Radiation Shields and Generic Shield Testing for Nuclear Power Plants”, Regulatory Guide 1.69, U.S. Nuclear Regulatory Commission, Washington, D.C.

94. Van Gerven, T, Van Baelen, D., Dutre, V., Van de casteele, C. (2004) “Influence of Carbonation and Carbonation Methods on Leaching of Metals from Mortars”, *Cement Concrete Research*, 34, 149–156.

95. Vodák, F., Trtík, K., Sopko, V., Kapičková, O., and Demo, P. (2005) “Effect of γ-Irradiation on Strength of Concrete for Nuclear Safety Structures”, *Cement and Concrete Research*, 35, 1447-1451.

96. Vodák, F., Vydra, V., Trtík, K., and Kapičková, O. (2011) “Effect of γ-irradiation on Properties of Harderned Cement Paste”, *Materials and Structures,* 44, 101-107.

97. Voyiadjis, G.Z., Taqieddin, Z.N., and Kattan, P.I. (2008) “Anisotropic Damage-plasticity Model for Concrete”, *Int. J. Plasticity*, 24, 1946–1965.

98. Voyiadjis, G.Z., Taqieddin, Z.N., and Kattan, P.I. (2009) “Theoretical Formulation of a Coupled Elastic-plastic Anisotropic Damage Model for Concrete Using the Strain Energy Equivalence Concept”, *Int. J. Damage Mech*., 18(7), 603- 638.

99. Walker, H.N., Lane, D.S., and Stutzman, P.E. (2006) “Petrographic Methods of Examining Concrete: A Petrographic Manual”, FHWA-HRT-04-150, U.S. Department of Transportation, Federal Highway Administration, McLean, Virginia.

100. Willam, K.J., and Warnke, E.P. (1974) “Constitutive Model for the Triaxial Behaviour of concrete”, Proc. Intl. Assoc. Bridge Structl. Engrs, Report 19, Section III, Zurich, p. 30.

101. Willam, K.J., Xi, Y., Lee, L., and Kim, B. (2009) “Response of Reinforced Concrete Structures in Nuclear Power Plants”, SESM No. 02-2009, Department of Civil, Environmental, and Architectural Engineering, University of Colorado, Boulder.

102. Wyckoff, J.M., and Chilton, A.B. (1973) “Dose Due to Practical Neutron Energy Distributions Incident on Concrete Shielding Slabs”, Proc. of the 3rd Int. Congress IRPA, p. 694, Washington, D.C.

103. Xotta G, Salomoni, V.A. and Majorana, C.E. (2013a) “Thermo-hygro-mechanical Meso-scale Analysis of Concrete as a Viscoelastic-damaged Material”, *Engineering Computations*, Volume 30, Issue 5.

104. Xotta G, Beizaee, S., Mousavi, R. and Willam, K. (2013b) “Comparisons of Damage and Plasticity Models in Uniaxial Tension, Compression and Simple Shear”, Internal Report - University of Houston, Texas.

105. Yevick, J.G. (Ed.) (1966) “Fast Reactor Technology: Plant Design, Shielding”, The M.I.T. Press, UK.

106. Yılmaz, E., Baltas, H., Kiris, E., Ustabas, I., Cevik, U., and El-Khayatt, A.M. (2011) “Gamma Ray and Neutron Shielding Properties of Some Concrete Materials”, *Ann. Nucl. Energy*, doi:10.1016/j.anucene.2011.06.011.

107. Yousef, S., AlNassar, M., Naoom, B., Alhajali, S., and Kharita, M.H. (2008) “Heat Effect on the Shielding and Strength Properties of Some Local Concrete”, *Progress in Nuclear Energy*, 50, 22-26.

108. Zanni, H., Nieto, P., Fernandez, L., Couty, R., Barret, P., Nonat, A., and Bertrandie, D. (1994) “Sol-gel Transition in Silica Alkaline Solutions: A NMR Study”, *J. Chim. Phys.*, 91, 901-908.

NRC FORM 335
(12-2010)
NRCMD 3.7

U.S. NUCLEAR REGULATORY COMMISSION

BIBLIOGRAPHIC DATA SHEET

(See instructions on the reverse)

1. REPORT NUMBER
(Assigned by NRC, Add Vol., Supp., Rev., and Addendum Numbers, if any.)

NUREG/CR-7171

2. TITLE AND SUBTITLE

A Review of the Effects of Radiation on Microstructure and Properties of Concrete Used in Nuclear Power Plants

3. DATE REPORT PUBLISHED

MONTH	YEAR
December	2013

4. FIN OR GRANT NUMBER

N6978

5. AUTHOR(S)

Kaspar Willam
Yunping Xi
Dan Naus

6. TYPE OF REPORT

Technical

7. PERIOD COVERED (Inclusive Dates)

09/10-08/13

8. PERFORMING ORGANIZATION - NAME AND ADDRESS (If NRC, provide Division, Office or Region, U. S. Nuclear Regulatory Commission, and mailing address; if contractor, provide name and mailing address.)

Oak Ridge National Laboratory, Managed by UT-Battelle, LLC
PO Box 2008
Oak Ridge, TN 37831-6283

9. SPONSORING ORGANIZATION - NAME AND ADDRESS (If NRC, type "Same as above", if contractor, provide NRC Division, Office or Region, U. S. Nuclear Regulatory Commission, and mailing address.)

Division of Engineering
Office of Nuclear Regulatory Research
U.S. Nuclear Regulatory Commission
Washington, DC 20555-0001

10. SUPPLEMENTARY NOTES

Herman L. Graves, III, NRC Technical Monitor

11. ABSTRACT (200 words or less)

The current understanding of the effects of radiation on concrete materials is summarized. Much of the research related to this topic was conducted from the 1960s into the 1970s in support of development of prestressed concrete reactor vessels for high-temperature reactors and radioactive waste storage facilities. Concrete structures used as biological shields and as support for the reactor pressure vessel in current light-water reactor plants are subjected to two types of radiation, gamma and neutron. Gamma and neutron radiation are described, and their interactions with concrete constituents noted. A summary of the effects of neutron and gamma radiation on the mechanical and physical properties of concrete is provided. Information is presented on thermal effects due to gamma heating of the concrete. Nondestructive testing methods are identified for assessment of the condition of reinforced concrete structures. Radiation limits for neutron and gamma exposure are listed. Finally, recommendations are provided to (1) expand limited database on the effect of neutron and gamma radiation on concrete's microstructure and properties, (2) conduct calculations to establish the neutron and gamma fields that develop in concrete shields and support structures after various operating periods, and (3) quantify the interaction of temperature and irradiation effects.

12. KEY WORDS/DESCRIPTORS (List words or phrases that will assist researchers in locating the report.)

alkali-silica reactions, carbonation, codes and standards, computational models, concrete aggregate, concrete cracking, concrete creep, concrete shrinkage, elevated temperature, gamma irradiation, mechanical properties, microcrystalline structure, microstructure, neutron irradiation, nondestructive testing methods, physical properties, Portland cement paste, radiation damage, radiation shielding, radiolysis, thermal stress

13. AVAILABILITY STATEMENT

unlimited

14. SECURITY CLASSIFICATION

(This Page)
unclassified

(This Report)
unclassified

15. NUMBER OF PAGES

16. PRICE

Federal Recycling Program

UNITED STATES
NUCLEAR REGULATORY COMMISSION
WASHINGTON, DC 20555-0001

OFFICIAL BUSINESS

NUREG/CR-7171

A Review of the Effects of Radiation on Microstructure and Properties of Concretes Used in Nuclear Power Plants

November 2013